AD-A057 664 MICHIGAN STATE UNIV EAST LANSING DIV OF ENGINEERING --ETC F/G 11/6
AN OPTICAL GAGE FOR STRAIN/DISPLACEMENT MEASUREMENT AT HIGH TEM--ETC(U)
SEP 77 W N SHARPE, D R MARTIN F33615-76-C-5059

UNCLASSIFIED AFML-TR-77-153 NL

1 OF 2
AD A057 664

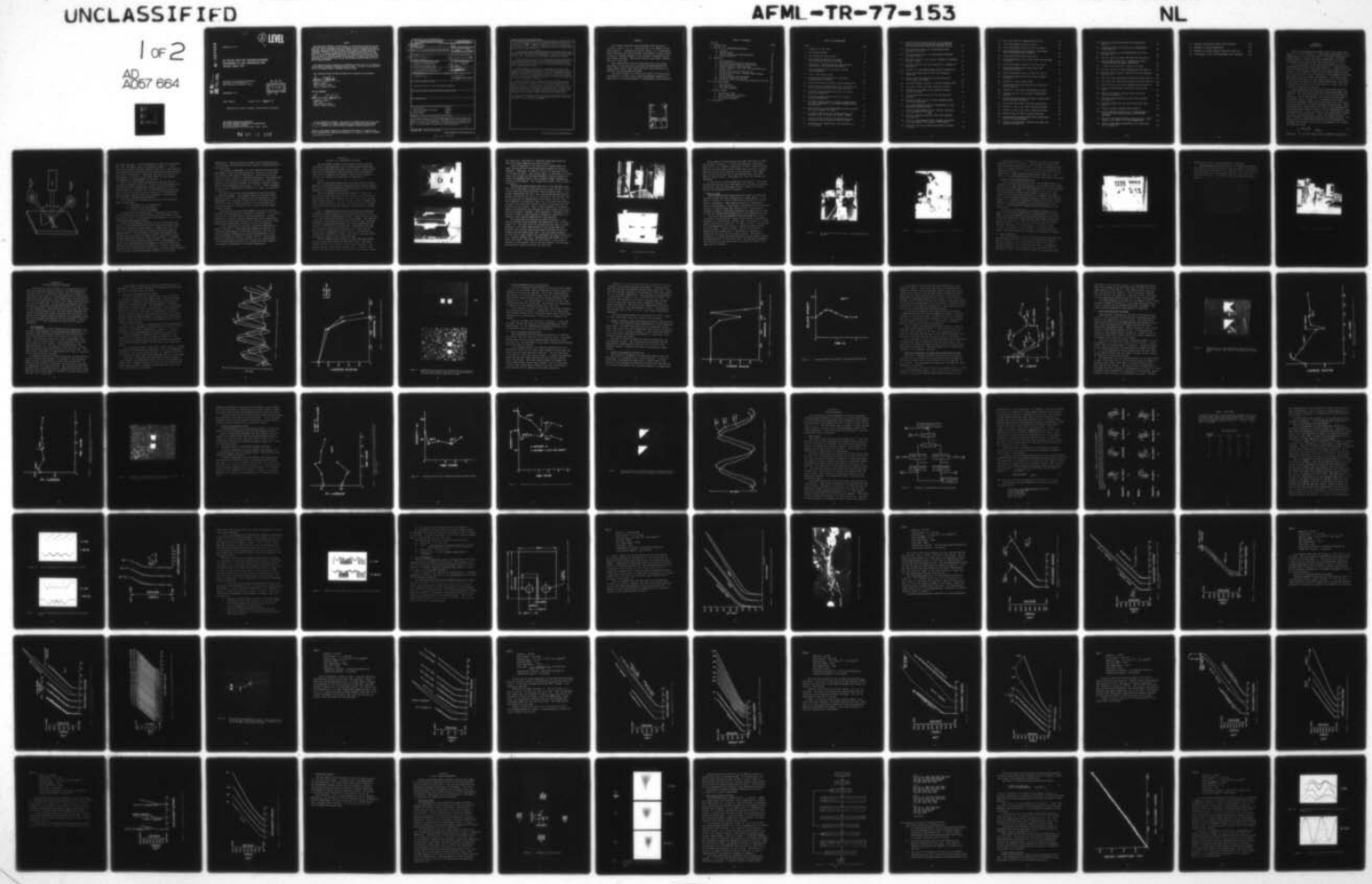

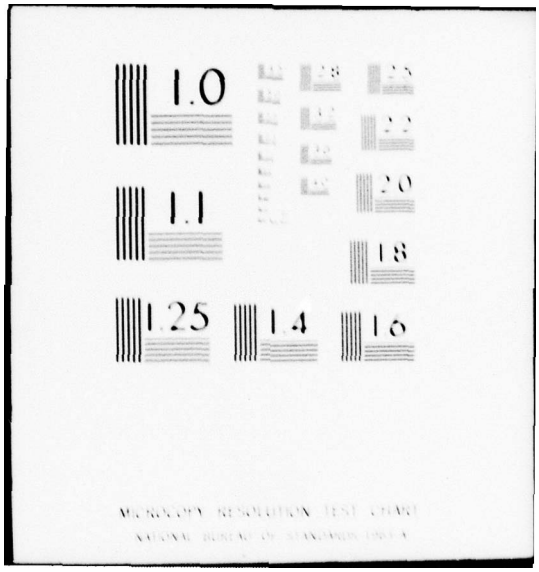
1.0
1.1
1.25
1.4
1.6
2.0
1.8

AD A057664

AD No.
DDC FILE COPY

(2) LEVEL II

AFML-TR-77-153

AN OPTICAL GAGE FOR STRAIN/DISPLACEMENT MEASUREMENT AT HIGH TEMPERATURE NEAR FATIGUE CRACK TIPS

Division of Engineering Research
Michigan State University
East Lansing, Michigan 48824

DDC
RECEIVED
AUG 15 1978
B

SEPTEMBER 1977

Final Report January 1976 - JULY 1977

Approved for public release; distribution unlimited.

AIR FORCE MATERIALS LABORATORY
AIR FORCE WRIGHT AERONAUTICAL LABORATORIES
Air Force Systems Command
Wright-Patterson Air Force Base, Ohio 45433

78 07 28 037

NOTICE

When Government drawings, specifications, or other data are used for any purpose other than in connection with a definitely related Government procurement operation, the United States Government thereby incurs no responsibility nor any obligation whatsoever; and the fact that the government may have formulated, furnished, or in any way supplied the said drawings, specifications, or other data, is not to be regarded by implication or otherwise as in any manner licensing the holder or any other person or corporation, or conveying any rights or permission to manufacture, use, or sell any patented invention that may in any way be related thereto.

This report has been reviewed by the Information Office (OI) and is releasable to the National Technical Information Service (NTIS). At NTIS, it will be available to the general public, including foreign nations.

This technical report has been reviewed and is approved for publication.

Dennis E. Macha

DENNIS E. MACHA
Metals Behavior Branch
Metals & Ceramics Division

FOR THE COMMANDER

Lawrence N. Hjelm

LAWRENCE N. HJELM
Actg. Chief,
Metals Behavior Branch
Metals & Ceramics Division

"If your address has changed, if you wish to be removed from our mailing list, or if the addressee is no longer employed by your organization please notify _____,W-PAFB, OH 45433 to help us maintain a current mailing list".

Copies of this report should not be returned unless return is required by security considerations, contractual obligations, or notice on a specific document.

AIR FORCE/56780/5 June 1978 — 300

SECURITY CLASSIFICATION OF THIS PAGE *(When Data Entered)*

REPORT DOCUMENTATION PAGE

READ INSTRUCTIONS BEFORE COMPLETING FORM

1. REPORT NUMBER: AFML-TR-77-153	2. GOVT ACCESSION NO.
3. RECIPIENT'S CATALOG NUMBER	
4. TITLE *(and Subtitle)*: AN OPTICAL GAGE FOR STRAIN/DISPLACEMENT MEASUREMENT AT HIGH TEMPERATURE NEAR FATIGUE CRACK TIPS.	5. TYPE OF REPORT & PERIOD COVERED: Final Technical Report. 1 January 76 - 31 July 77
	6. PERFORMING ORG. REPORT NUMBER
7. AUTHOR(s): William N. Sharpe, Jr.; Donald R. Martin	8. CONTRACT OR GRANT NUMBER(s): F 33615 — 76 — C — 5059
9. PERFORMING ORGANIZATION NAME AND ADDRESS: Division of Engineering Research, Michigan State University, East Lansing, Michigan 48824	10. PROGRAM ELEMENT, PROJECT, TASK AREA & WORK UNIT NUMBERS: 2307-05 (61102F)
11. CONTROLLING OFFICE NAME AND ADDRESS: Air Force Materials Laboratory (LLN), Wright-Patterson Air Force Base, Ohio 45433	12. REPORT DATE: September 1977
	13. NUMBER OF PAGES: 126
14. MONITORING AGENCY NAME & ADDRESS *(if different from Controlling Office)*	15. SECURITY CLASS. *(of this report)*: Unclassified
	15a. DECLASSIFICATION/DOWNGRADING SCHEDULE

16. DISTRIBUTION STATEMENT *(of this Report)*

Approved for public release; distribution unlimited.

17. DISTRIBUTION STATEMENT *(of the abstract entered in Block 20, if different from Report)*

18. SUPPLEMENTARY NOTES

19. KEY WORDS *(Continue on reverse side if necessary and identify by block number)*

Interferometry	IN-100
Crack tip opening displacements	Overload
High Temperature	Creep
Biaxial Strain	Closure

20. ABSTRACT *(Continue on reverse side if necessary and identify by block number)*

The interferometric strain/displacement gage (ISDG) relates the motion of fringe patterns generated by a laser beam impinging upon closely-spaced indentations to local surface deformation. The purpose of this research was to extend the technique to real-time crack tip opening displacement (CTOD) and biaxial strain measurements on superalloys at high temperatures.

DD FORM 1 JAN 73 1473 EDITION OF 1 NOV 65 IS OBSOLETE

SECURITY CLASSIFICATION OF THIS PAGE *(When Data Entered)*

401 086

LB

The indentations must remain relfective at temperature; they can be protected with a coating. A coating was developed to protect Incolloy 901 for several hours at 650°C. IN-100 will remain reflective if it is preoxidized in an rf furnace, but an electroplated chromium and vapor-plated platinum coating produces better fringe patterns.

The measurement systems were evaluated with fifteen demonstration experiments using an IN-100 compact tension specimen. Tests were run at room temperature and 732°C. The loading spectrum consisted of fatigue crack growth at a constant stress intensity factor interspersed with single peak overloads.

Fringe motions were monitored with a minicomputer-controlled system which used oscillating mirrors to move the patterns across photomultiplier tubes. Two software packages were used for the two kinds of measurements--CTOD and biaxial strain. In each case, the output of the system was a voltage proportional to displacement or strain.

CTOD measurements were made using two indentations placed across the fatigue crack. Typically the spacing was 50 or 100 microns, and the indentations were located 100 microns behind the crack tip. Displacements were measured with a resolution of 0.12 micron at a rate of $\sim$ 10 microns per second. This meant that cyclic load-displacement curves could usually be recorded at 1 Hz; the overloads were recorded at a slower rate. The system functioned well for tests at room and high temperatures.

Strain was recorded in two orthogonal directions at various locations ahead of the crack tip. Spacing of the set of three indentations was 150 microns, and they were located at 0, 100, or 200 microns ahead of the tip along the crack line. The resolution of the system is $\sim$ 0.004 percent strain and the recording rate is $\sim$ 0.01 percent strain per second. A typical load-strain plot would take 50-100 seconds. Strains were easily recorded at room and elevated temperature for fatigue cracks, but the overloads produced a spreading plastic zone which usually destroyed one of the indentations.

Both of the measurement systems were shown to have excellent stability at high temperature. In addition to recording strain/displacement versus load, they would be useful for creep measurements.

PREFACE

This report describes work performed under Air Force contract F 33615 - 76 - C - 5059 with Mr. D. E. Macha as technical monitor. Professor William N. Sharpe, Jr., of Michigan State University was the principal investigator, and Mr. Donald R. Martin, graduate student in the College of Engineering was the project engineer. The project duration was from 1 January 1976 to 31 July 1977.

The authors would like to acknowledge the very capable assistance of two Electrical Engineering undergraduates--Mr. Thomas Payne and Mr. Dale Koch--who built the electronics and modified the minicomputer programs.

This work is part of a continuing effort of the principal investigator to develop this unique measurement technique for application to various problems in experimental solid mechanics.

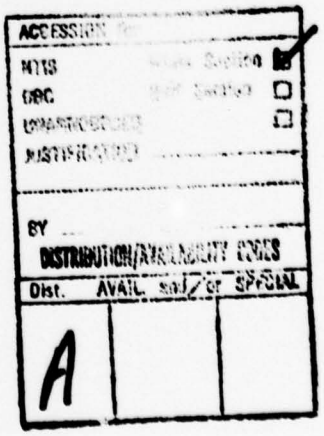

TABLE OF CONTENTS

SECTION		Page
I.	INTRODUCTION	1
II.	BIAXIAL HIGH TEMPERATURE FACILITY	5
	1. Furnace	5
	2. Scanner Board	9
	3. Mirror Drivers and PMT Amplifiers	12
	4. Other Equipment	12
III.	OXIDATION	16
	1. Test Procedure	16
	2. Bare Metal--Incolloy 901 and IN-100	17
	3. Platinum-Rhodium Tabs on Incolloy 901	21
	4. Nickel Plating on Incolloy 901	21
	5. Copper. Chomium, Gold, and Platinum Plating on Incolloy 901	22
	6. Chrome Electroplated Incolloy 901	22
	7. Chrome Electroplated, Platinum Vapor-Plated Incolloy 901	25
	8. IN-100 Oxidized with RF Heater	27
	9. Chrome-Electroplated IN-100	32
	10. Chromium, Oxide, and Platinum Coatings on IN-100	32
IV.	CTOD MEASUREMENT	38
	1. CTOD Software	38
	2. CTOD Measurements	48
	3. Concluding Remarks	75
V.	BIAXIAL STRAIN	76
	1. The Biaxial ISDG	76
	2. Small Displacement Software	79
	3. Biaxial Strain Results	82
	4. Concluding Remarks	114
VI.	DISCUSSION	116

LIST OF ILLUSTRATIONS

Figure		Page
1.	Schematic of the ISDG	2
2.	The Hotrod furnace	6
3.	The resistance wire furnace	8
4.	The scanner board with the laser, servocontrolled mirrors, and PMTs	10
5.	Closeup of a scanning mirror, PMT, resistor network box, and adjusting mechanism	11
6.	The 4-channel mirror controller and PMT signal amplifier	13
7.	View of the entire setup	15
8.	Fringe pattern intensities at different temperatures for IN-100	18
9.	Normalized fringe intensity versus temperature	19
10.	Indentations in Incolloy 901 (a) and IN-100 (b) after heating to 593°C and furnace cooling	20
11.	Intensity versus temperature plot for nickel-plated Incolloy 901	23
12.	Intensity versus time at 650°C for nickel-plated Incolloy 901	24
13.	Intensity versus time at different temperatures for three specimens of platinum/chromium plated Incolloy 901	26
14.	Indentations in platinum/chromium plated Incolloy 901 after exposure at 650°C	28
15.	Intensity-time curve for IN-100 specimen pre-oxidized in an rf furnace at 650°C at AFML	29
16.	Intensity-time curve for IN-100 specimen pre-oxidized in an rf furnace at 650°C at MSU	30
17.	Indentations in IN-100 after pre-oxidizing in an rf furnace	31

18. Intensity-time curves at 732°C for a chromium plated and preoxidized IN-100 specimen and for same specimen with additional platinum coating 33

19. Intensity-time curve for chromium/platinum/ pre-oxidized IN-100 34

20. Intensity-time curve for chromium/pre-oxidized/ platinum IN-100 35

21. Photomicrograph of the original indents of specimen 19 after tests. 36

22. Intensity traces for the second set of indents of specimen 19 37

23. Flowchart of maximum/minimum counting subroutine 39

24. Output from PMTs when mirrors are scanning 3 locations 44

25. Output from PMTs when mirrors are stationary and specimen is loaded 44

26. Load-displacement curves at various loading rates 45

27. Intensity versus time when cycling at 10 Hz. 47

28. Dimensions in inches of the modified compact tension specimen 49

29. Load-displacement plots for the Incolloy 901 specimen 51

30. Photomicrograph of the Incolloy specimen after the crack had grown 52

31. Load-displacement plots for indentations at two distances from crack tip. 54

32. Plots of displacement before, during, and after the overload of 1.73 K_{max}. 55

33. Plots at various intervals after the overload of Figure 32

34. Plots of displacement before, during, and after the overload of 1.73 K max at 732°C Test 3 58

35. Plots for the first 1000 cycles after overload at 732°c. 59

36. The crack after the completion of Test 3. 60

37. Load-displacement plots for Test 4 62

38. Load-displacement plots at 732°c for Test 5 64

39. Load-displacement plots taken at 732°C after the overload and hold of Test 5 65

40. Load-displacement plots for Test 6 67

41. Load-displacement plots taken after the overload for Test 6 68

42. Load-displacement plots at 732°C for Test 7 70

43. Load-displacement plots taken after the overload for Test 7 71

44. Load-displacement plots at 732°C for Test 8 73

45. Load-displacement plots after the overload of Test 8 74

46. Schematic of the biaxial ISDG 77

47. Photographs of fringe patterns for different biaxial spacing 78

48. Flowchart of the small displacement program 80

49. Calibration plot for the small displacement program 83

50. Fringe pattern signals from three indentations spaced 100 microns apart 85

51. Fringe pattern signal from two indentations 85

52. Strains ε_x and ε_y for Test 9 before overload 86

53. Strains ε_x and ε_y for Test 9 during overload 88

54. Indentations for Test 10 before overload 90

55. Fringe pattern signals from three indentations spaced 150 microns apart 90

56. Biaxial strains before, during, and after the overload for Test 10 91

57. Biaxial strains taken after the overload for Test 10 93

58. Photomicrograph of the crack and indentations after Test 10 94

59. Biaxial strains at room temperature and 732°C for Test 11 96

60. Biaxial strains versus load and time for Test 11 97

61. The specimen after Test 11 showing the crack growing through the upper indentation 98

62. ε_x during the overload of Test 11 at 732°C 99

63. Biaxial strains at three temperatures for Test 12 101

64. Biaxial strains before, during and after overload for Test 12 102

65. The crack and indentations before and after Test 12 103

66. The crack and indentations before and after Test 13 105

67. Baixial strains at three temperatures for Test 13 106

68. Biaxial strains before and during overload for Test 13 107

69. Biaxial strains at various cycles after the overload of Test 13 108

70. Biaxial strains before and after the overload for Test 14 110

71. Photomicrographs of the crack before and after Test 15 112

72. Biaxial strains recorded during Test 15 113

73. Fringe patterns from sets of 3 indentations on the plated and unplated sides of the IN-100 specimen 118

74. Opening load versus distance from tip for a crack grown at 25.5 MN/m $^{3/2}$ at room temperature 119

75. Opening load versus temperature for crack grown at 25.5 MN/m $^{3/2}$ 121

76. Opening load versus cycles after overload 122

77. Maximum ε_y versus temperature 123

78. Maximum ε_y versus distance from the crack tip 123

79. Photograph of the IN-100 specimen crack surfaces 124

SECTION I
INTRODUCTION

Relative displacement measurement over a very short gage-length is in itself difficult. Displacement measurement at high temperatures is in itself difficult. This report describes a system capable of making real-time displacement (or strain) measurements with a gage-length of 50-100 microns at 732°C.

Other displacement/strain measuring devices for use at high temperatures have larger gage-lengths.[1] Electro-optical and electro-mechanical extensometers have gage-lengths of 12.5 mm or more. Wire resistance gages can have gage-lengths as small as 1.6 mm, but their lack of stability at high temperatures makes them useful only for dynamic measurements. Capacitance gages have better stability, but their gage-length is 6.4 mm or more. If one wishes to measure crack-opening-displacement (COD) near a fatigue crack tip or the strains ahead of a crack tip, then a different approach is required.

COD measurements over short gage-lengths have been made using the laser-based interferometric strain/displacement gage (ISDG)[2]. The basic principles of the ISDG are described in that paper and its bibliography, but a very brief description is probably useful. Figure 1 is a schematic of the ISDG. Two square pyramidal indentations are pressed into the surface of the specimen with a Vicker's hardness tester diamond. These indentations may either straddle a crack for COD measurements or be placed away from the crack for strain measurements. When illuminated with a laser, the sides of the indentations diffract the light in four directions. Since the indentations are so close together, interference patterns are formed in space. The motion of two of these fringe patterns can be recorded and averaged and related to the relative displacement (δd) between the indentations by

$$\delta d = \frac{\delta m_1 + \delta m_2}{2} \qquad \frac{\lambda}{\sin \alpha_o} \tag{1}$$

Where δm_1, δm_2 are the fringe pattern movements normalized on

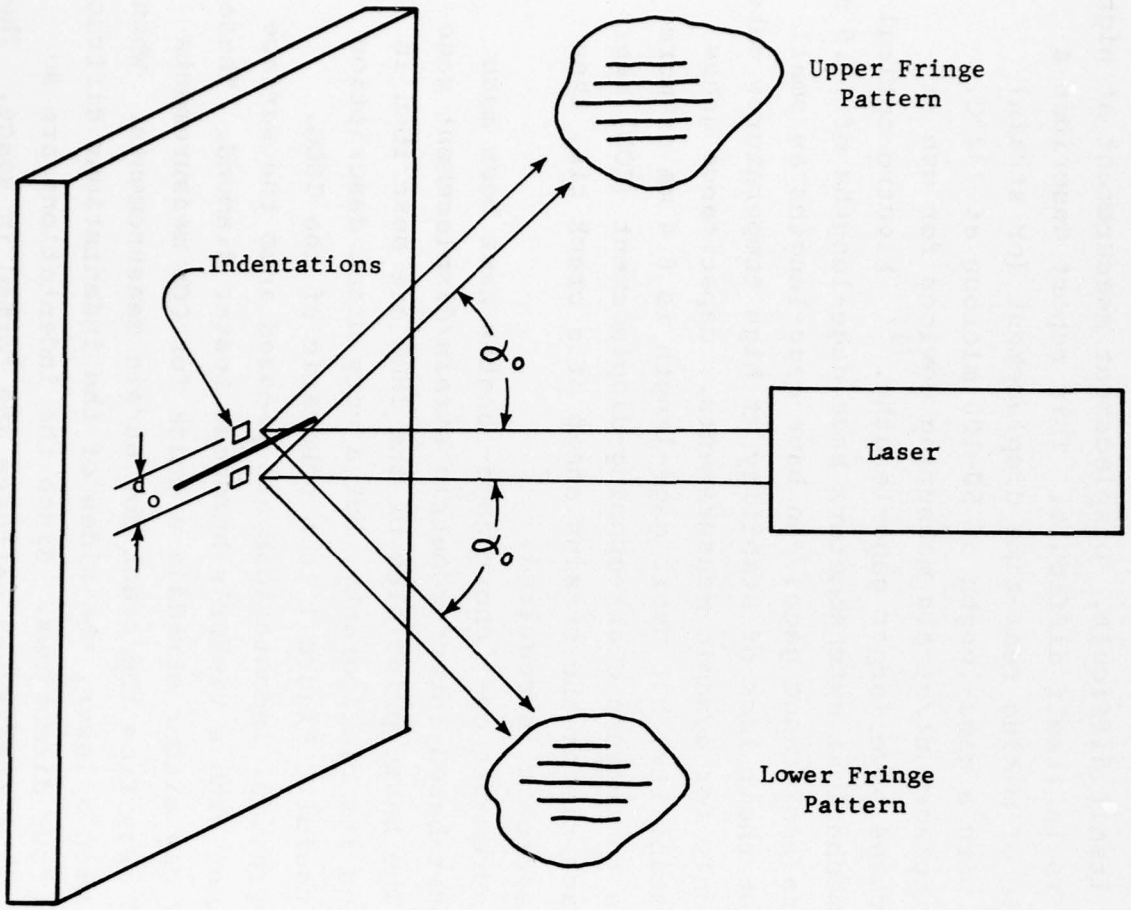

Figure 1. Schematic of the ISDG

the fringe spacing, λ is the wavelength of light (0.633 microns for a He - Ne laser) and α_o is defined in Figure 1. Strain on a solid specimen would be computed from $\delta d/d_o$. More details about the optics of the gage and the effects of rigid body motion are given in reference 3. Typically the quantity $\lambda/\sin \alpha_o$ is approximately 1 micron, so one fringe shift on each pattern corresponds to a displacement of 1 micron.

Use of the ISDG at high temperatures requires that the indentations remain reflective. Biaxial strain measurement can be made with three indentations and with detectors for four fringe patterns. Previous uses of the ISDG have not been real-time, but the fringe motion was recorded using photodetectors and the output analyzed after the experiment. Fringe motion has also been recorded photographically.

This research then extends the existing state-of-the-art ISDG in three ways:

1) Measurement at high temperature
2) Biaxial strain measurement
3) Real-time strain measurement

A previous brief investigation [4] indicated that biaxial strain measurement at elevated temperatures was possible, and an earlier project [5] was devoted to development of a real-time displacement measurement system.

Real-time measurement requires that the fringe motion be monitored with photodetectors and the resulting electrical signals then converted to displacement. A simple way to do this is to use an analog circuit that counts fringes and feeds a summing counter. An instrument for biaxial displacement measurements has been built for NASA Lewis [6] using this concept. Though simple and economical, this instrument has a resolution of only 1/2 micron and cannot measure cyclic displacements. One needs a more sophisticated, minicomputer-controlled system for improved resolution and cyclic capability. Section 2 describes the facilities constructed on this project to attain high-resolution, cyclic, biaxial strain/displacement capability at elevated

temperatures. These facilities include a multi-ported furnace, a four-channel servocontrolled mirror system, and photomultiplier tube detectors.

The premiere requirement for high temperature displacement measurement is that the indentations are capable of reflecting the incident laser beam at temperature. Most metals will not maintain a mirror finish at elevated temperature. The superalloys tested in this research (in particular IN-100) are oxidation-resistant, but special treatment is required to prepare a specimen so that measurements can be made at 732°C. These treatments, as well as the investigations leading up to them, are presented in Section 3.

Section 4 deals with the minicomputer controlled system for CTOD measurement. The software used was available from a previous project[5]. The capabilities and limitations of the measurements are examined in seven cyclic tests with single overloads. Four of these tests were at 732°C and three were at room temperature; all were run on a single IN-100 compact tension specimen.

The software for strain measurement available at the beginning of the project had the required resolution (~0.01 percent strain) but no provisions for cyclic measurements. It was necessary to develop a biaxial version with cyclic capability. This system is described in Section 5, and the results of seven demonstration experiments (three at 732°C) are presented.

A final appraisal of the ISDG at elevated temperature is given in Section 6. The system has adequate resolution for real-time measurements of both CTOD and strain, but the frequency response (especially for strain measurements) is not as high as would be liked for fatigue testing. On the other hand, its stability is quite suitable for creep measurements. It is believed that this work is a significant step forward in mechanical measurement at elevated temperatures.

SECTION II

BIAXIAL HIGH TEMPERATURE FACILITY

The electronic hardware and multiport furnace required for biaxial high temperature strain/displacement measurement are specialized items developed on this project. When coupled with an electrohydraulic testing machine and a minicomputer, they form the complete test system. The various components of this test facility are described in this chapter.

1. Furnace

Two furnaces were constructed; one using silicon-carbide heating elements and one using resistance wire heating elements. The first one reached temperature more quickly, but the thermal gradient in the specimen was larger.

The first furnace is pictured in Figure 2. There are five ports in the front half of the furnace; one in the center for the entering laser beam and four at 45 degrees for the exiting fringe patterns. Each port is made with an alundum tube with a quartz window on each end. The front half is attached to the two posts of the test machine; the back half is hinged to it.

Heat is supplied to the furnace with three Hotrods manufactured by Norton Company (3/8-inch diameter with a 5-inch long heating zone) mounted horizontally. These rods are located 1 1/4 inch from the rear surface of the specimen. The specimen is mounted in clevises and pins made from 713C steel and manufactured by Applied Test Systems, Inc. The clevises are connected to the load cell and hydraulic ram by steel rods that are internally cooled with running water. These rods are hollow with a concentric internal tube that carries the entering water to within 1/2 inch of the clevis; the water exits through the annular region around the tube.

The two shells of the furnace are made from sheet metal on the outside and transite on the inner faces. The space inside the shell is filled with bulk fiber insulation. The various joints are made with ceramic cement. Figure 2 shows half of the plug that fits in the bottom of the furnace around

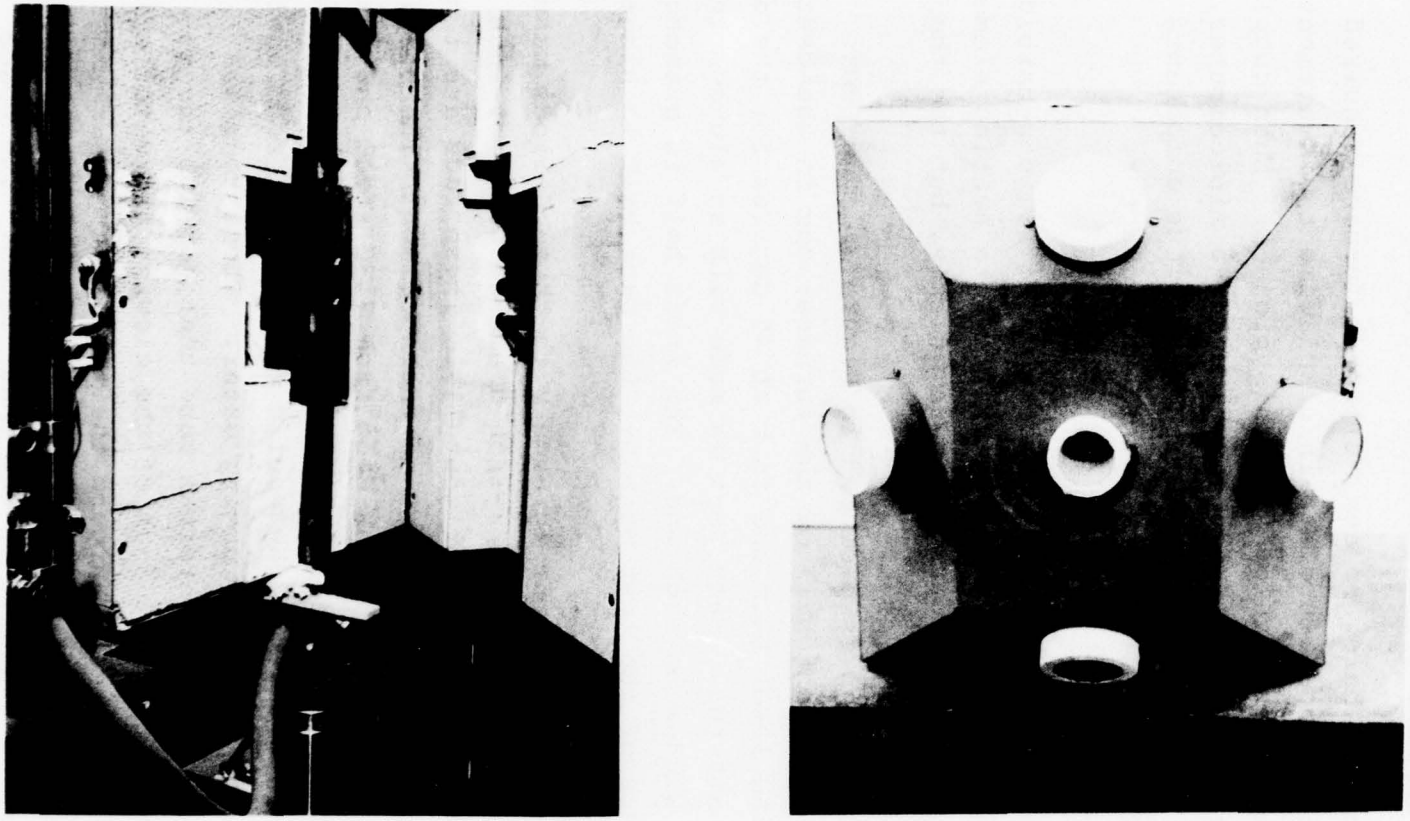

Figure 2. The Hotrod furnace

the lower rod. Fracture of a specimen would then knock the plug out without damaging the whole furnace.

Power is supplied to the Hotrods by a Phaser Model 646 power controller with distributed zero-crossing and current feedback. Typically, 15 amps at 70 volts is required to hold the furnace at 732°C. The control signal to the power controller comes from a Leeds and Northrop Micromax controller which receives its feedback signal from a chromel-alumel thermocouple mounted in the furnace. The furnace would reach 732°C in about 30 minutes.

Thermocouple measurements were made on the specimen along the line of the notch at positions 1.27 cm and 3.18 cm in front of the notch tip--front and back (nearest heating rods). At a nominal temperature of 732°C, the 3.18 cm position was approximately 22°C hotter than the 1.27 cm position, and the back side of the specimen was approximately 79°C hotter than the front. This gradient is excessively large, but could have been reduced by using 713C load links instead of water cooled rods that extended into the furnace. Also, transite shields to eliminate some of the radiation loss through the rather large ports would have been helpful. However, after examining a resistance wire furnace at AFML, it was decided to construct a new furnace to achieve a more uniform temperature in the specimen.

The resistance wire furnace is shown in Figure 3. The heating elements were purchased from Thermcraft, Inc., Winston-Salem, N.C. The wire coils are arranged on the front to permit entrance of the laser beam and exit of the fringe patterns. Firebrick was used as insulating material between the heating elements and the sheet metal case. The five quartz windows on the front of the furnace were purchased from Quartz Scientific, Inc., Fairport Harbor, Ohio. The specimen was loaded via 713C steel load links. The lower one (see Figure 3) was attached directly to the actuator ram of the test machine, and the upper one was water cooled to protect the load cell.

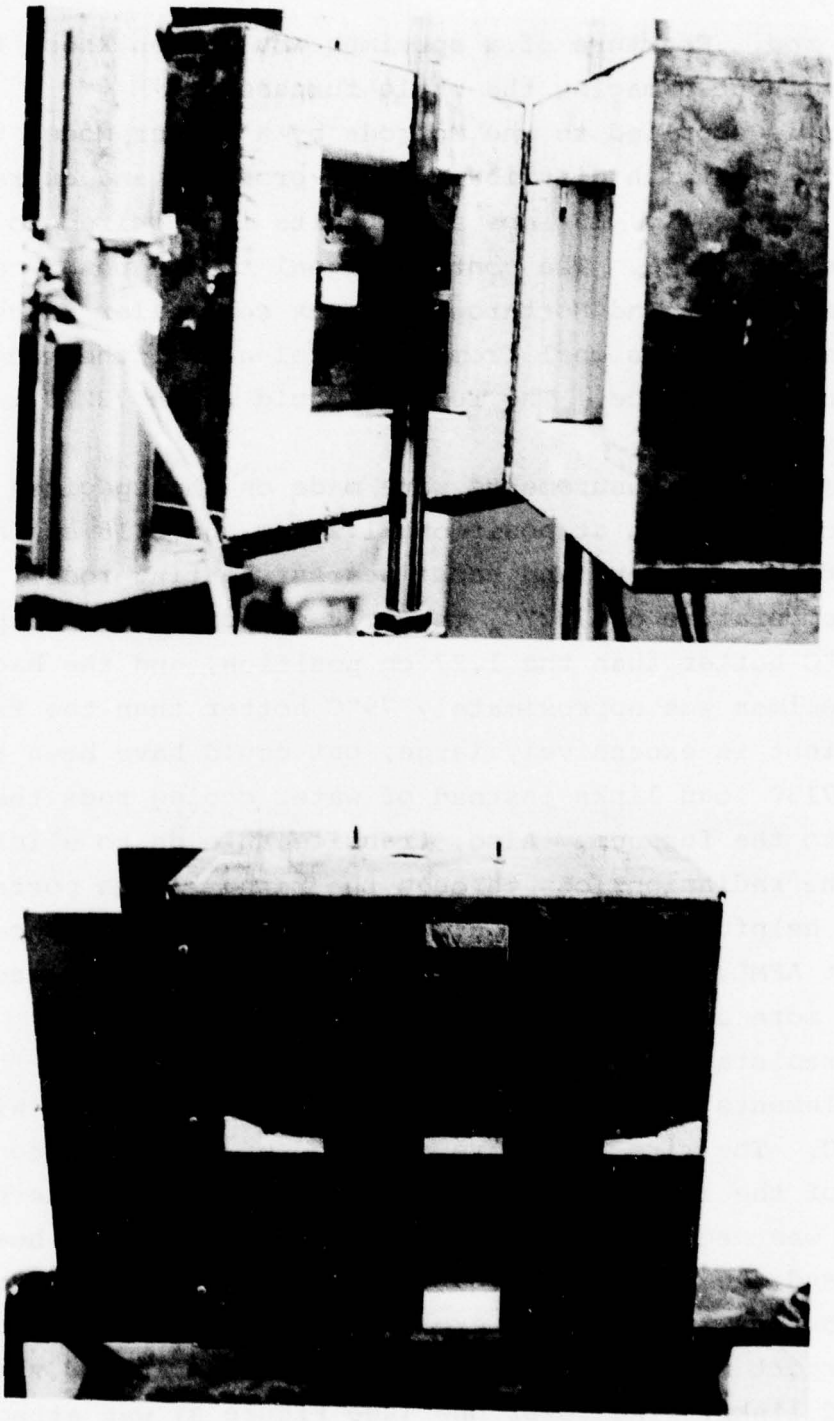

Figure 3. The resistance wire furnace

This furnace is controlled by the same controller as used for the Hotrod furnace. It takes approximately 50 minutes to reach 732°C. At a nominal temperature of 593°C, there was less than 8°C variation among seven thermocouples placed at various positions on the front and back of the specimen. The temperature in the central portion of the specimen where the crack grows is quite uniform - both along the crack and through the thickness.

A coil for an rf furnace has been constructed. This would be used with an available 5 KVA Lepel unit, and may be a better heat source than the resistance furnace. There is no need to provide quartz ports on an rf furnace.

2. Scanner Board

The aluminum scanner board holds the laser, the servocontrolled mirrors, and the photomultiplier tubes (PMTs). It is shown in Figure 4. A heavy tripod holds the board and allows vertical adjustment. The board is mounted on a machinist's rotary indexing table. This allows translation in two directions as well as rotation about the vertical axis. A convenient alignment system is required to position the laser beam so that it hits the indentations perpendicular to the specimen surface.

The key to the minicomputer-controlled ISDG is a servocontrolled scanning mirror. Model PD 100 mirrors from General Scanning Inc. of Watertown, MA were used. The mirror is 6.4 mm square and rotates as much as ± 15° about an axis. It is driven by a servoamplifier and contains a capacitance-based angular position sensor. Figure 5 shows a closeup of one mirror mounted on the scanner board. The mirror is attached to a mount with circular fins to provide cooling. This mount is attached to an adjusting mechanism which permits motion parallel and perpendicular to the mirror axis. The adjusting mechanism for the mirror on the other side of the board is shown in the upper part of Figure 5.

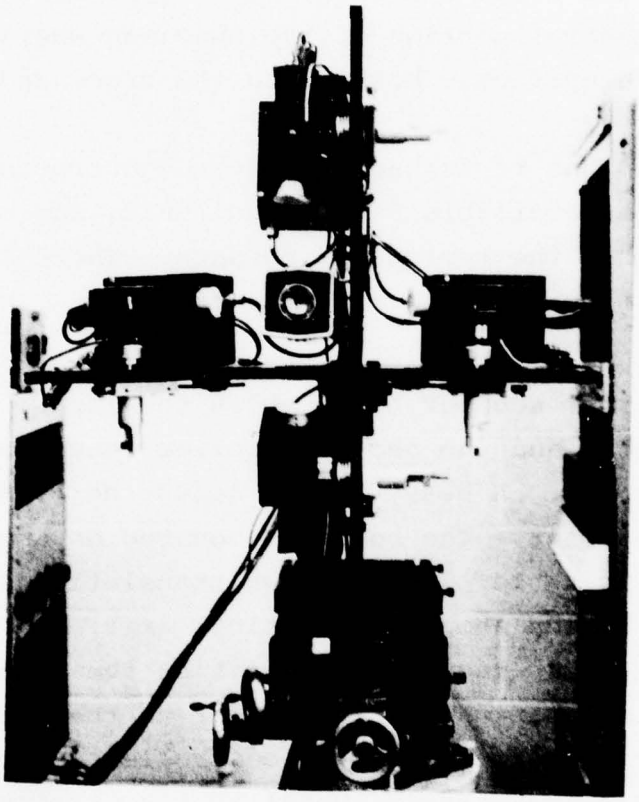

Figure 4. The scanner board with the laser, servocontrolled mirrors, and PMTs

Figure 5. Closeup of a scanning mirror, PMT, resistor network box, and adjusting mechanism

The fringe pattern is reflected by the mirror onto PMTs provided with a slit aperture. Narrow-band interference filters are mounted behind the slits. The PMTs are Amperex XP1117, and one is shown mounted in its light-tight case with mu metal shielding in Figure 5. The divider network for the PMT is also shown there. These tubes were operated at 1500 volts. The laser is a Spectra-Physics model 120 He-Ne laser with 5 mw output.

3. Mirror Drivers and PMT Amplifiers

The mirrors are driven by a servo circuit which takes its command signal from the minicomputer. Four A-600 printed circuit boards from General Scanning were assembled into a scanner control unit--pictured in Figure 6. Each channel has an input from the minicomputer, a drive signal output to the mirror, and a position signal input from the mirror to complete the feedback loop. The gain knob adjusts the amount of angular sweep of the mirrors. A screwdriver adjustable resistor on the board itself permits an angular adjustment of the static position of the mirror. Feedback gain and damping must also be adjusted for each channel.

The output from the PMTs is a negative voltage of less than 2 volts that is proportional to fringe pattern intensity. Small operational amplifier circuits were built to invert the signal and amplify it to meet the 0-10 volt input requirements of the A/D converters. These are mounted on the same chassis shown in Figure 6. The two knobs for each channel adjust the gain and offset of the PMT signal. A low-pass filter (~10 Hz) is included in each channel to eliminate electrical noise. The power supply for the PMTs is also shown in Figure 6.

4. Other Equipment

The electrohydraulic cyclic testing machine was manufactured by MTS Systems and has a 22,000 lb. (98,000 Newton) capacity and a 6 gpm pump. It is controlled by a Model 410 digital function generator and a Model 406 controller. The system is limited to cycling at 15 Hz because of a resonance point of the floor at 22Hz. This system was bought in conjunction with

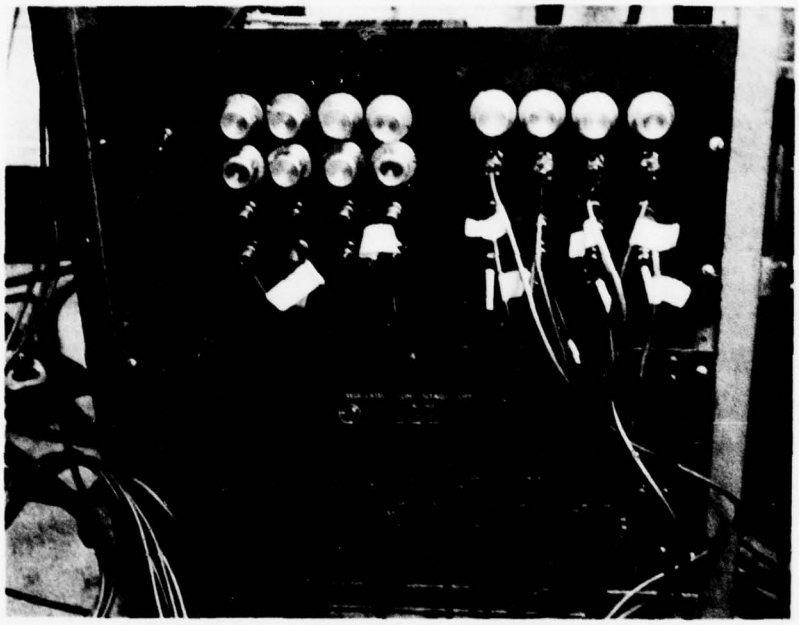

Figure 6. The 4-channel mirror controller and PMT signal amplifier

AFOSR Grant 75-2817 and has performed as expected.

The minicomputer system consists of a Computer Automation Inc. Model LSI-2/10G minicomputer with 8K memory, a Datel Model 256 A/D and D/A converters, and a teletype. The fringe patterns were monitored on an oscilloscope, and the plots taken on a two-pen X-Y plotter. A picture of the total setup is shown in Figure 7.

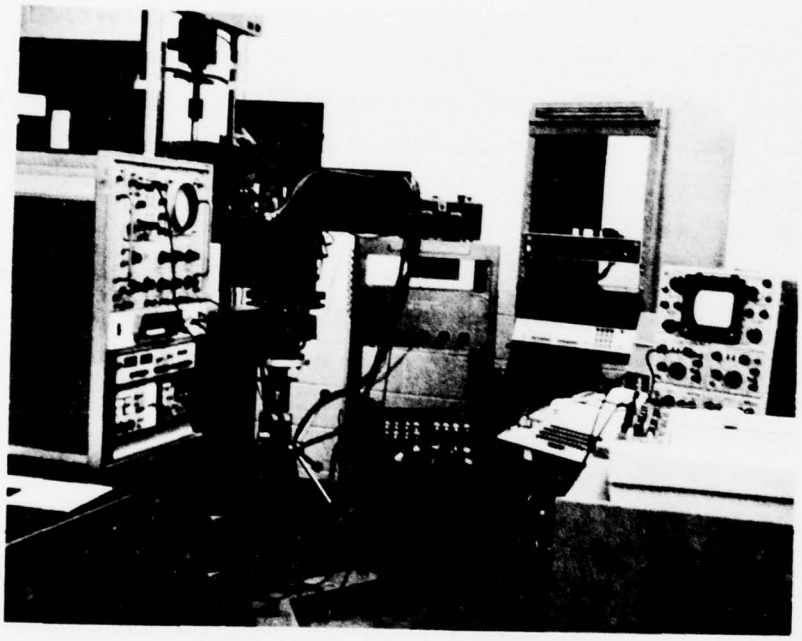

Figure 7 View of the entire setup

SECTION III
OXIDATION-RESISTANT COATINGS

It would be an ideal situation if the indentations in the metal test specimen remained reflective at high temperatures for long times. The superalloys under study are resistant to oxidation in that their surface smoothness does not deteriorate drastically upon exposure to high temperature, but the requirement that the indentations preserve their shape and reflectivity is a very stringent one. It was hoped, nevertheless, that indentations in bare metal specimens would last for a few hours at test temperature. This turned out not to be the case (except for specially-oxidized IN-100), and this section describes the various processing and coating procedures that were tried in a search for a suitable reflective coating. An acceptable coating was found for both the Incolloy 901 and the IN-100. Various references [7-20] were consulted to select the best coating procedures.

1. Test Procedure

The reflectivity of the indentations was measured by illuminating a test specimen in the large Hotrod furnace with a 20 milliwatt laser and scanning across the fringe pattern with a slit-covered photomultiplier tube mounted on a translation stage. The stage was connected to a DCDT displacement transducer, and the resulting plot of fringe intensity versus angle was recorded on an X-Y plotter. The photomultiplier tube (Amperex type XP 1117) was powered at 1500 volts and a narrow-band interference filter was placed in front of the tube. Thus 100mv output corresponds to approximately 10^{-9} watts of radiation through the filter into the tube.

A Lindberg laboratory furnace was used for "before-and-after" tests of surfaces and coatings. The volume of this resistance-heated furnace is approximately 11,000 cubic centimeters. Indentations were placed on a specimen and the specimen subjected to temperature for a specified time. The indentations were then examined under a microscope and by illuminating them with a laser. This was a qualitative means of evaluating coatings, but was very efficient for a "first-look".

A small Lepel furnace was also used to process and test specimens. It has a power output of 2.0 KVA, and the coil used was 2.5 cm in diameter by 5 cm long.

2. Bare Metal--Incolloy 901 and IN-100

Figure 8 is a print of a fringe pattern scan of IN-100 in the Hotrod furnace at four temperatures. The scan at room temperature is typical of the quality of the fringe patterns produced by indentations that are approximately 25 microns square and 200 microns apart. The "noise" on the signal comes from manual turning of the translation stage; the electrical signal is excellent. The effect of temperature in Figure 8 is also typical in that as the indentations oxidize the fringe pattern gradually becomes dimmer. Eventually the indentations become so dark that one records only randomly scattered laser light from the specimen.

The relative intensity (normalized to the room temperature pattern) for two specimens of IN-100 and one of Incolloy 901 is plotted as a function of temperature in Figure 9. It takes the Hotrod furnace approximately 30 minutes to reach 650°C.

Photomicrographs of indentations on both metals after heating in the Hotrod furnace are shown in Figure 10. The Incolloy 901 has merely darkened, but the IN-100 has developed an oxide with grains roughly 1/10 the size of the indentation sides.

It is clear from these results that simply taking a polished specimen with indentations and heating it to a test temperature of 650°C or 732°C is not going to work. It appears that 430°C is probably the upper limit for testing bare metals of this type.

Specimens of Incolloy 901 were treated with a stream of argon flowing over them while in the furnace; this produced no improvement. A small specimen sealed in a glass tube that had been evacuated with a laboratory vacuum pump was tested, but the indentations still oxidized.

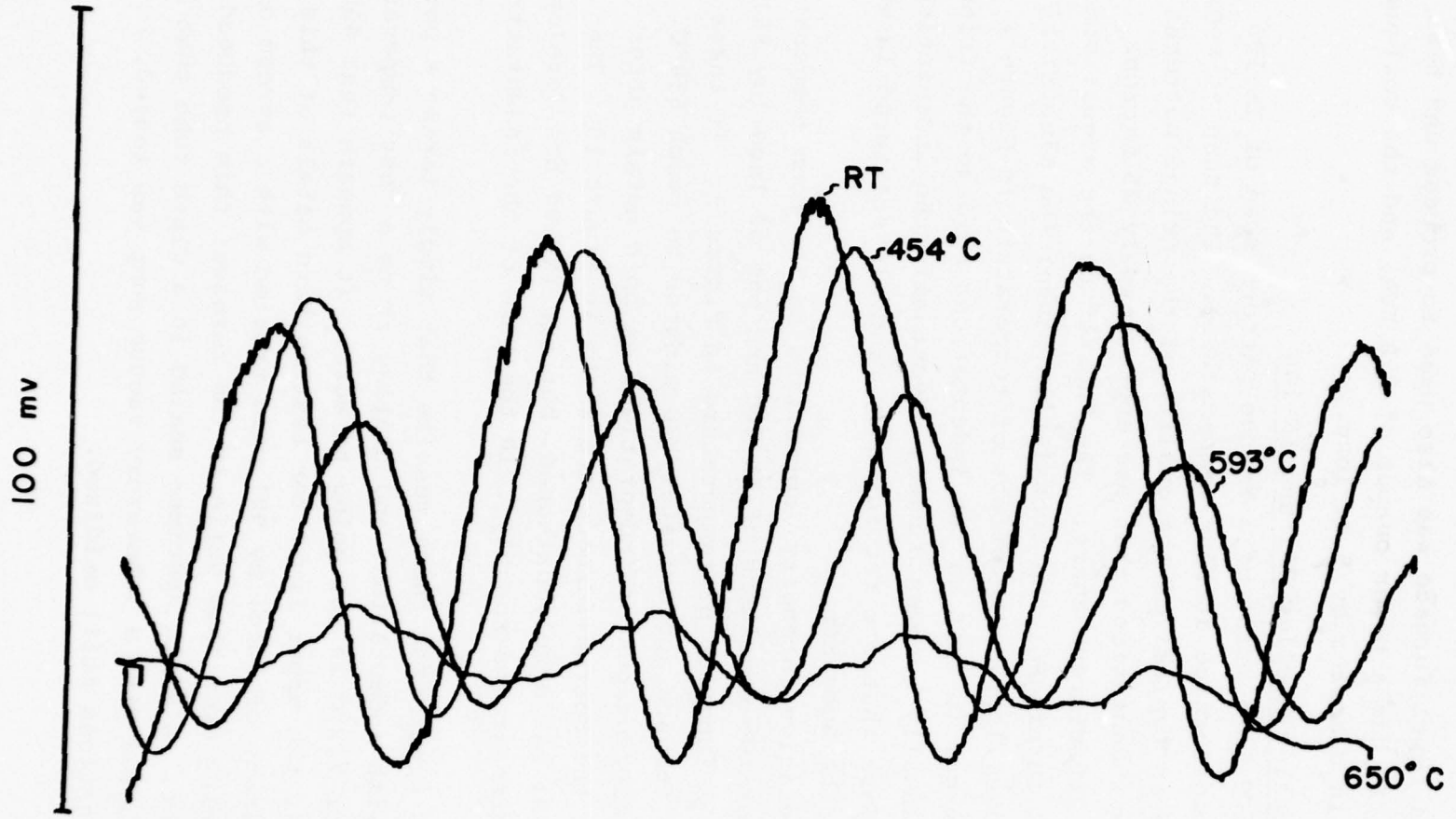

Figure 8 - Fringe pattern intensities at different temperatures for IN-100.

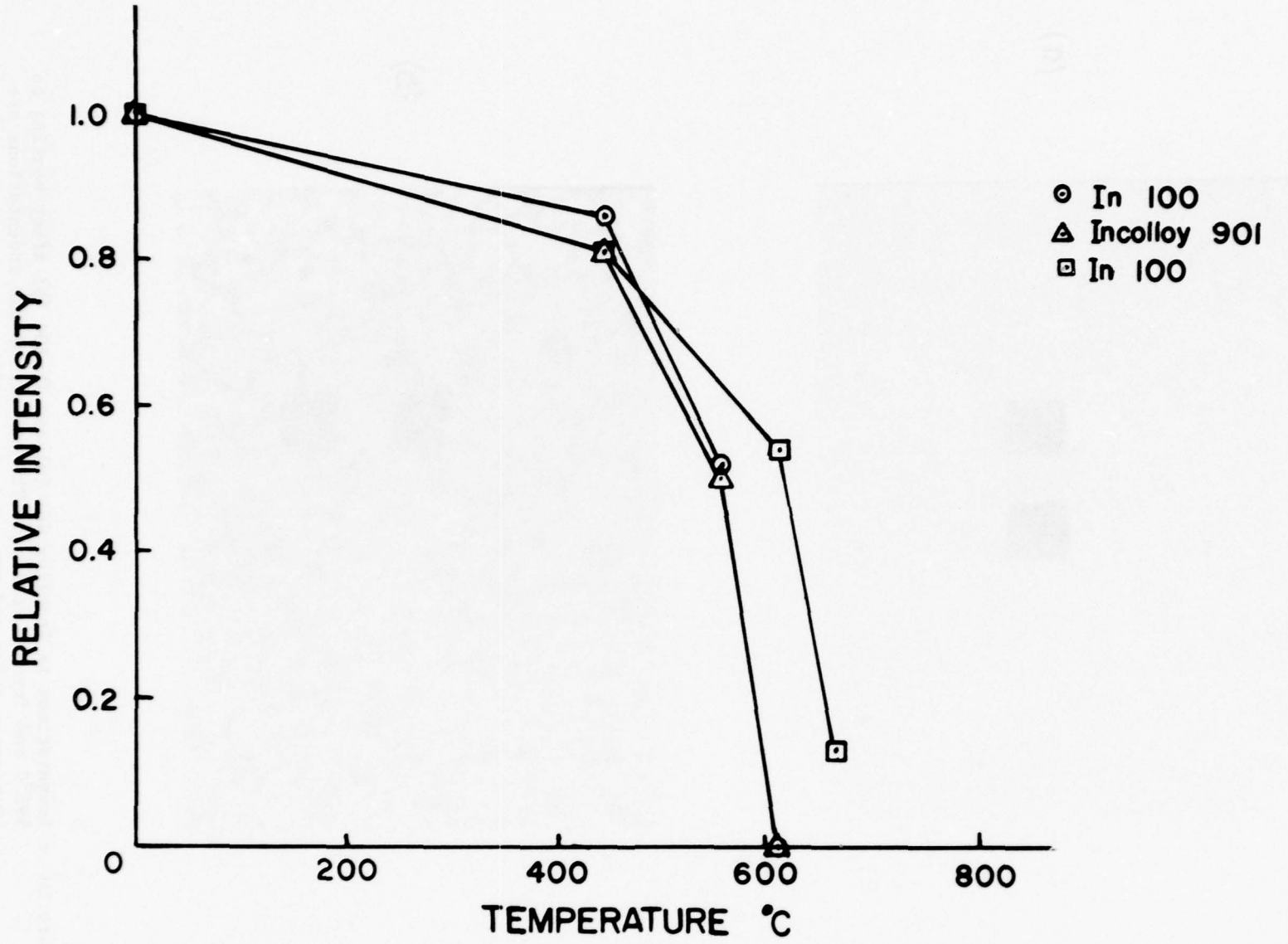

Figure 9 - Normalized fringe intensity versus temperature.

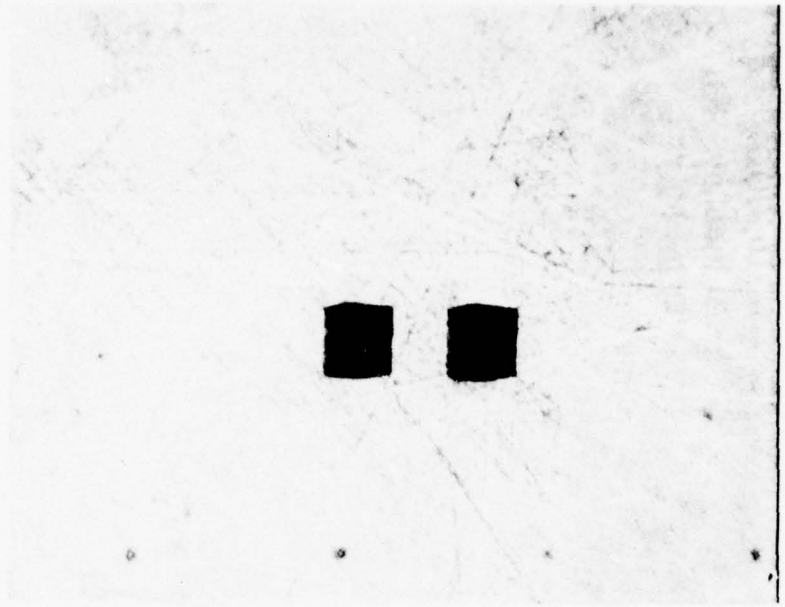

(a)

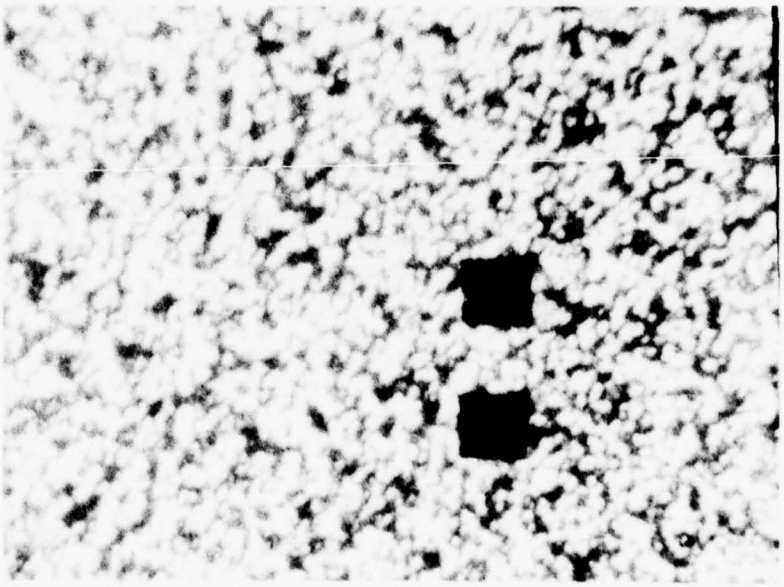

(b)

Figure 10 - Indentations in Incolloy 901 (a) and IN-100 (b) after heating to 593°C and furnace cooling. The centers of the indentations are 50 microns apart and the exposures are the same.

3. Platinum-Rhodium Tabs on Incolloy 901

One way to measure displacements or strains at high temperatures is to glue small tabs of nonoxidizing material such as a platinum alloy onto the specimen. Small tabs (approximately 2mm square) of Pt-13% Rh were glued onto an Incolloy specimen with ceramic cement (Aremco Bond 503, Aremco Products, Inc., Ossining, N.Y.). For the purposes of an oxidation test, both indentations were put in one tab. In practice, the tabs would be smaller and one indentation applied to each tab.

After exposure to 732°C for one hour, the fringe intensity had decreased by 20 percent. Examination of the indentations and specimen surface with a microscope showed that a thin oxide layer with very large grains (~200 microns in diameter) had formed.

This is a viable, but difficult, technique. It may turn out that this is the only way to make measurements at higher temperatures [4], but indentations impressed directly in to the specimen surface are much to be preferred.

4. Nickel Plating on Incolloy 901

Vapor-deposited coatings appeared promising for oxidation protection, and nickel was the first material tried. All vapor-plating was done in a Consolidated Vacuum Corporation model LC1-14B unit. The thickness of the nickel coatings was estimated to be less than 0.1 micron.

It was learned that if the Incolloy specimens were pre-oxidized at 538°C for one hour in the Lindberg furnace then the nickel coatings were much more effective. This pre-oxidation is in effect a first protective coating. It leaves the specimen quite dark and the fringe pattern dim, but coating restores their brightness. This step could probably be skipped if a thick enough nickel coating were applied, but it is difficult to make a very thick vapor coating in one step and multiple-step coatings did not adhere to each other very well.

Figure 11 is a plot of the relative intensity as the pre-oxidized, then coated, specimen was heated. A flow of argon was directed over the specimen surface during this test. Note that the specimen regained its brightness at 650°C, but quickly lost it at higher temperature. This increase in reflectivity is also shown in Figure 12 for a specimen held at 650°C. Apparently, the forming of the oxide or perhaps some alloying with the superalloy material cause a momentary increase in surface brightness. The surface and indentations look quite smooth and bright after the exposure at 650°C. Upon heating the specimen held at 650°C to 732°C, the fringes disappeared completely.

This coating would work for Incolloy 901 at 650°C. Based on later experience, the argon stream is not necessary.

5. Copper, Chromium, Gold, and Platinum Plating on Incolloy 901

Various vapor-plated coating combinations of these materials were tried. The copper was used only as an undercoat for the other three materials, and chromium was used as both an undercoat and a final coat. Another parameter in this series was whether or not the surface had been pre-oxidized; in every case a pre-oxidized surface was better.

The best of these coatings was simply chromium over the pre-oxidized surface. The fringes were quite bright and the indentations looked smooth after one hour at 732°C in the Lindberg furnace. Almost as good was a platinum over copper coating.

6. Chrome Electroplated Incolloy 901

The success of chromium as a protective coating led to an evaluation of electroplating as a coating method. It was expected that electroplating would give a tighter bond of the coating to the specimen and improve the protection, particularly for indentations applied after specimen exposure to temperature.

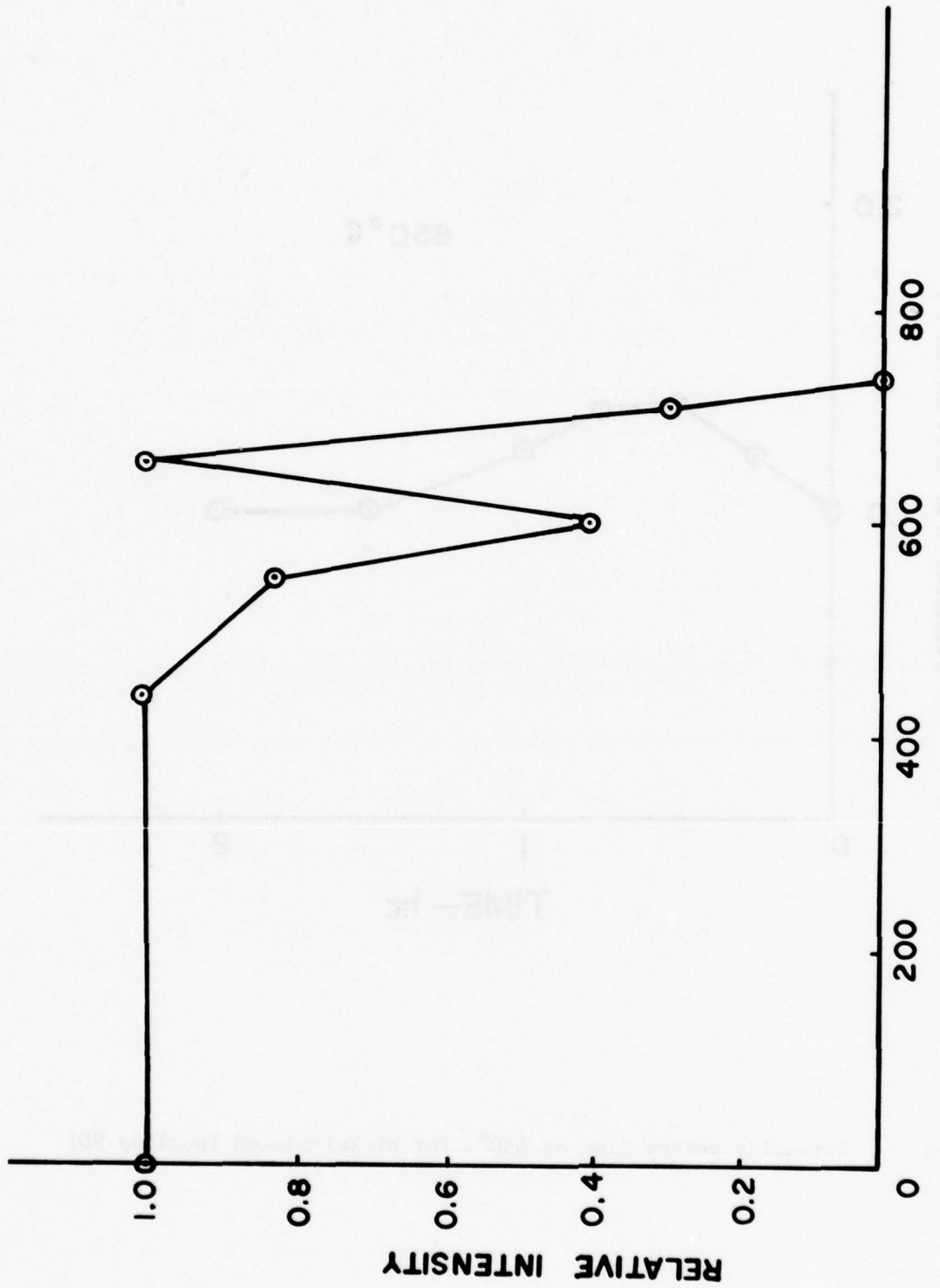

Figure 11 - Intensity versus temperature plot for nickel-plated Incolloy 901.

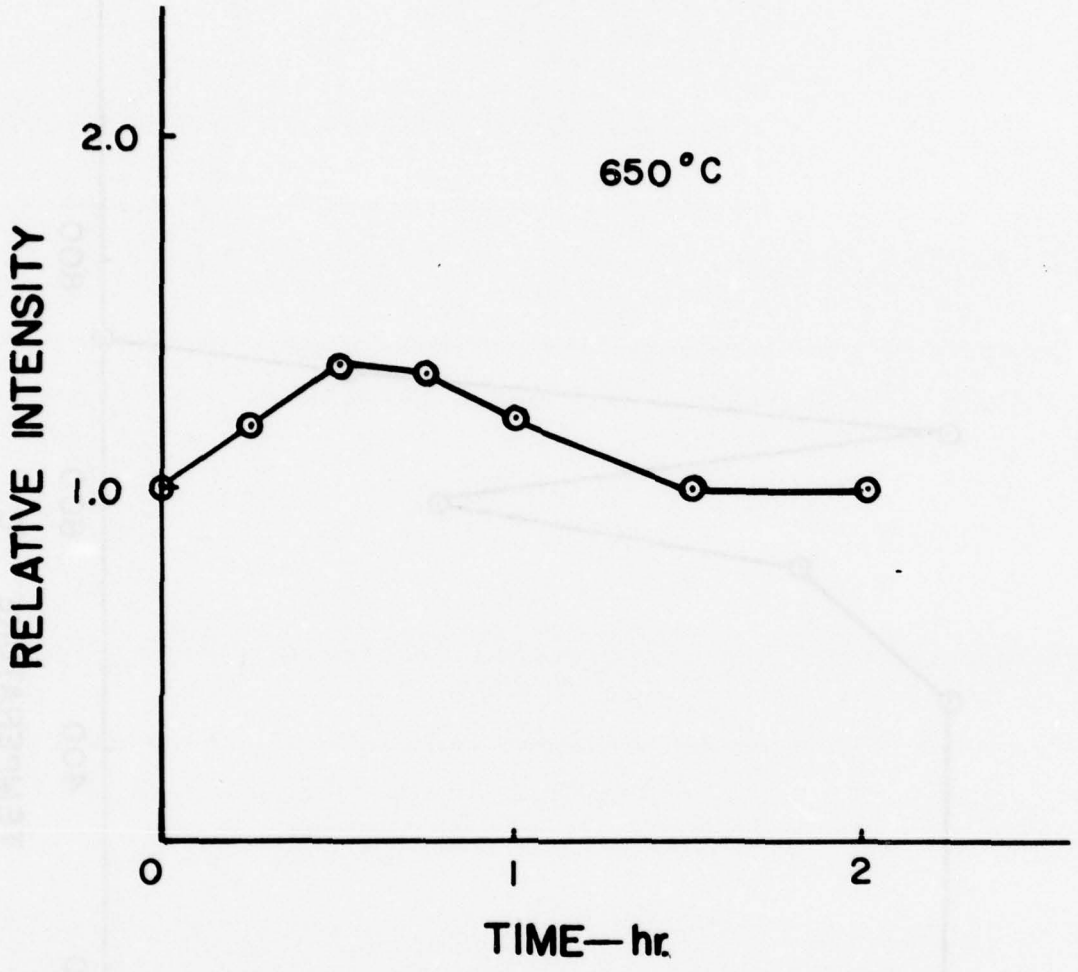

Figure 12 Intensity versus time at 650°C for nickel-plated Incolloy 901.

A specimen of Incolloy 901 was electroplated by a local commercial plater. The coating was thick (~25 microns) but bright--a thicker coating would have become a matte gray color. Indentations placed in the specimen before coating were still sharp and the fringe patterns were excellent after coating. Indentations were also applied after coating. After 732°C for one hour in the Lindberg furnace, the fringe patterns were still quite good and the specimen surface was bright. Another 16 hours at 650°C did not change the indentations. The indentations applied after coating remained slightly brighter.

A laboratory chrome-plating operation was set up using a commercial plating solution and commercial anodes. This was operated at 49°C and 4-6 amps. A plating current of 1 amp/in^2 was aimed for and times were 10 minutes or less. The coatings were calculated to be from 0.5 -1 micron thick. Reference 7 was used as a basis for these calculations.

None of these laboratory-applied coatings were as good as the commercially applied coating. In fact, they did not last to 650°C. The solution is the same, the temperature is the same, and the times are the same as the commercial system, only the size of the bath and the applied voltage are different.

Note that none of these Incolloy specimens were pre-oxidized. Electroplating did not work well over the oxide layer. The specimens were simply polished and then cleaned and neutralized with M-Prep Conditioner A and M-Prep Neutralizer 5 (Micro Measurements, Inc., Romulus, Michigan).

7. Chrome Electroplated, Platinum Vapor-Plated Incolloy 901

The final coating arrangement and the one that is quite satisfactory for Incolloy is a vapor-plated layer of platinum ~0.1 micron thick over an electroplated layer of chromium ~ 1 micron thick. Its performance at temperature is shown for three specimens in Figure 13.

In each case, the reflectivity of the indents drops at 650°C, usually a considerable amount. After being held at 650°C for an hour or so, two of the specimens maintained usable fringe

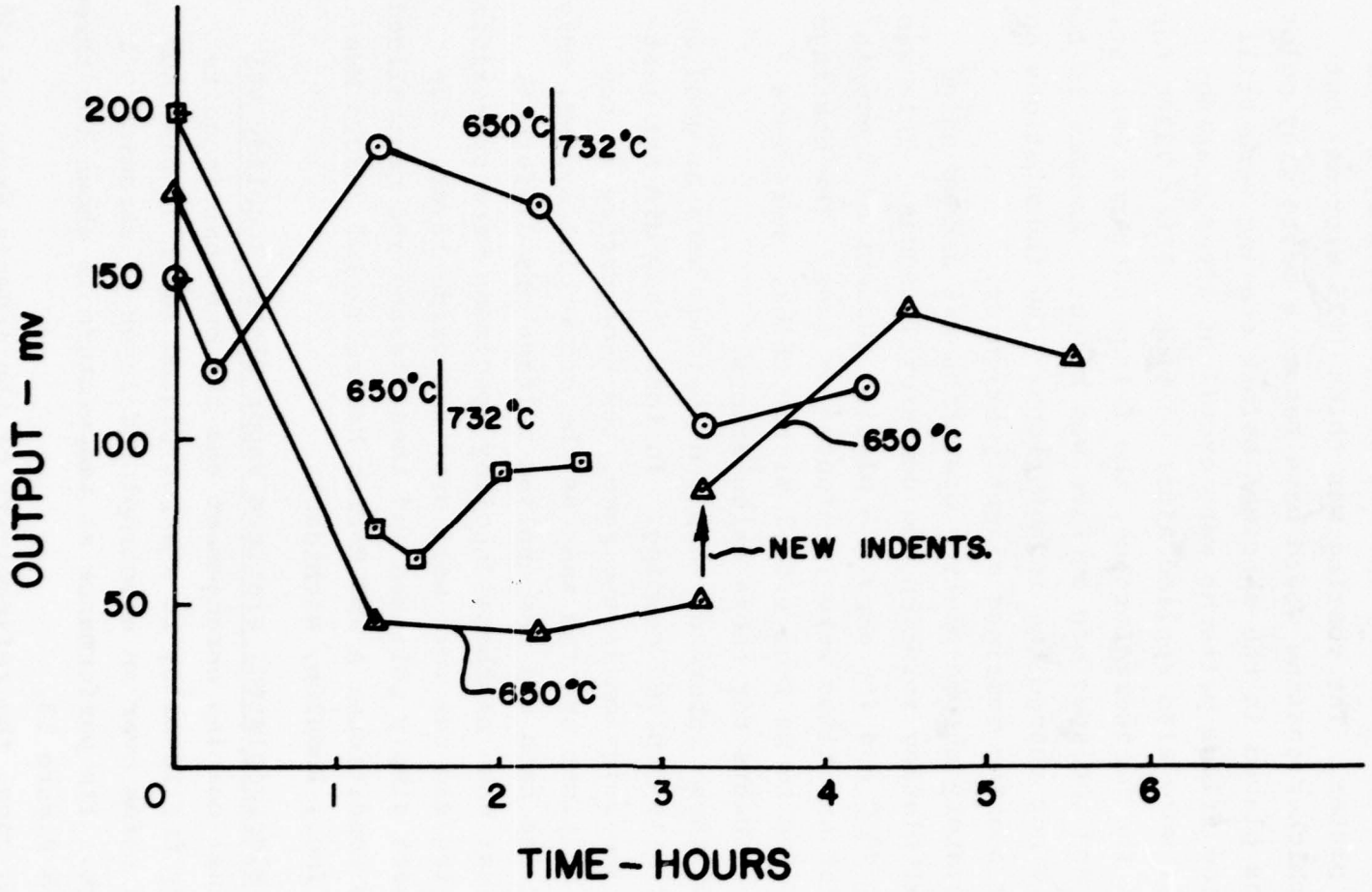

Figure 13 - Intensity versus time at different temperatures for three specimens of platinum/chromium plated Incolloy 901.

patterns at 732°C for over an hour. One specimen was cooled down after slightly more than three hours at 650°C and new indents applied to the surface. The indents held up very well when the specimen was reheated. This is excellent, because one can then put new indents in a specimen as the crack grows at high temperature without having to re-plate the specimen.

A photomicrograph of the last set of indents in this latter specimen is shown in Figure 14. It is seen that the surface is still bright and the indents still sharp and smooth. The fringe pattern produced by these indents is excellent.

8. IN-100 Oxidized with RF Heater

AFML supplied a specimen of IN-100 that had been treated to 650°C in an rf heater for two half-hour intervals and then held at that temperature for 5 1/2 hours. The indentations that had been put in the polished specimen before heating were still sharp and smooth and the fringe patterns were well-defined and reasonably bright. This is contrary to the earlier results in the Hotrod furnace at M.S.U. This specimen was tested with the results shown in Figure 15. After a total of 24 hours at 650°C plus a short time at the higher temperature, the indents and fringes were still usable.

This test was duplicated with a specimen prepared at M.S.U. by oxidizing it at 650°C for 1 hour in the rf heater. It was tested, with the results shown in Figure 16. A photomicrograph of the indentations after the preoxidation is shown in Figure 17. It is not apparent from that picture, but the oxide layer is very much smoother than that shown in Figure 10 for a specimen oxidized in the Hotrod furnace.

The hypothesis for this strange behavior of the bare IN-100 is that in the open coil of the rf furnace plenty of oxygen is available and a finer oxide layer is produced quickly which then protects the surface. The heating time to temperature in both AFML and M.S.U. furnaces is approximately the same ($\sim$1/2 hour). A specimen was prepared with 0_2 impinging on the specimen during heating in the rf furnace; no improvement was noted. Another

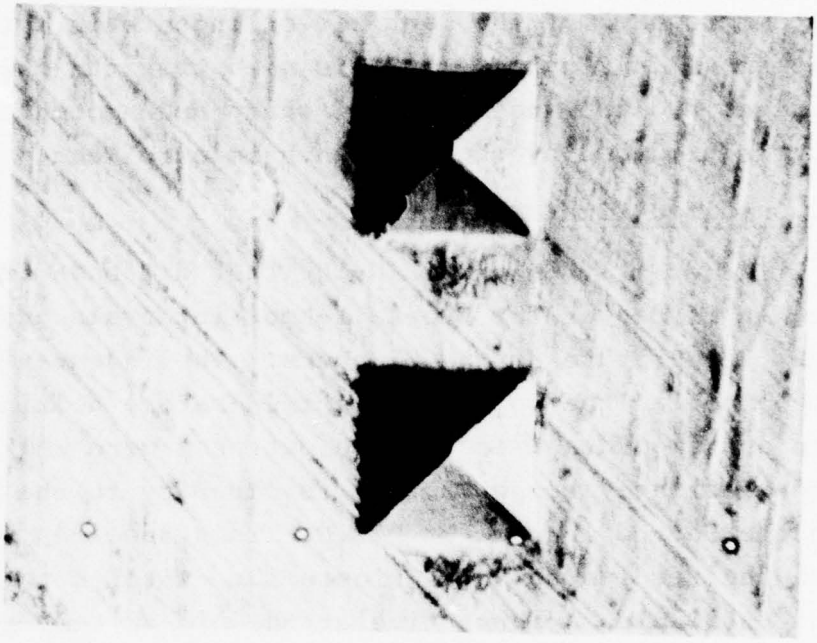

Figure 14 Indentations in platinum/chromium plated Incolloy 901 after exposure at 650°C. The centers of the indents are 50 microns apart.

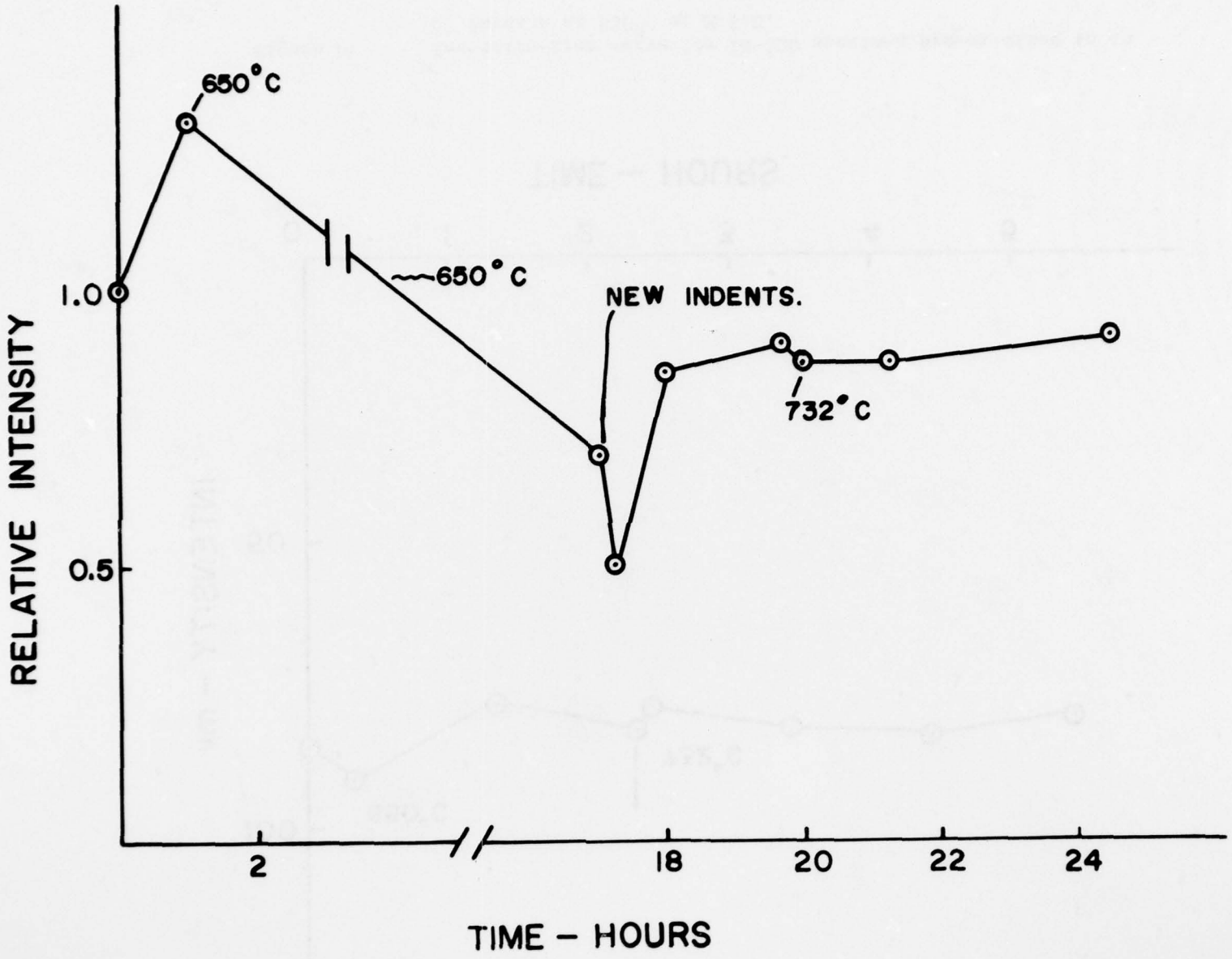

Figure 15 Intensity-time curve for IN-100 specimen pre-oxidized in an rf furnace at 650°C at AFML.

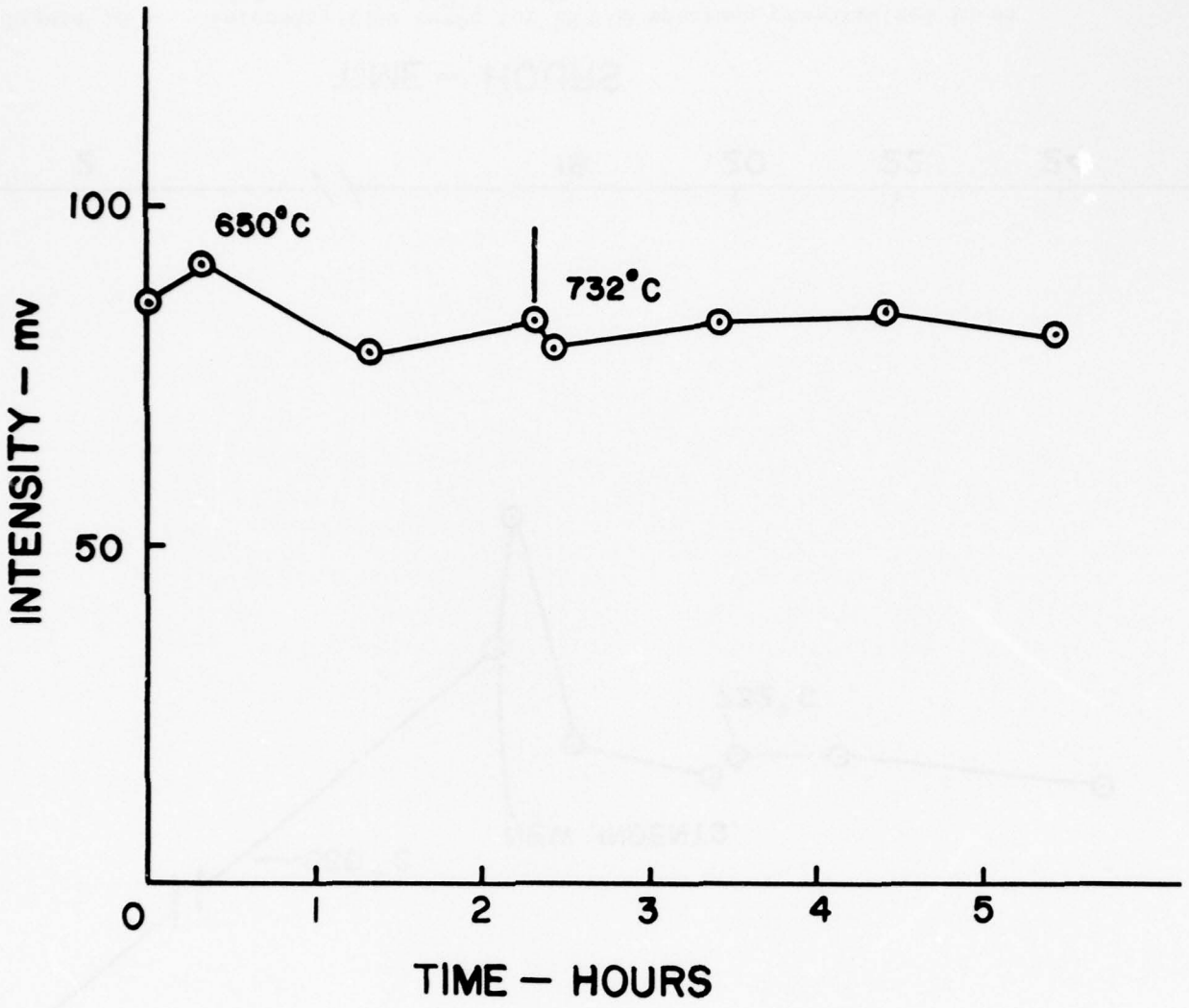

Figure 16 Intensity-time curve for IN-100 specimen pre-oxidized in an rf furnace at 650°C at M.S.U.

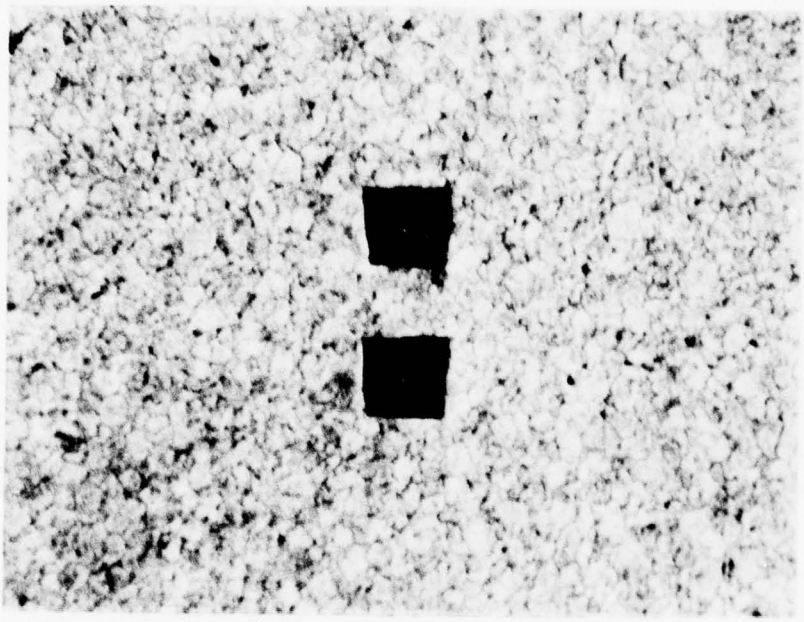

Figure 17 - Indentations in IN-100 after pre-oxidizing in an rf furnace. The centers of the indents are 50 microns apart.

specimen was heated in the Hotrod furnace while 0_2 was incident on it, and the surface, indentation, and fringe patterns looked very much like they did for specimens heated in the rf furnace.

It should be noted that fringe patterns from IN-100 specimens pre-oxidized in this manner are satisfactory. It was felt that brighter fringe patterns could be obtained if a coating was applied in conjunction with the pre-oxidized coating.

9. Chrome-Electroplated IN-100

IN-100 specimens were electroplated at M.S.U. in the same manner as the Incolloy ones, with the same negative results.

When a chrome-plated specimen was then oxidized in the rf furnace, the results under test were satisfactory as shown in Figure 18. After the specimen was tested at 732°C, it was coated with platinum and retested as shown in Figure 18. Again, the results are good.

10. Chromium, Oxide, and Platinum Coatings on IN-100

A logical extension was to pre-oxidize the specimen after a platinum coating over the chrome plating. This produced good results as shown in Figure 19.

A better arrangement is to pre-oxidize the chrome-plated specimen before platinum plating. This gives better results; see Figure 20. A set of indents applied after the first test also gave good results as shown in Figure 20. A photomicrograph of the original indentations is given in Figure 21. The good quality of the indentations is evident. Figure 22 reproduces plots of the intensity from the second set of indents taken at 732°C.

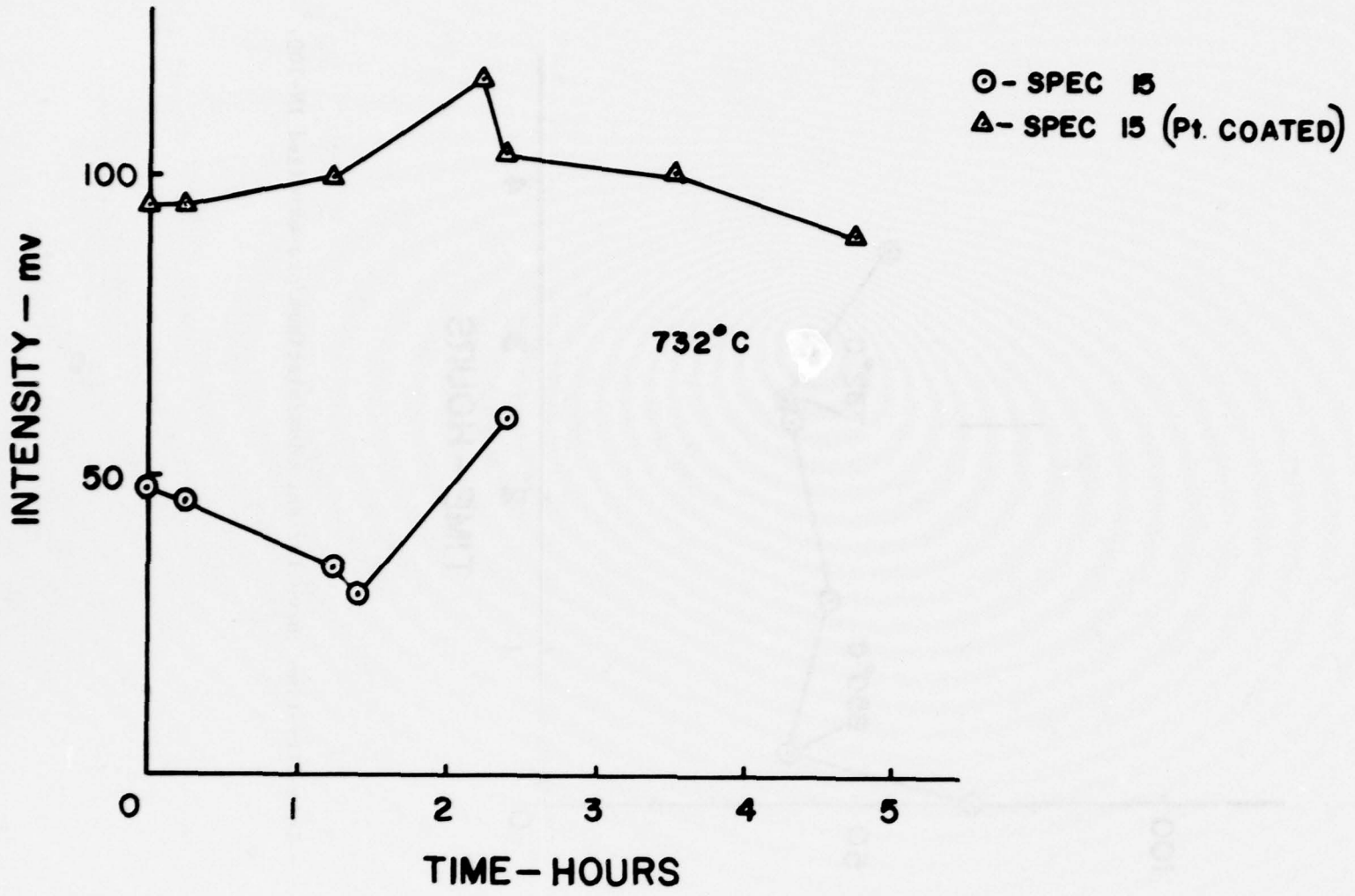

Figure 18 - Intensity-time curves at 732°C for a chromium-plated and pre-oxidized IN-100 specimen and for same specimen with additional platinum coating.

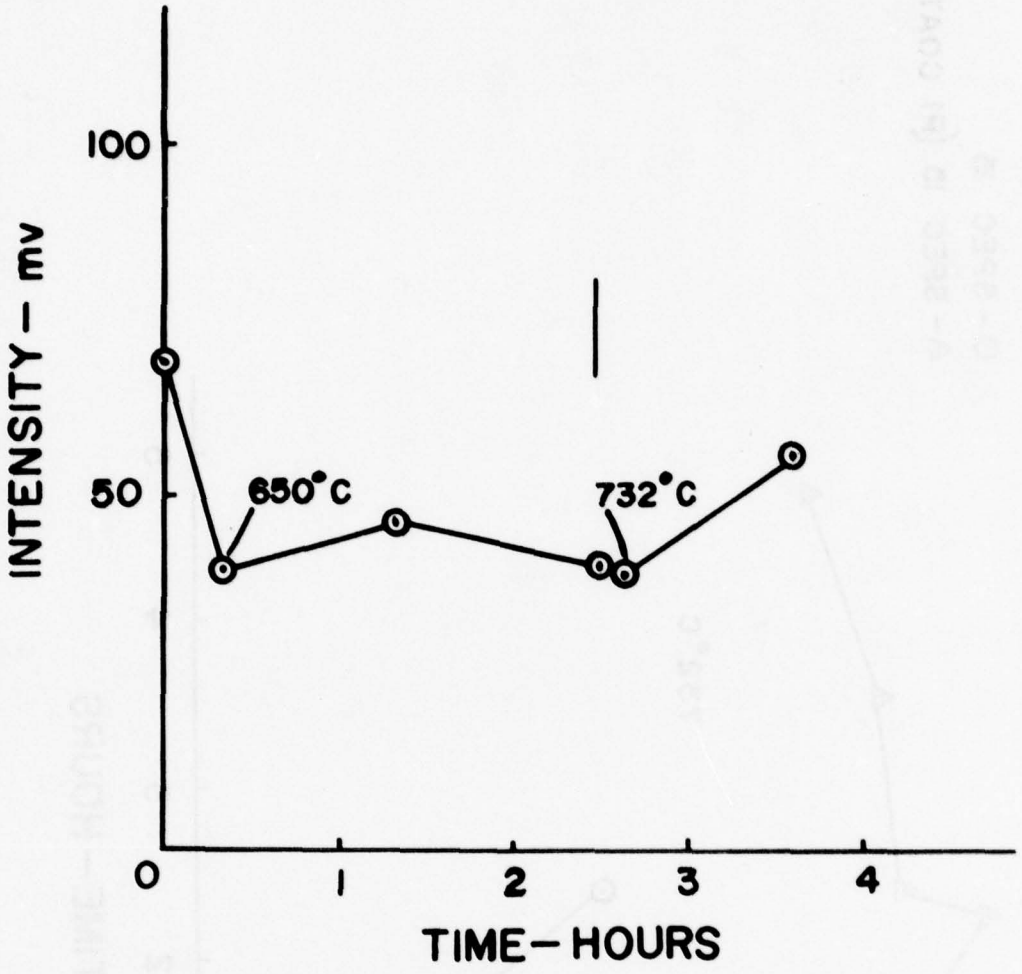

Figure 19 - Intensity-time curve for chromium/platinum/pre-oxidized IN-100.

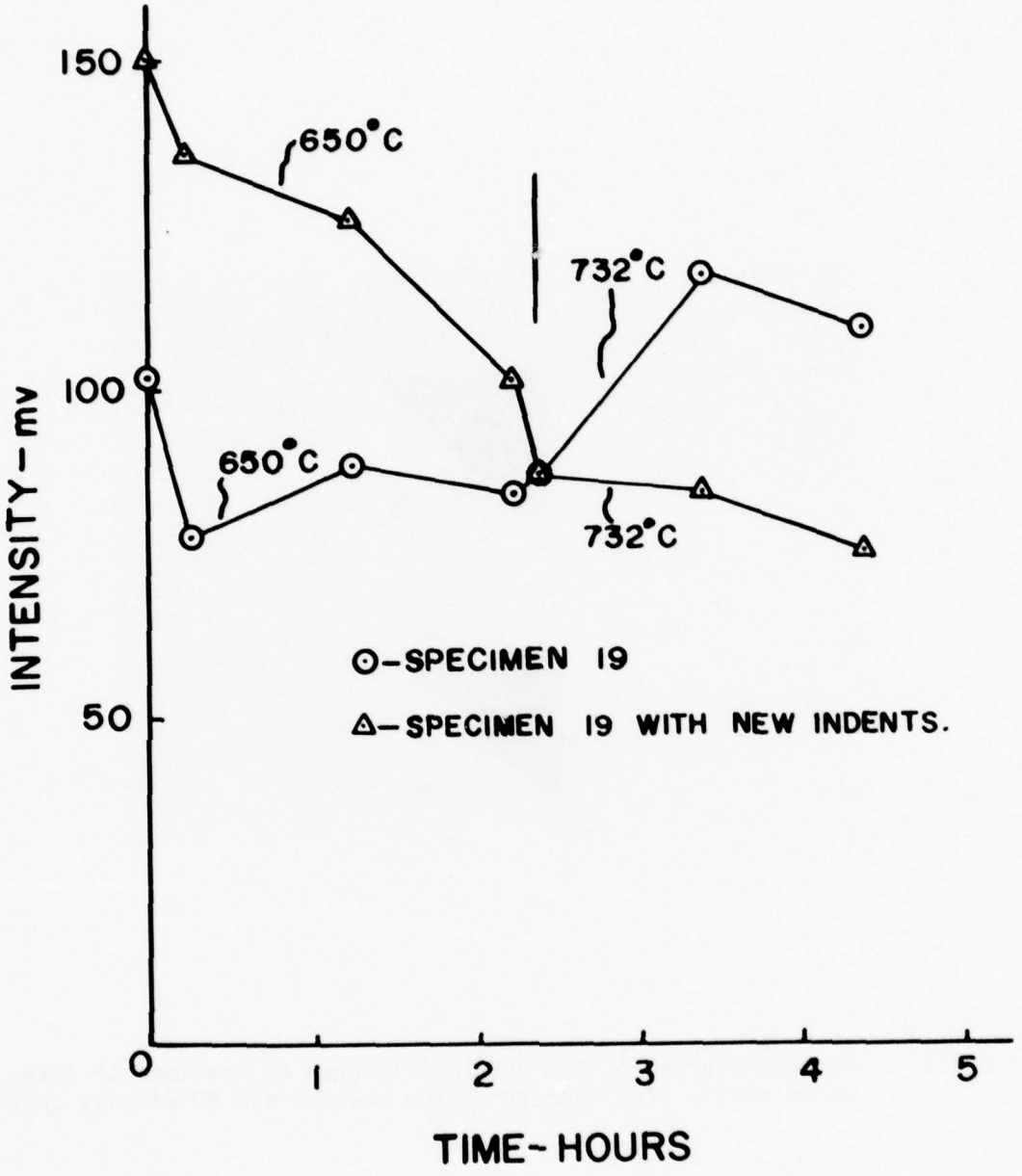

Figure 20 - Intensity-time curve for chromium/pre-oxidized/platinum IN-100.

Figure 21 - Photomicrograph of the original indents of specimen 19 (Fig. 20) after tests. The centers of the indents are 50 microns apart.

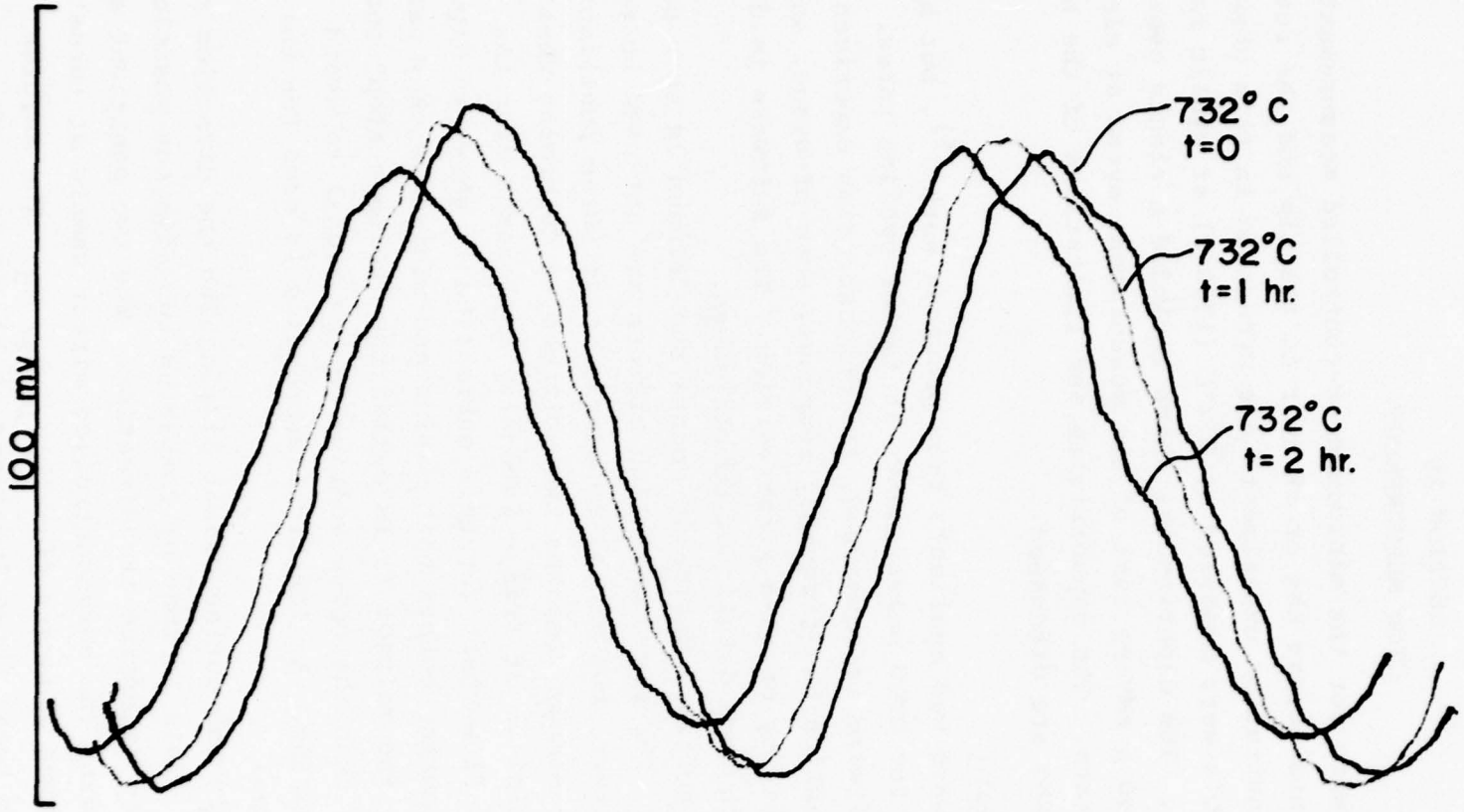

Figure 22 - Intensity traces for the second set of indents of specimen 19 (Fig. 20)

SECTION IV
CTOD MEASUREMENT

The software for the minicomputer-controlled measurement of displacements across the crack near to the tip and the results of eight demonstration experiments are presented in this chapter. Real-time CTOD's were measured at 732°C (1350°F) at cyclic rates of up to 1 Hz. The experiments, which included a single overload cycle, provided a severe test of the measurement sytem at elevated temperature. The capabilities and limitations of the high temperature ISDG are discussed.

1. CTOD Software

The software was available from previous work [5], but had not been used for CTOD measurements at faster cycling rates. As far as the software is concerned, the demonstration experiments served to establish the frequency response, ease-of-usage, and general reliability of this first version. The software is described here in some detail for completeness.

The CTOD software basically counts the fringes as they pass the PMT slits. The servocontrolled mirrors are not used to scan the fringe pattern, but merely to sample it at three positions. One subroutine simply compares two voltages to determine whether a maximum or minimum of fringe intensity has passed over the PMT slit. The flow-chart for this subroutine is shown in Figure 23. The subroutine counts both maxima and minima as they pass the PMT slit. The voltage Δv is called the "voltage step" and is set greater than the noise voltage on the signal to avoid spurious triggering. An identical subroutine is used for the second PMT signal.

The max/min subroutine cannot distinguish the direction of fringe motion. This is done by comparing two adjacent positions on the fringe to determine its direction. The two positions are obtained by having the servocontrolled mirror sample at three locations and thus generate signals V_1, V_2, V_3. The angular spacing between these three locations is adjustable. The signals V_i and V_2 establish position A; V_2 and V_3 position B. The order in which maximums (or minimums) are seen at these two positions

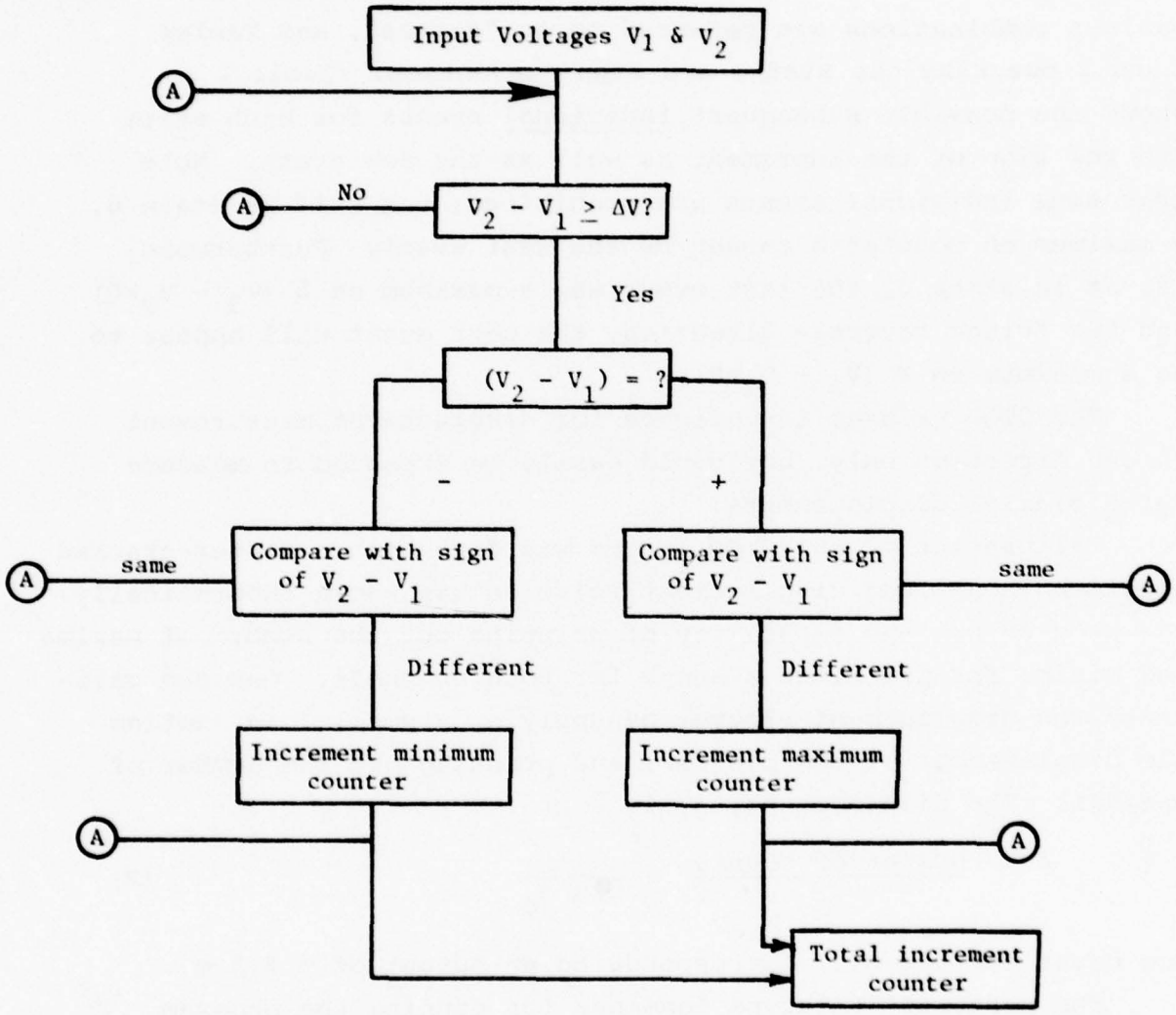

Figure 23 Flowchart of maximum/minimum counting subroutine.

determines the fringe direction. For example, a max at A followed by a max at B indicates a fringe movement opposite in direction to one showing a max at B followed by a max at A. The situation is more complicated than this; there are four combinations of max/min that indicate the same direction as well as some combinations that are not allowed after an existing combination. These various combinations are referred to as "states", and Tables 1 and 2 describe the states and sign convention. Table 2 shows the possible subsequent individual events for each state and the sign of the increment as well as the new state. Note that some individual events are prohibited; e.g., if in state 0, a maximum on counter A cannot be the next event. Furthermore, if, as in state 0, the last event was a maximum on B ($V_3 - V_2 > 0$) and the fringe reverses direction, the next event will appear to be a minimum on B ($V_3 - V_2 > 0$).

The CTOD program is designed for displacement measurement in one direction only, but could easily be expanded to measure large biaxial displacements.

Calibration of the CTOD system was done with a center-cracked specimen whose load displacement relation was known theoretically.[5] The program has the capability of printing out the number of maxima and minima for positions A and B for both channels. One can calibrate the displacement plotter by applying a small load, noting the displacement of the plotter, and printing out the number of max/min. The displacement, δ, is

$$\delta = \frac{\text{Number of counts}}{8} \quad \frac{\lambda}{\sin \alpha_o} \qquad (2)$$

One count (or one bit) corresponds to an output of $\sim$ 2.5 mv.

The pertinent teletype commands for running the program are shown below:

```
INITIALIZE: FULL,PARTIAL,NONE? (F,P,N)>F
SCAN SEPARATION=1000
VOLTAGE STEP=100
TRIAL RUN? (Y,N)>N
TYPE G TO GO>G
```

Table 1 - SCHEMATIC OF VARIOUS FRINGE MOTION SEQUENCES

The dashed fringe is the position before motion; the solid fringe the position after a max or min has been observed on counter A or B. The designated state is stored in the minicomputer and used to give the proper sign to subsequent motion.

Motion				
Sequence	Max A, Max B	Min A, Min B	Max B, Min A	Min B, Max A
State	0	1	2	3

Motion				
Sequence	Min B, Min A	Max B, Max A	Max A, Min B	Min A, Max B
State	4	5	6	7

TABLE 2. STATE TABLE

The entries in the table list the sign of the increment output to the totalizing counter and the next state of fringe motion. For example, if a fringe is in state 0 and sees a minimum on counter A, it will output a + increment and change the state to 2. x denotes a sequence that is not allowed.

Existing State	Next Input Detected			
	Max A	Min A	Max B	Min B
0	x	+,2	x	-,6
1	+,3	x	-,7	x
2	-,5	x	x	+,1
3	x	-,4	+,0	x
4	+,3	x	-,7	x
5	x	+,2	x	-,6
6	x	-,4	+,0	x
7	-,5	x	x	+,1

One simply sets the "scan separation" 0-3000; with a value of 1000 corresponding to mirror rotation of approximately 0.04 degre between locations. A "voltage step" of 100 corresponds to 0.2 volts.

A photograph of the signals V_1, V_2, V_3 for both channels is shown in Figure 24. The synchronization of the inputs is of course controlled by the minicomputer.

The fringe patterns, as they sweep past the PMT slit (mirrors stationary), are shown in Figure 25. The specimen was loaded and unloaded in 10 seconds for this particular photograph. Note the difference in number of fringes on the upper and lower traces; this is caused by rigid-body motion which is averaged out in the computation of displacement.

Figure 25 shows a total fringe shift on loading of approximately 6. This corresponds to a displacement of approximately 3 microns. Plots of the displacement output obtained at different loading rates (single cycles) are shown in Figure 26. Note that there is no difference in the output until the time for loading and unloading is reduced to one second. The frequency response of the X-Y plotter begins to affect the output then.

When the sequence of fringe motions of Table 2 is violated, the program "crashes". This can be caused by noise on the PMT signal, improper alignment of fringe patterns onto the PMT, fringes moving faster than the sampling rate, oscillation of the fringes when the load changes direction, etc. Experience has shown that there is no problem with the program crashing for cycling frequencies 0.1 hz or less. When one tries to record at rates faster than 1 hz, the program simply will not run reliably. The speed of cycling is important, but so is the maximum displacement; really it is the speed with which the fringes move past the PMT that counts. Figure 24 shows that each three-location scan takes approximately 4 milliseconds, i.e., a scan rate of 250 scans/second. If the small displacement of Figure 25 is generated at a rate of 1 hz, then the fringes move past the PMT slit at a rate of 10 fringes/second.

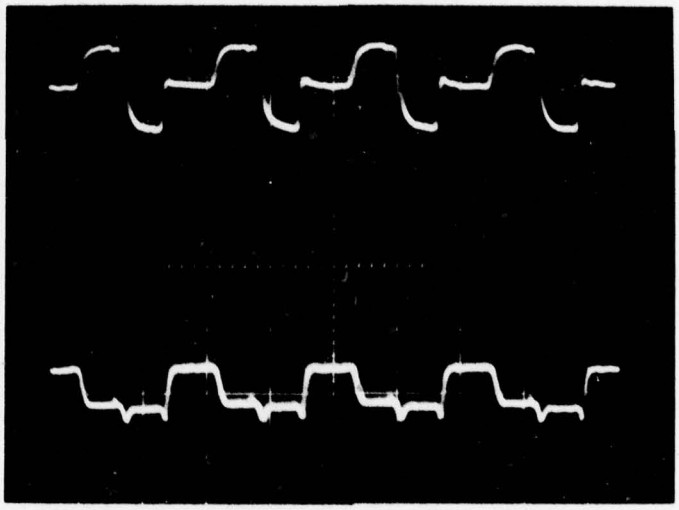

Figure 24 Output from PMTs when mirrors are scanning 3 locations.

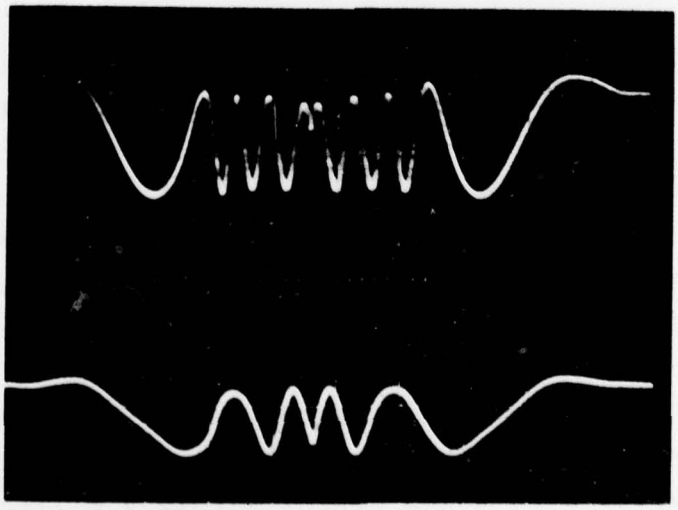

Figure 25 Output from PMTs when mirrors are stationary and specimen is loaded.

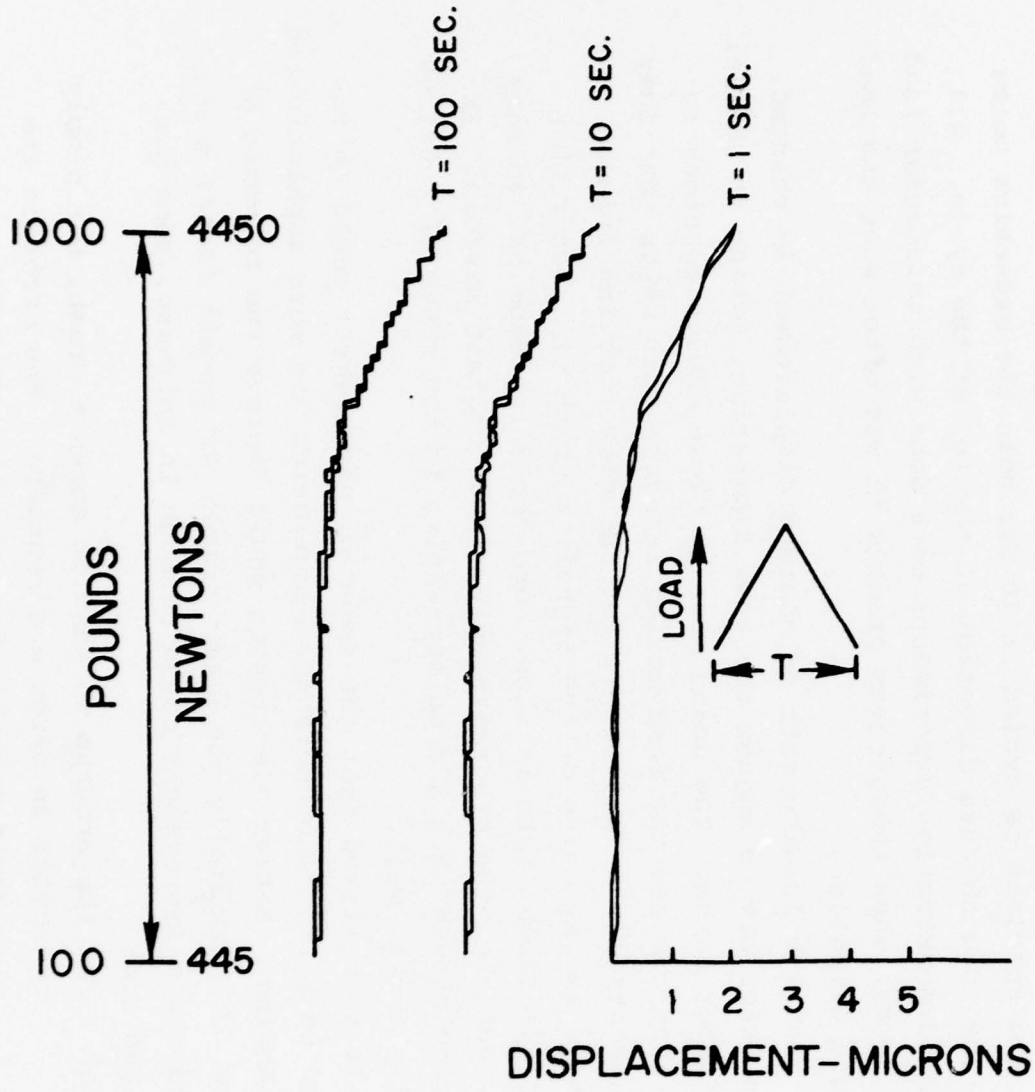

Figure 26 Load-displacement curves at various loading rates

The program handles this fine, but larger diaplacements or faster rates cause problems.

Part of the problem with higher speed response is mechanical motion between the testing machine and the scanning board. This motion can cause the fringe pattern to look different than the one expected by the software. Figure 27 shows the PMT output when the specimen is cycled at 10 Hz; note the excessive noise when the load changes direction at the top of the cycle. All of the demonstration experiments were done with triangular load wave forms; when the program crashed it was often when the load changed direction.

When the loading rate or maximum displacement is changed, it is necessary to adjust the scan separation, making it smaller for faster rates. The scans must be close enough together so that they can see the fast-moving fringes; this means that they see essentially a flat signal for the slower moving fringes. If there is any noise on the signal, a crash will occur when the displacement rate is slow. One could increase the voltage step, but then the program simply misses certain max/min. Experience showed that a scan separation in the range of 800-1200 usually worked well.

It is believed that the speed of measurement could be improved by better photodetector electronics and more sophisticated programming. Better electronics would improve the response of Figure 24 (especially the upper trace) and permit faster scans. Considerable improvement could be made in software; some suggestions are:

a) Fix the program so that it doesn't crash, but simply indicates an error and restarts. The error on the plot could probably be corrected after the test, and one wouldn't lose critical data.

b) Develop a feedback system that adjusts the scan separation according to the speed with which max/min were being counted.

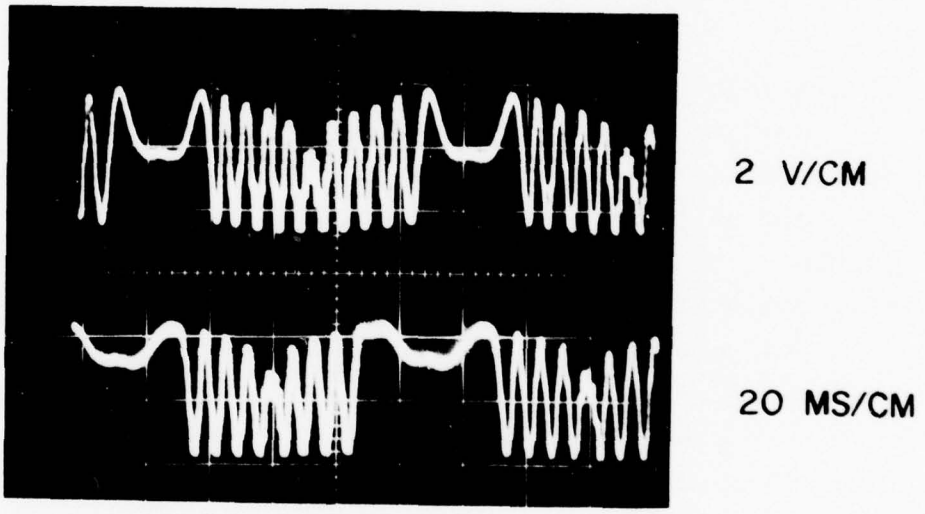

Figure 27 Intensity versus time when cycling at 10 Hz. Mirror was stationary.

c) Set separate scan separations for each channel.

If the speed of the system were increased, another method of recording the data would have to be devised as the X-Y plotter is too slow. It might be possible to store the load-displacement data on floppy disks for later plotting.

The present system has the following characteristics:

a) resolution - $\sim$ 0.12 microns

b) range - $\sim$ 400 microns; the fringes become too closely spaced when the indents are too far apart.

c) gage-length - 50-400 microns

d) cycling rate - 1 hz for maximum displacements of 5 microns.

2. CTOD Measurements

Results of the experiments used to evaluate the CTOD system capabilities are reported in this section. The results are in the form of plots of load versus displacement taken with the X-Y plotter. No attempt is made to interpret the results in light of closure or crack growth theories.

One test was run on a specimen of Incolloy 901 to a maximum temperature of 650°C. The rest of the experiments were performed on one specimen of IN-100.

All specimens were the modified compact tension type shown in Figure 28 (also called "T" type W.O.L.[21]) and were 7.6 mm thick. The surfaces were prepared by lapping for 25 minutes on a Lapmaster machine and then polished with 1 micron diamond paste on a cloth polishing wheel; the oxidation-resistant coatings were then applied. A triangular load waveform with R = 0.1 was used for all experiments on the IN-100 specimen. Most of the tests involved application of a single overload. The overload ratio is defined as $k_{overload}/k_{max}$.

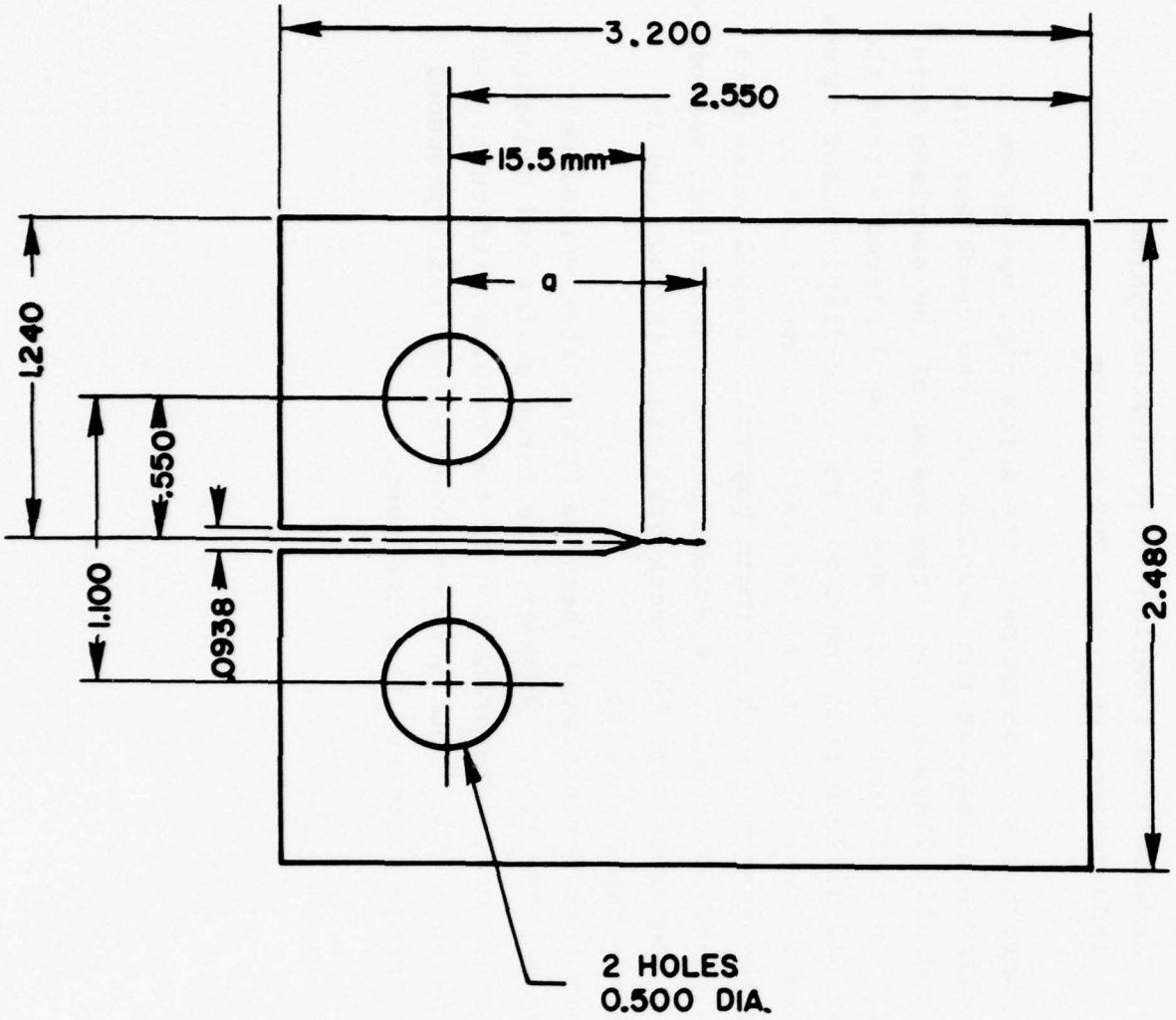

Figure 28 Dimensions in inches of the modified compact tension specimen.

Test 1

Material - Incolloy 901
Crack length - a = 19.35 mm
Baseline K_{max} - 27.4 ksi $\sqrt{in}$ (30.1 $MN/m^{3/2}$)
Overload - none
Test temperature - 650°C
Hold-time - none
Indentations location - 510 microns behind tip
Indentations spacing - 200 microns

A short crack, 0.85 mm past the notch tip, was grown in the Incolloy specimen at the baseline K. The crack was very jagged and slip lines in the large grains of the specimen were evident. Indentations 200 microns apart were placed across the crack at 510 microns from the tip. The load-displacement curves of Figure 29 were obtained at the various temperatures by loading the specimen with a single haversine-shaped pulse with a duration of 50 seconds. A second set of indentations was placed ahead of the crack tip; the crack grew right through one indentation - see Figure 30.

This test demonstrated that the CTOD system worked well at 650°C for Incolloy. However, the large grains and branching of the crack make interpretation of the results difficult. It should be noted that both sets of indentations still produced useable fringe patterns after the test.

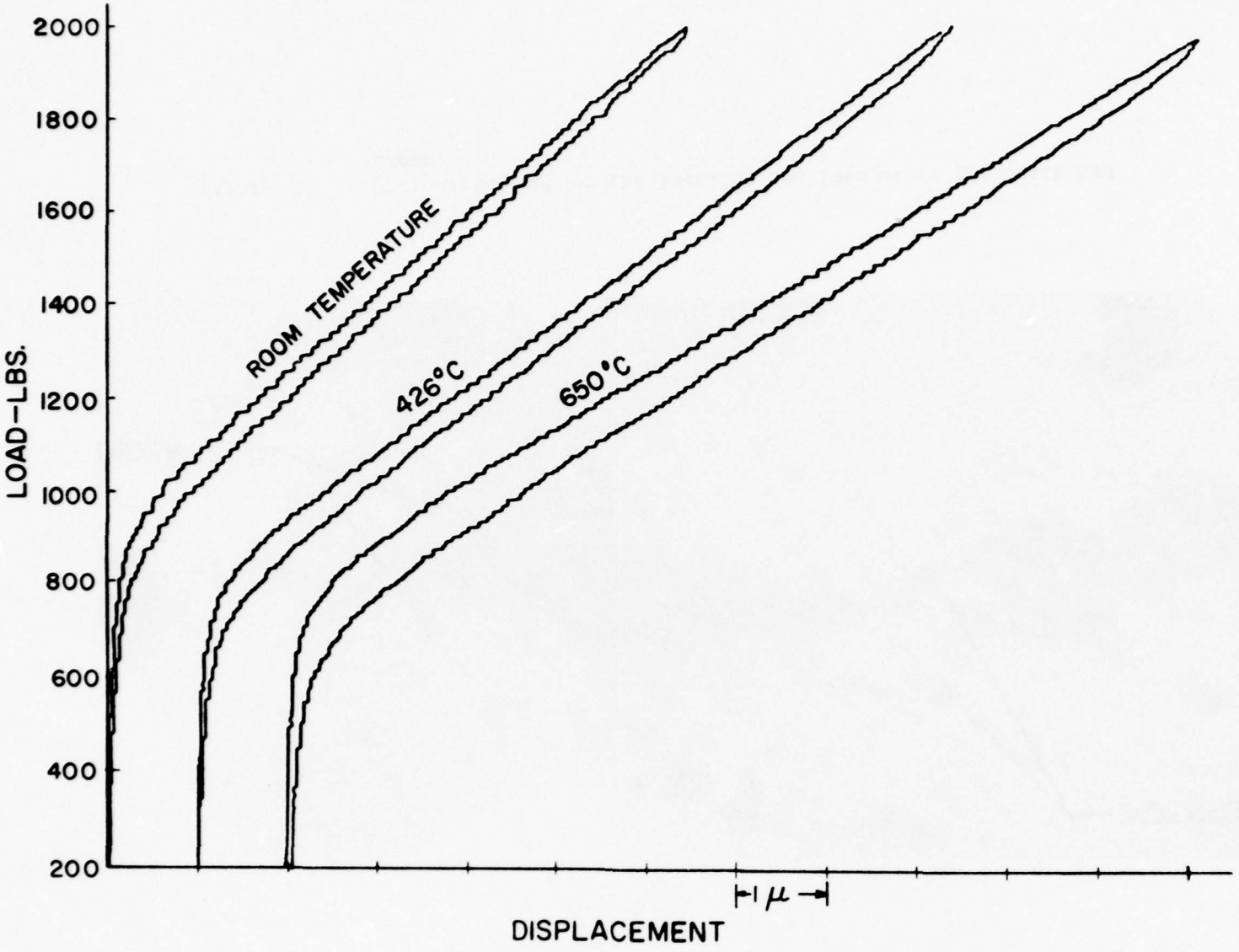

Figure 29 Load-displacement plots for the Incolloy 901 specimen.

V_i and V_2 establish position A; V_2 and V_3 position B. The order in which maximums (or minimums) are seen at these two positions

Figure 30 Photomicrograph of the Incolloy specimen after the crack had grown.

Test 2

Material - IN-100
Crack length - a = 21.0 mm
Baseline K_{max} - 23.2 ksi-$in^{1/2}$ (25.5 $MN/m^{3/2}$)
Overload Ratio - 1.73
Test temperature - Room
Hold-time - None
Indentation location - 700 and 2200 microns behind tip
Indentations spacing - 50 microns

The crack in the IN-100 specimen is very fine and straight, and its tip is hard to locate--even with a microscope. The indentations were placed 50 microns apart, but mistakenly placed 700 microns behind the tip. A second set of indentations was placed 2200 microns behind the tip. The load-displacement curves for the two sets of indentations are shown in Figure 31. Note that the loading rate was slowed for the larger displacement. Note also that the "knee" in the curve occurs at a lower load for the indentations furthest from the tip.

The load-displacement plot for the overload is shown in Figure 32. One thousand cycles were run at the baseline K and a rate of 1 Hz before the overload. Then ten more cycles were run at 0.1 Hz; these are shown in the figure. After the single overload, ten more cycles were run. One thousand more cycles were run at 1 Hz and displacements recorded at intervals; these are shown in Figure 33.

The CTOD system performed flawlessly for these experiments.

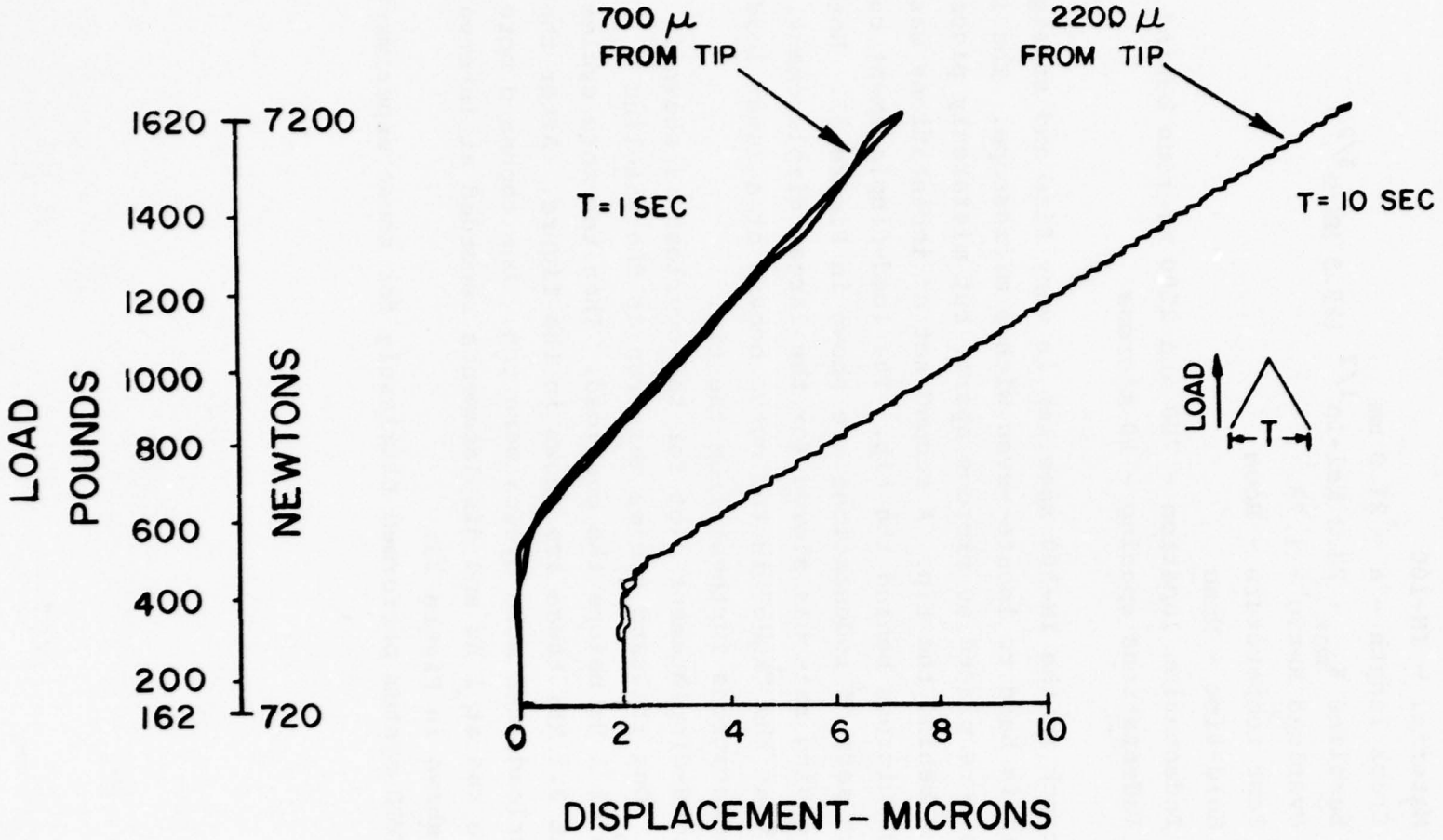

Figure 31 Load-displacement plots for indentations at two distances from crack tip.

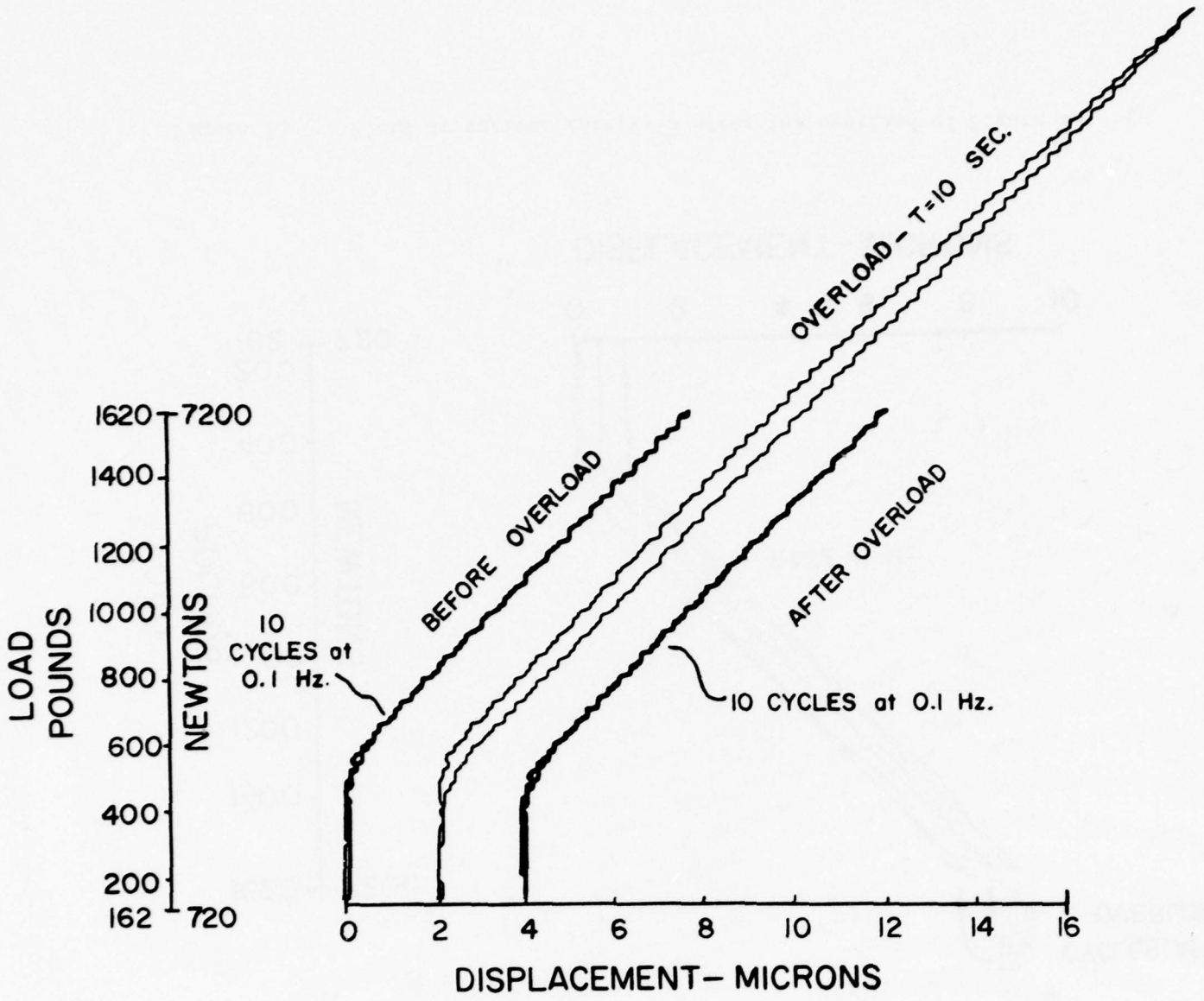

Figure 32 Plots of displacement before, during, and after the overload of 1.73 $K_{max.}$ Test 2

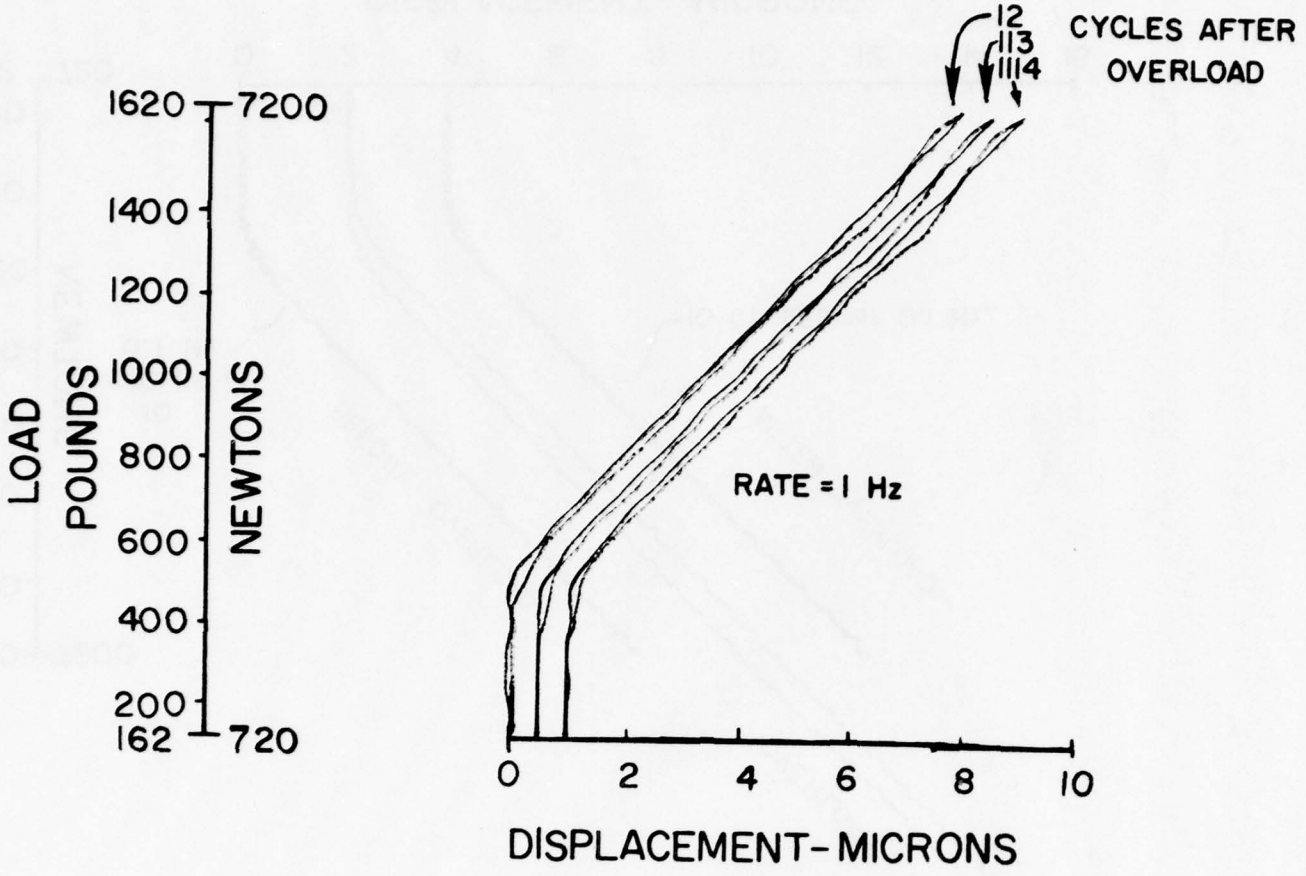

Figure 33 Plots at various intervals after the overlaod of Figure 32.

Test 3

Material - IN-100
Crack length - a = 22.6 mm
Baseline K_{max} - 23.2 ksi-$in^{1/2}$ (25.5 $MN/m^{3/2}$)
Overload ratio - 1.73
Test temperature - 732°C
Hold-time - none
Indentations location - 130 microns behind tip
Indentation spacing - 50 microns

One hundred cycles were run at K_{max} at 732°C prior to the overload. Plots were taken by dropping the pen on the plotter for ten cycles--see Figure 34. The overload was applied at a rate of 0.1 Hz, and then ten load-displacement cycles were recorded immediately after overload. Figure 35 shows plots recorded every 50 cycles for 1000 cycles after the overload. All of these were recorded at 1 Hz without stopping or slowing the load application.

Again, the system performed flawlessly.

A photomicrograph of the crack and indentations after the overload and cycling is shown in Figure 36. The crack was always observed to deviate slightly from its original straight path when it grew past the plastic zone caused by the overload.

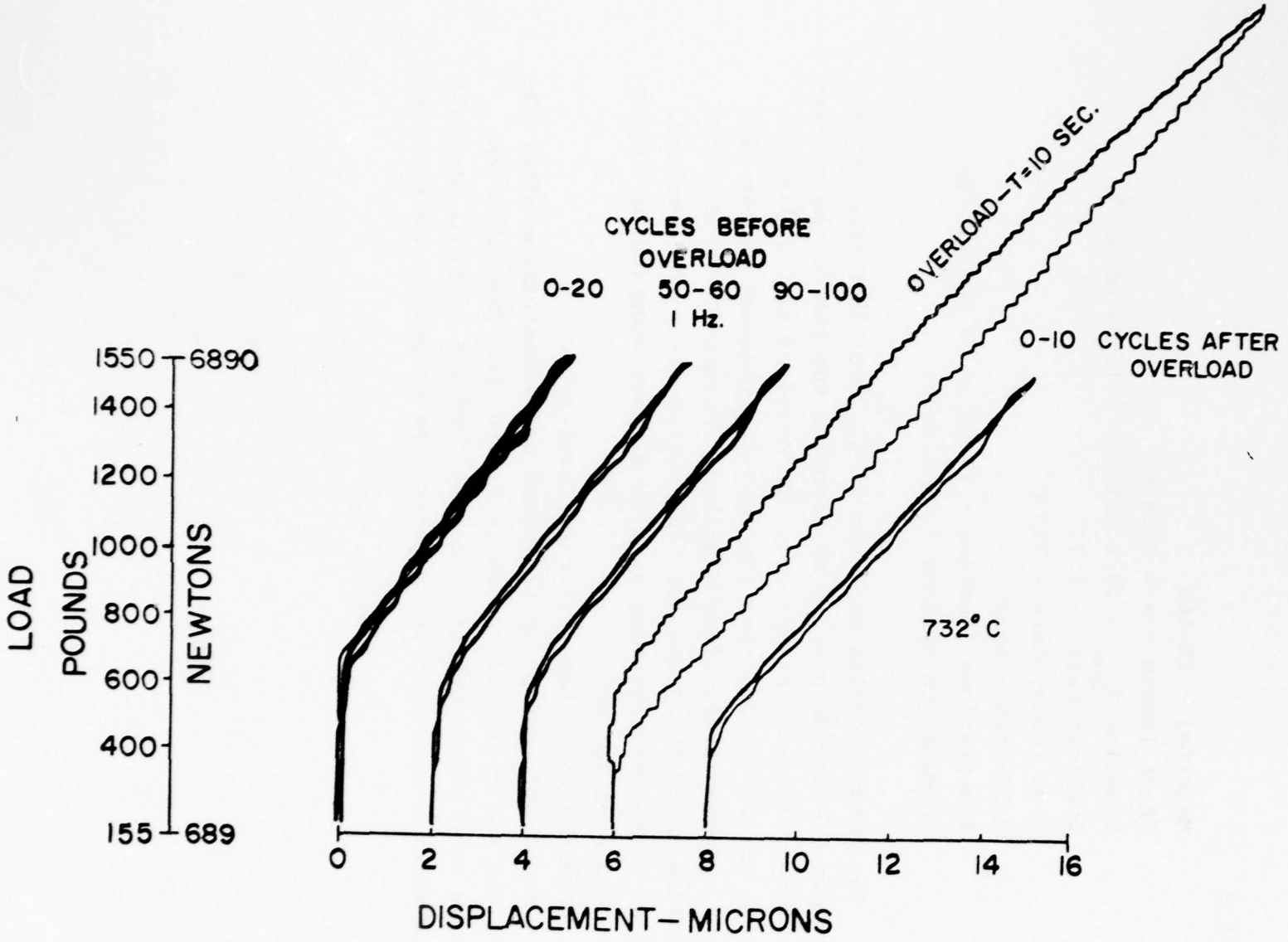

Figure 34 Plots of displacement before, during, and after the overload of 1.73 K max at 732°C Test 3.

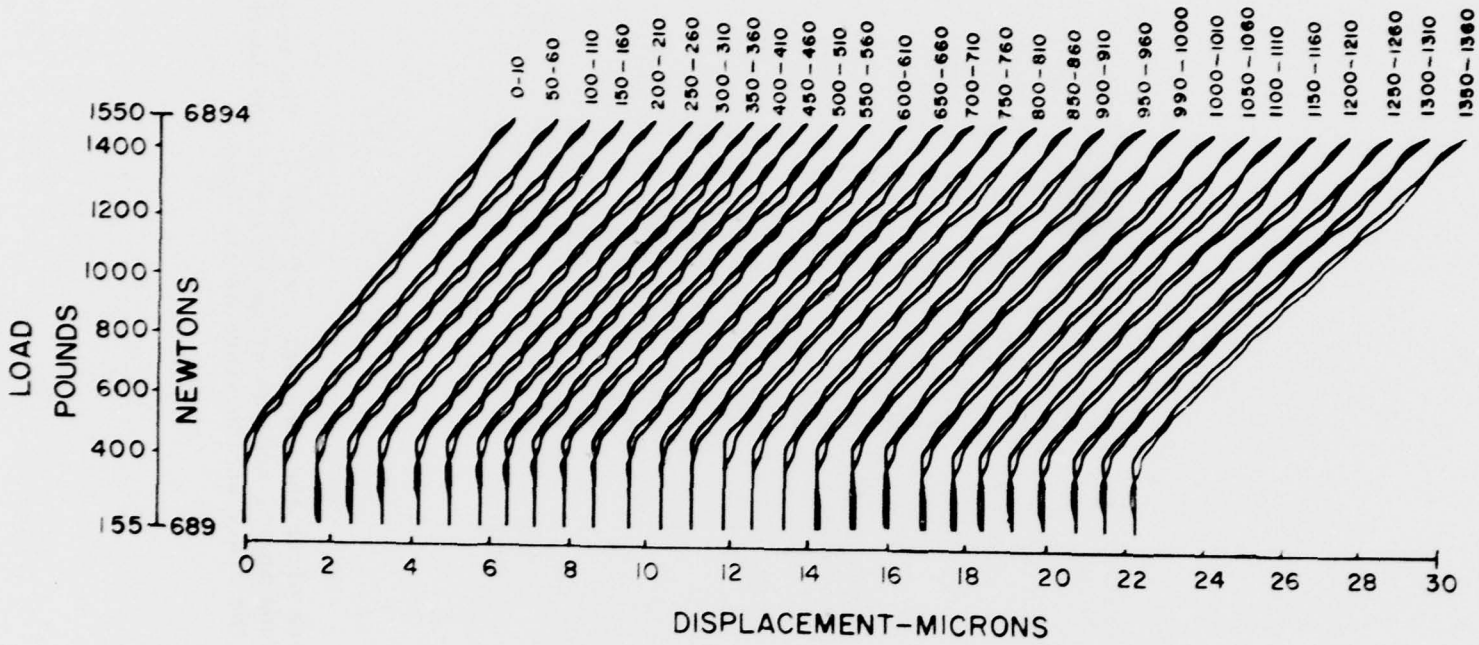

Figure 35 Plots for the first 1000 cycles after overload at 732°C. Test 3.

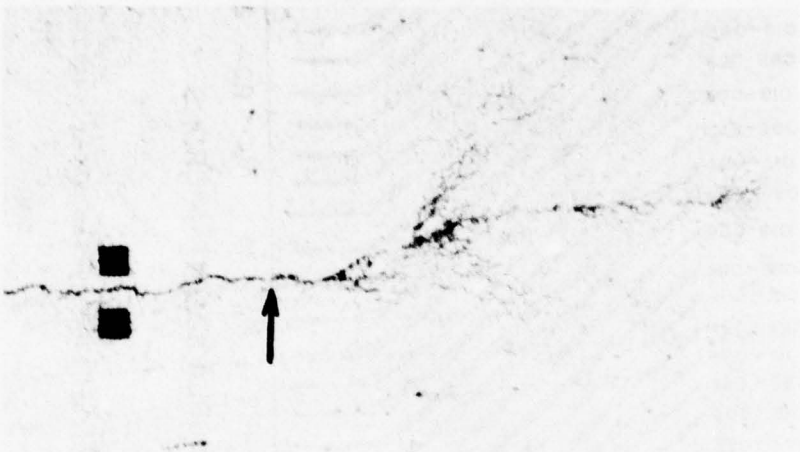

Figure 36 The crack after the completion of Test 3. The indentations are 50 microns apart, and the arrow indicates the location of the tip of the crack at the start of the test.

Test 4

Material - IN-100
Crack length - a = 23.64 mm
Baseline K_{max} - 23.2 ksi-$in^{1/2}$ (25.5 $MN/m^{3/2}$)
Overlaod ratio - 1.73
Test temperature - Room
Hold-time - None
Indentation location - 100 microns behind tip
Indentation spacing - 50 microns

This is basically a repeat of Test 2, but the deflection was monitored for more cycles after the overload. Figure 37 shows the load-displacement plots. For some reason (probably the adjustment of the fringe patterns on the PMT), the ISDG wouldn't function at 1 Hz after 9000 cycles. The testing rate was maintained at 1 Hz, but loading was stopped to take a plot at 0.1 Hz. Note the dramatic change between 11,000 and 12,000 cycles; presumably this is where the crack grew through the plastic zone associated with the overload.

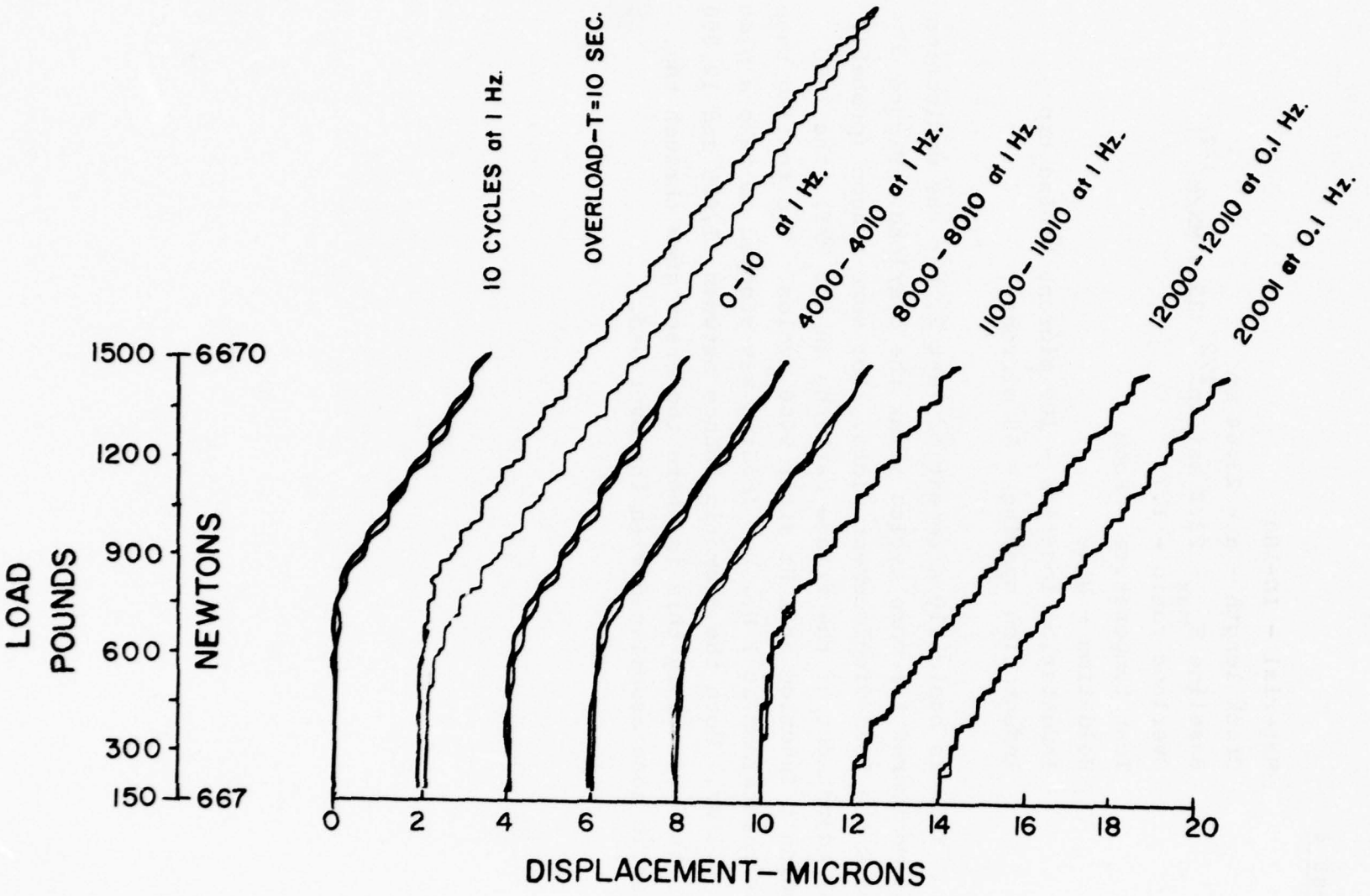

Figure 37 Load-displacement plots for Test 4.

Test 5

Material - IN-100

Crack length - 25.37 mm

Baseline K_{max} - 23.3 ksi - $in^{1/2}$ (25.5 $MN/m^{3/2}$)

Overload ratio - 1.73

Test temperature - 732°C

Hold-time - 1 hr at baseline K_{max} on first cycle after overload

Indentations location - 100 microns behind tip

Indentation spacing - 50 microns

In this test at high temperature the specimen was overloaded, then the load was raised to the baseline K_{max} and held there for 1 hour. It was then unloaded and cycled until changes in the plots were observed.

The plots are shown in Figure 38. The ISDG could not be made to run at 1 Hz, but ran fine at 0.71 Hz. When the specimen was loaded after the overload and held at K_{max}, the plotter was switched to a slow time sweep - plotting displacement versus time. No displacement occurred; the line was straight with occasional jumps of 1 bit back and forth. This demonstrates the stability of the ISDG.

Figure 39 shows the plots after the overload and hold. As the displacement got larger, it was necessary to reduce the rate in order to get a plot.

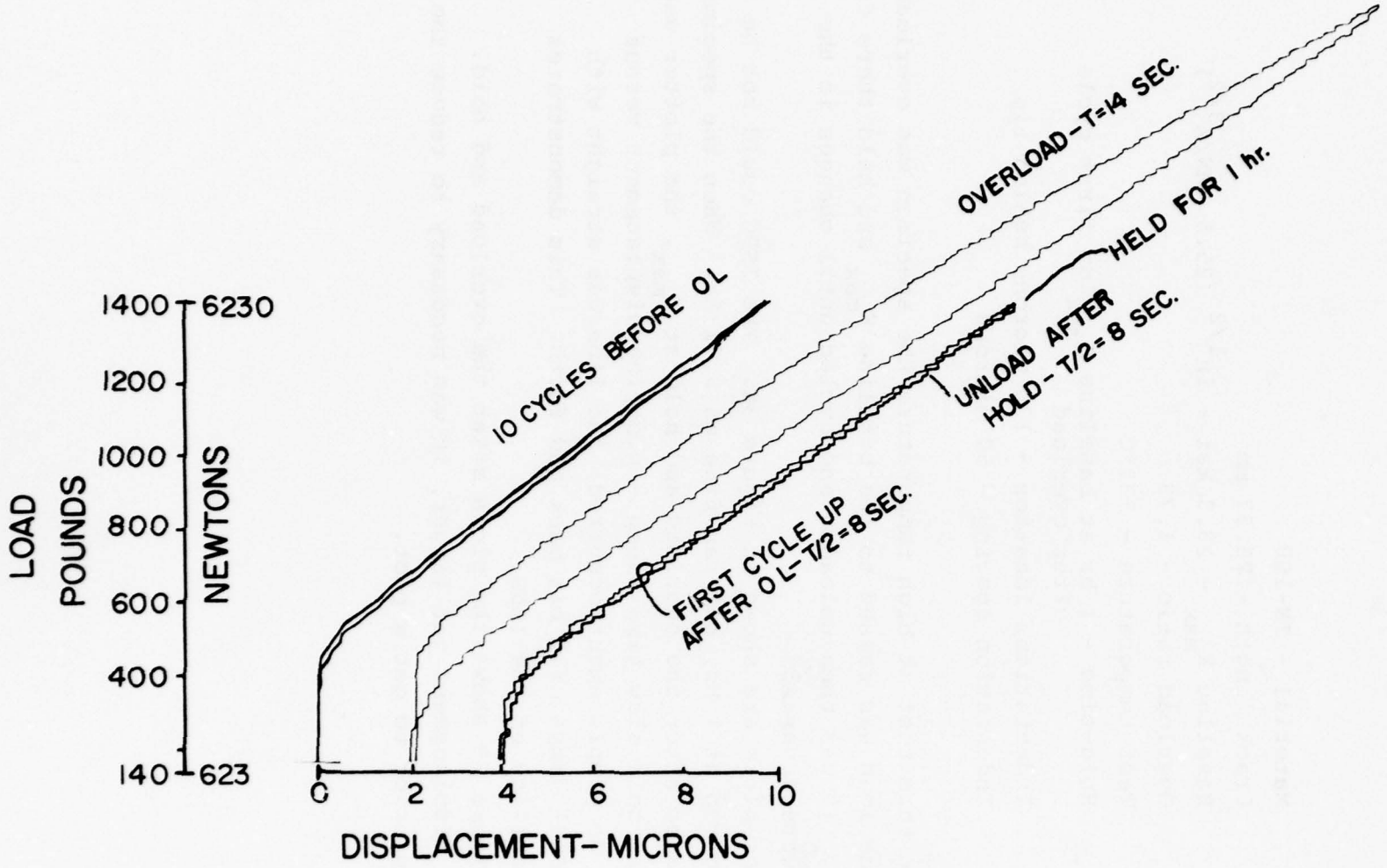

Figure 38 Load-displacement plots at 732°C for Test 5.

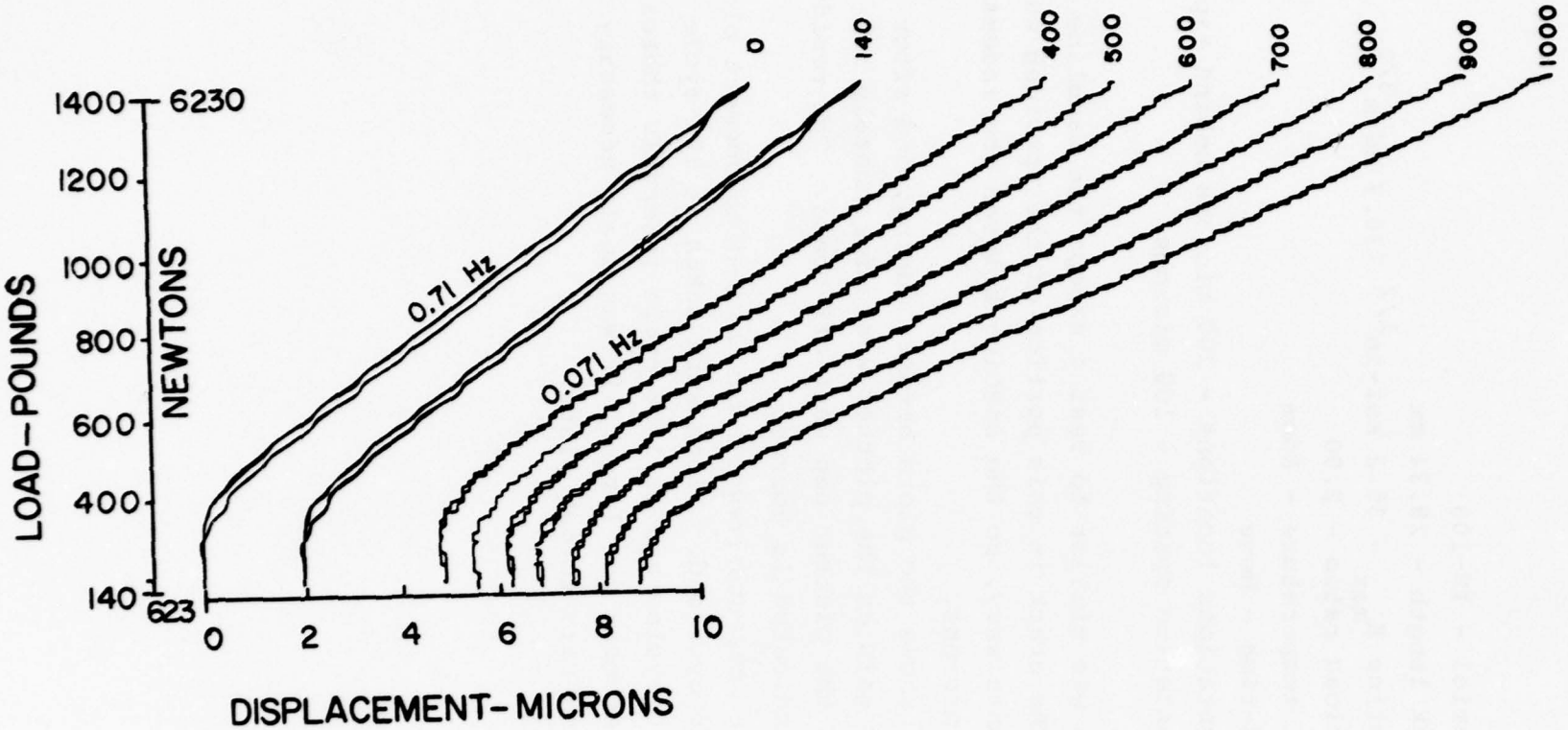

Figure 39 Load-displacement plots taken at 732°C after the overload and hold of Test 5.

Test 6

Material - IN-100
Crack length - 28.34 mm
Baseline K_{max} - 35.2 ksi-$in^{1/2}$ (38.7 $MN/m^{3/2}$)
Overload ratio - 2.00
Test temperature - Room
Hold-time - None
Indentations locations - 200 microns behind tip
Indentation spacing - 100 microns

This test was similar to Test 4 except the baseline K_{max} was larger. The crack in this portion of the specimen was becoming a bit more wavy, so the spacing between the indents was raised to 100 microns.

Figure 40 shows the plots before, during, and after the overload. The gain on the plotter was unfortunately set incorrectly, and the plotter pen went off-scale. The residual displacement indicated is correct.

Figure 41 presents some of the load-displacement plots taken after the overload. Plots were taken at 100 cycle intervals up to 2000 cycles and at 1000 cycle intervals thereafter. When the displacement got larger, it was again necessary to slow the loading rate to get plots.

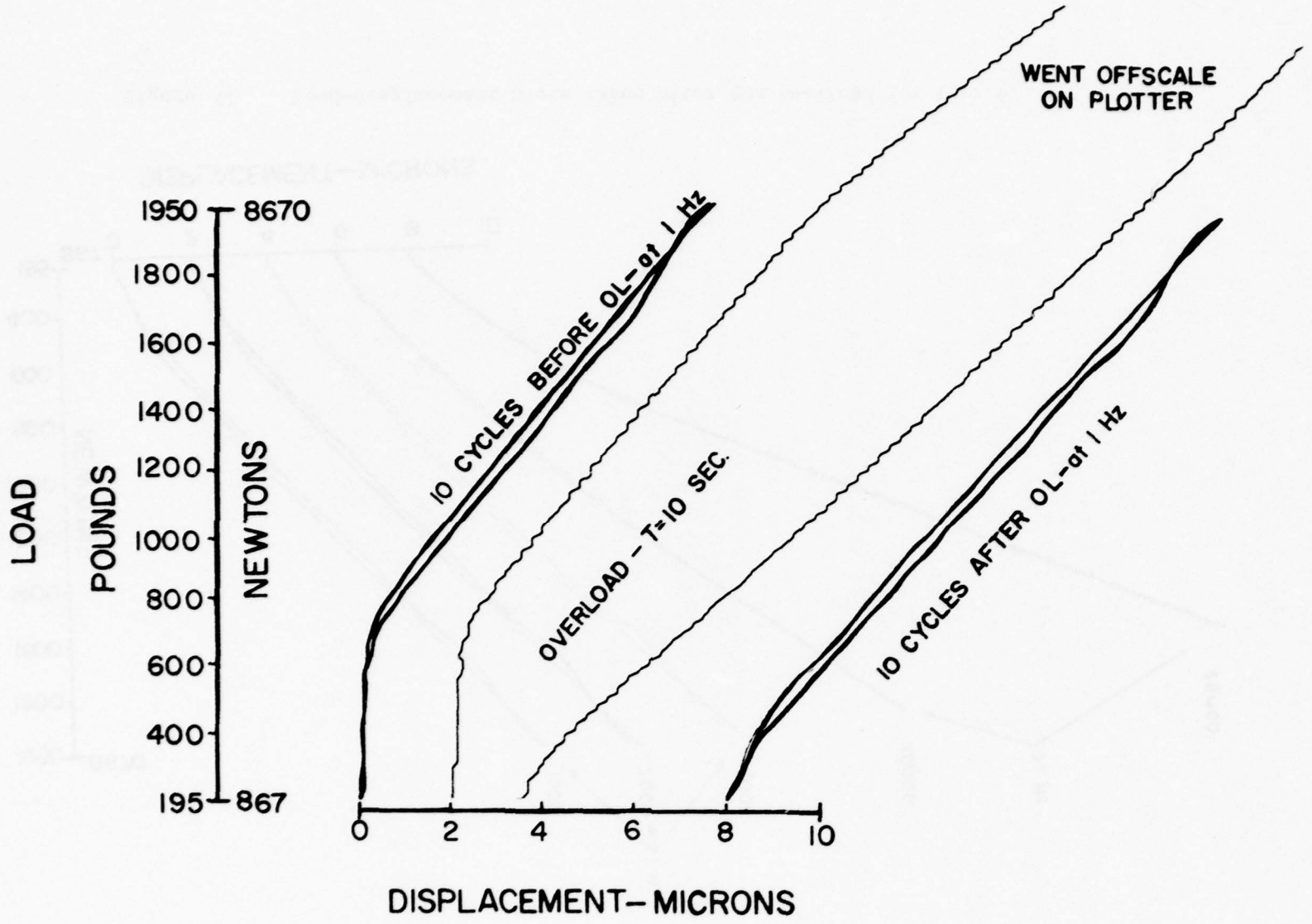

Figure 40 Load-displacement plots for Test 6.

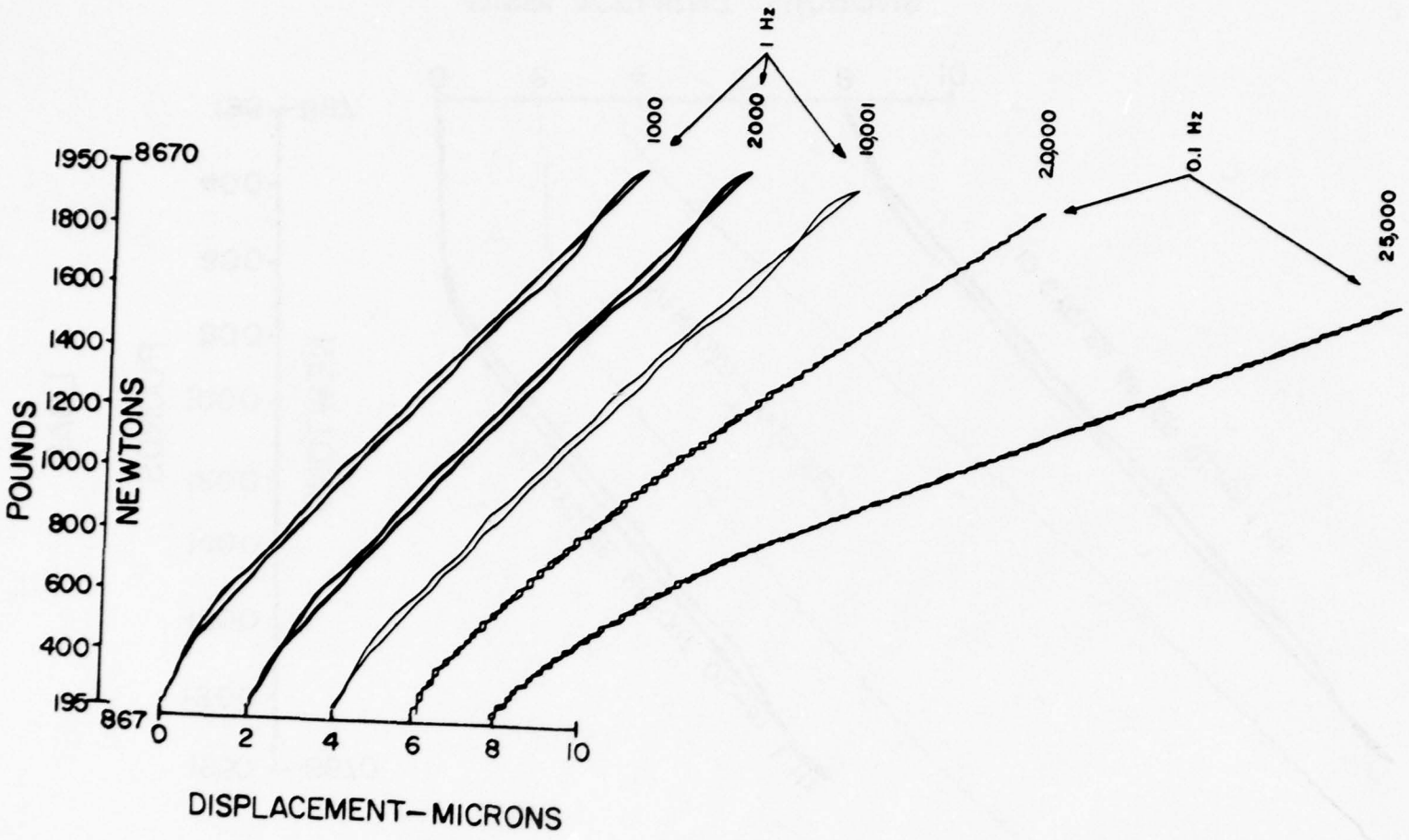

Figure 41 Load-displacement plots taken after the overload for Test 6.

Test 7

Material - IN-100
Crack length - 29.63 mm
Baseline K_{max} - 35.2 ksi-$in^{1/2}$ (38.7 $MN/m^{3/2}$)
Overload ratio - 2.00
Test temperature - 732°C
Hold-time - None
Indentations location - 200 microns behind tip
Indentation spacing - 100 microns

Figure 42 shows the load-displacement plots before, during, and after the overload. Because of the large displacement associated with a high K_{max} at elevated temperature, it was necessary to record at 0.25 Hz. The incident laser beam was not carefully positioned on the indentations, and when the specimen was loaded, they moved out of the beam. The program picked up the displacement again when the specimen unloaded, but the absolute value of the displacement is not known.

Figure 43 presents some of the load-displacement plots taken after the overload.

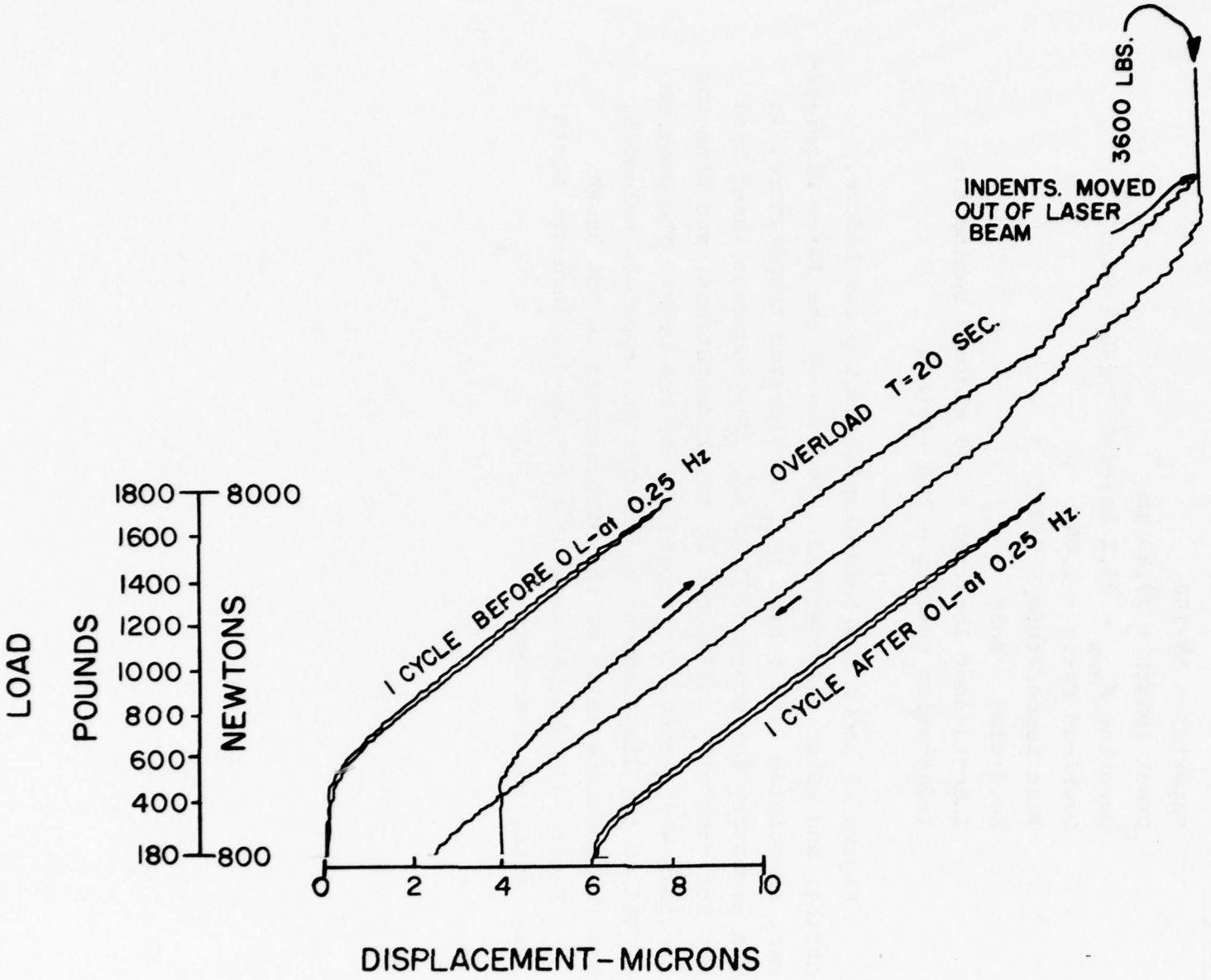

Figure 42 Load-displacement plots at 732°C for Test 7.

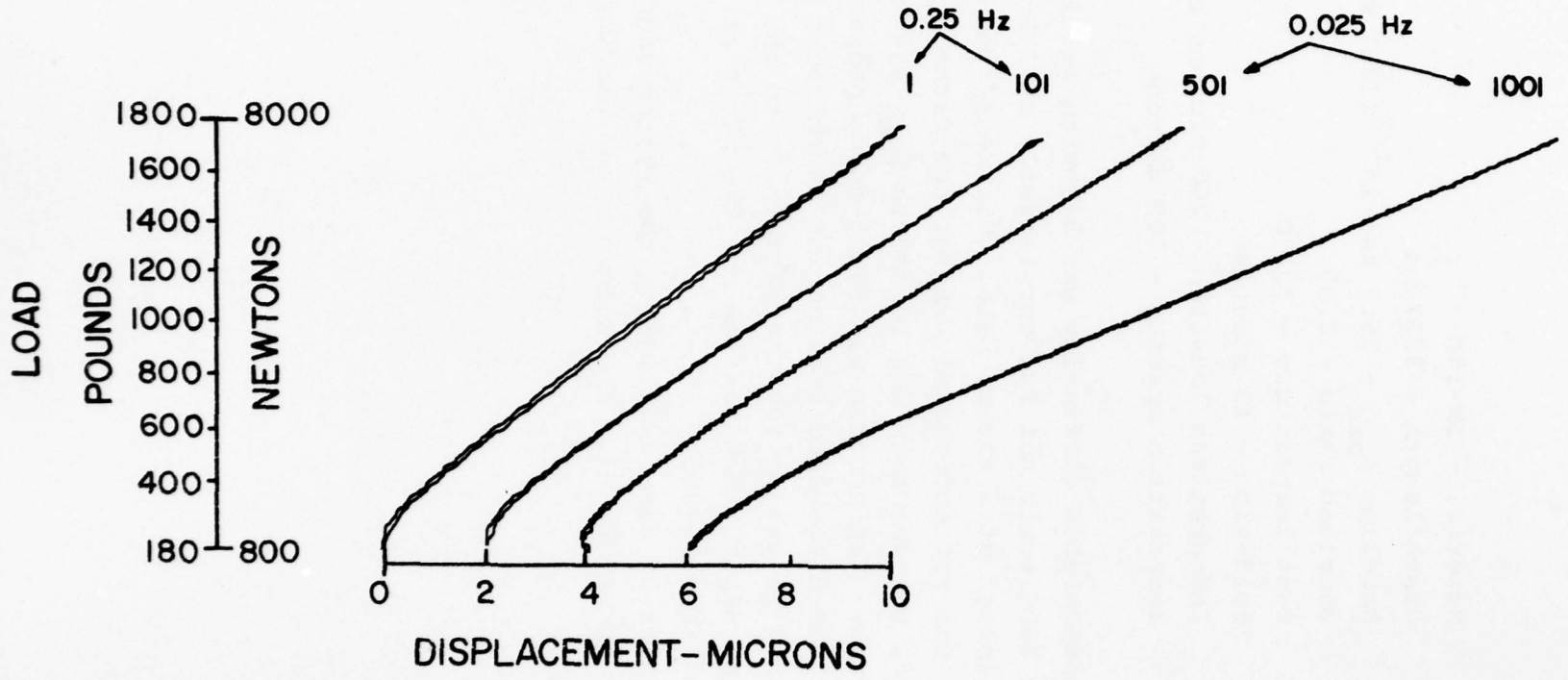

Figure 43 Load-displacement plots taken after the overload for Test 7.

Test 8

Material - IN-100
Crack length - 32.7 mm
Baseline K_{max} - 35.2 ksi-in$^{1/2}$ (3817 MN/m$^{3/2}$)
Overload ratio - 2.00
Test temperature - 732°C
Hold-time - 13 minutes
Indentations location - 200 microns behind tip
Indentation spacing - 100 microns

Considerable difficulty was had with setting up for Test 8. The ISDG would not run consistently at 1 Hz, so the overload was attempted at a slower rate. Figure 44 shows that this attempt was not successful. After the first cycle after the overload, the specimen was loaded to K_{max} and held there for 13 minutes. The program was functioning properly then.

It was discovered that one of the mirrors was slightly misaligned in projecting the pattern on to the PMT. This was corrected after the hold-time and the plots of Figure 45 were obtained at 0.25 Hz.

A lack of care in aligning the system caused the difficulties of Figure 44. The software and hardware worked fine.

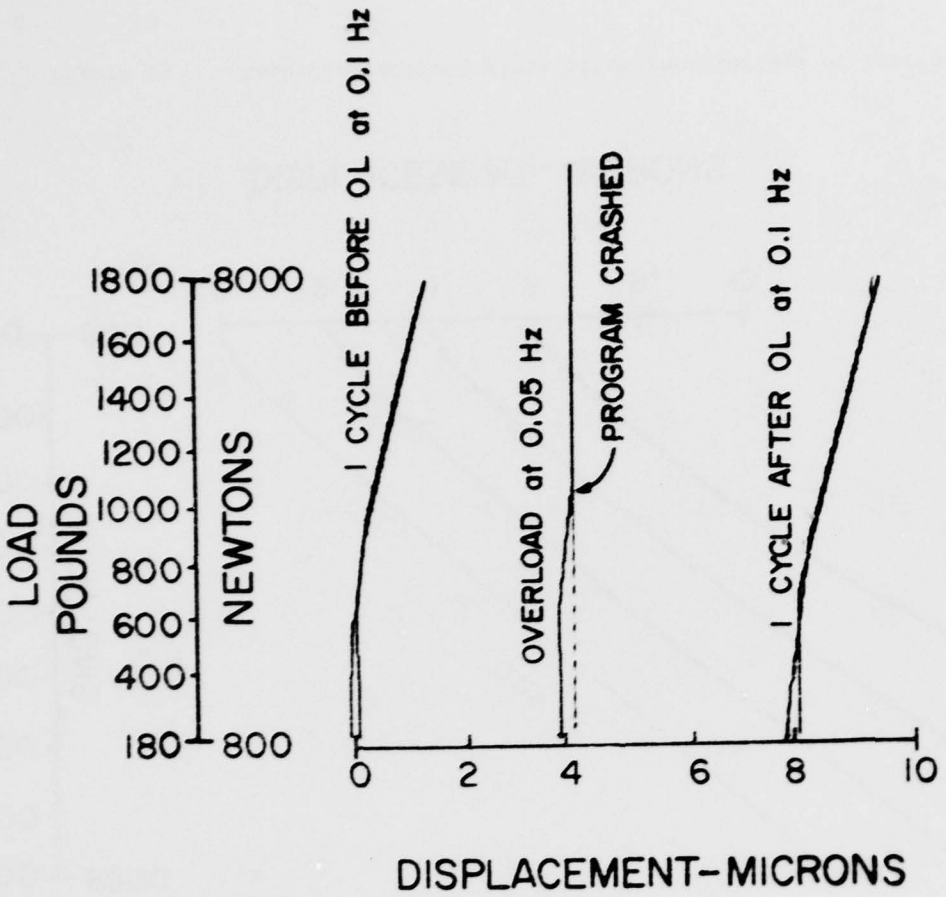

Figure 44 Load-displacement plots at 732°C for Test 8.

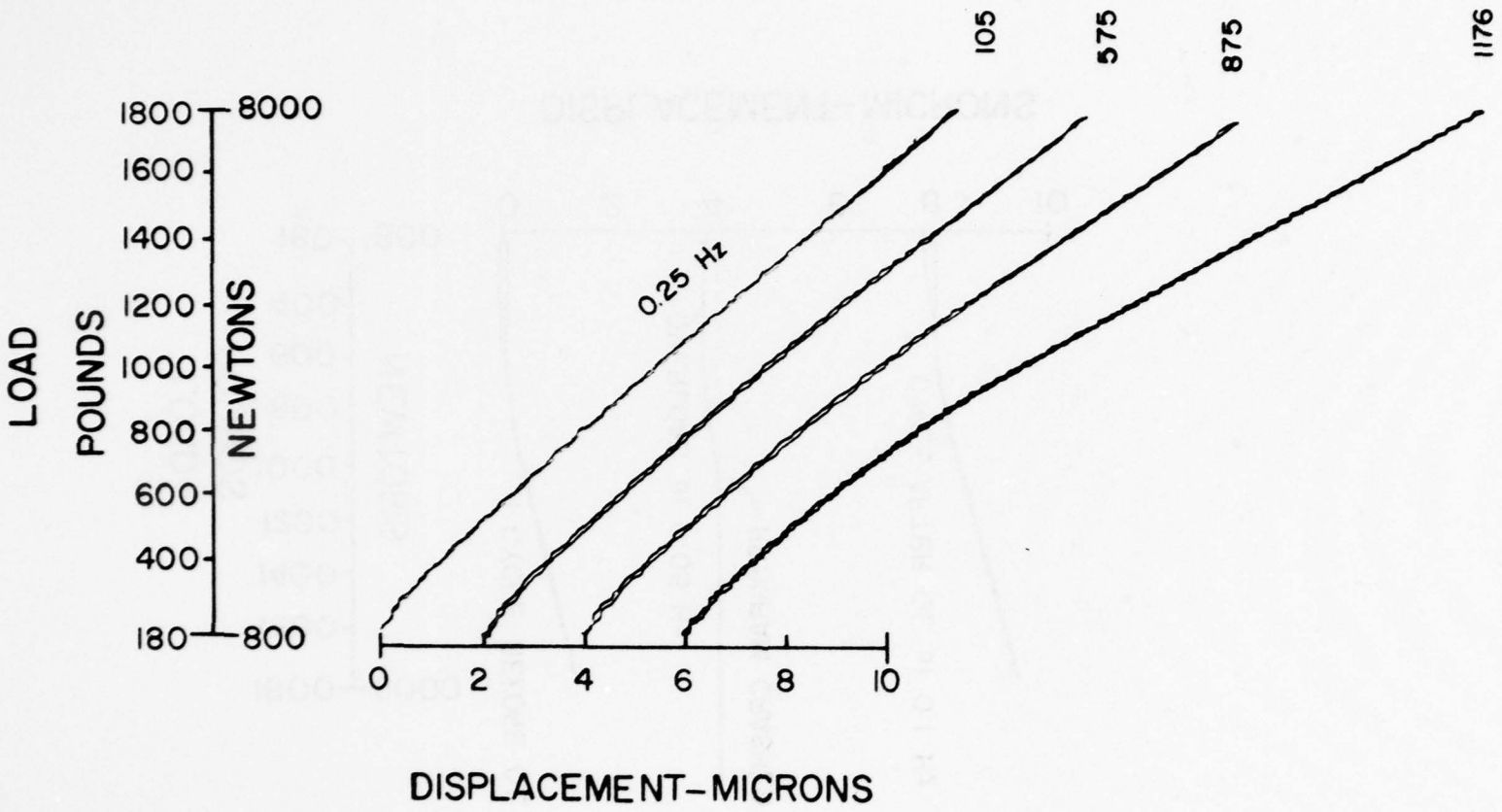

Figure 45 Load-displacement plots after the overload of Test 8.

3. Concluding Remarks

One can expect to obtain results as good as those in Tests 2-5 with this ISDG system. In other words, load-displacement can be monitored at 1 Hz; this cycling rate must be lowered if the displacement becomes larger than approximately 5 microns. The overload cycles of tests 6-8 were not recorded because of carelessness in setting up the measurement system. The system is not particularly difficult or time-consuming to set up.

The resolution, life at high temperature, ease of specimen preparation, and convenience of data recording are all satisfactory. The main improvement that may be desirable is a faster cycling rate. As mentioned in Section 1, the present rate of 1 Hz could probably be improved upon.

SECTION V
BIAXIAL STRAIN MEASUREMENT

Biaxial strain measurement requires increasing the number of fringe-monitoring channels from two to four and measuring smaller values of fringe shifts. The system becomes more complicated in terms of both hardware and software. The optics associated with biaxial measurement are discussed first, and then the software used to measure smaller relative displacements is described. The capabilities and limitations of the system are evaluated with demonstration experiments.

1. The Biaxial ISDG

The configuration of two indentations shown in Figure 1 permits measurement of displacement in one direction only even though four fringe patterns are generated. The horizontal fringe patterns (on a line parallel to the slot in Figure 1) are not used. If three indentations are applied as shown in Figure 46, then all four fringe patterns are used, and the relative displacement or strain can be measured in orthogonal directions. Strain in the Y direction is measured with patterns B and D; in the X direction with patterns A and C. A more complete analysis of the relation between indentation orientation and fringe orientation is given in Reference 22.

The interaction of the four fringe patterns from the two sets of indentations causes the fringe pattern to have a "checkered" appearance. Representative fringe patterns are shown in Figure 47 for different values of d_o. The overall triangluar shape of the pattern is caused by the triangular side of the indentation. In each case, the bottom of the pattern would point toward the incident laser beam. When a slit is placed over the PMT with its orientation horizontal (for Figure 47), the PMT senses fringe motion in only one direction--perpendicular to the slit. If the slit is long enough to contain several "spots", then the PMT response is the same as it would be for fringes generated from two indentations. As the specimen is loaded, the spots move at an angle to the slit; the PMT senses only motion perpendicular to it.

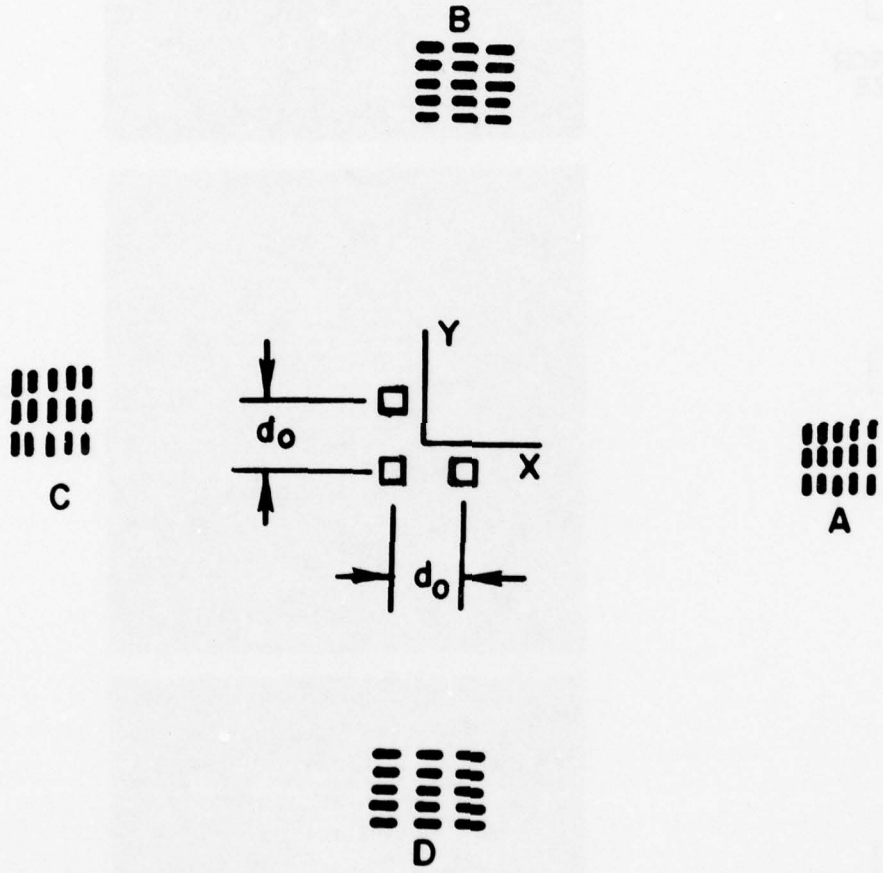

Figure 46 Schematic of the biaxial ISDG.

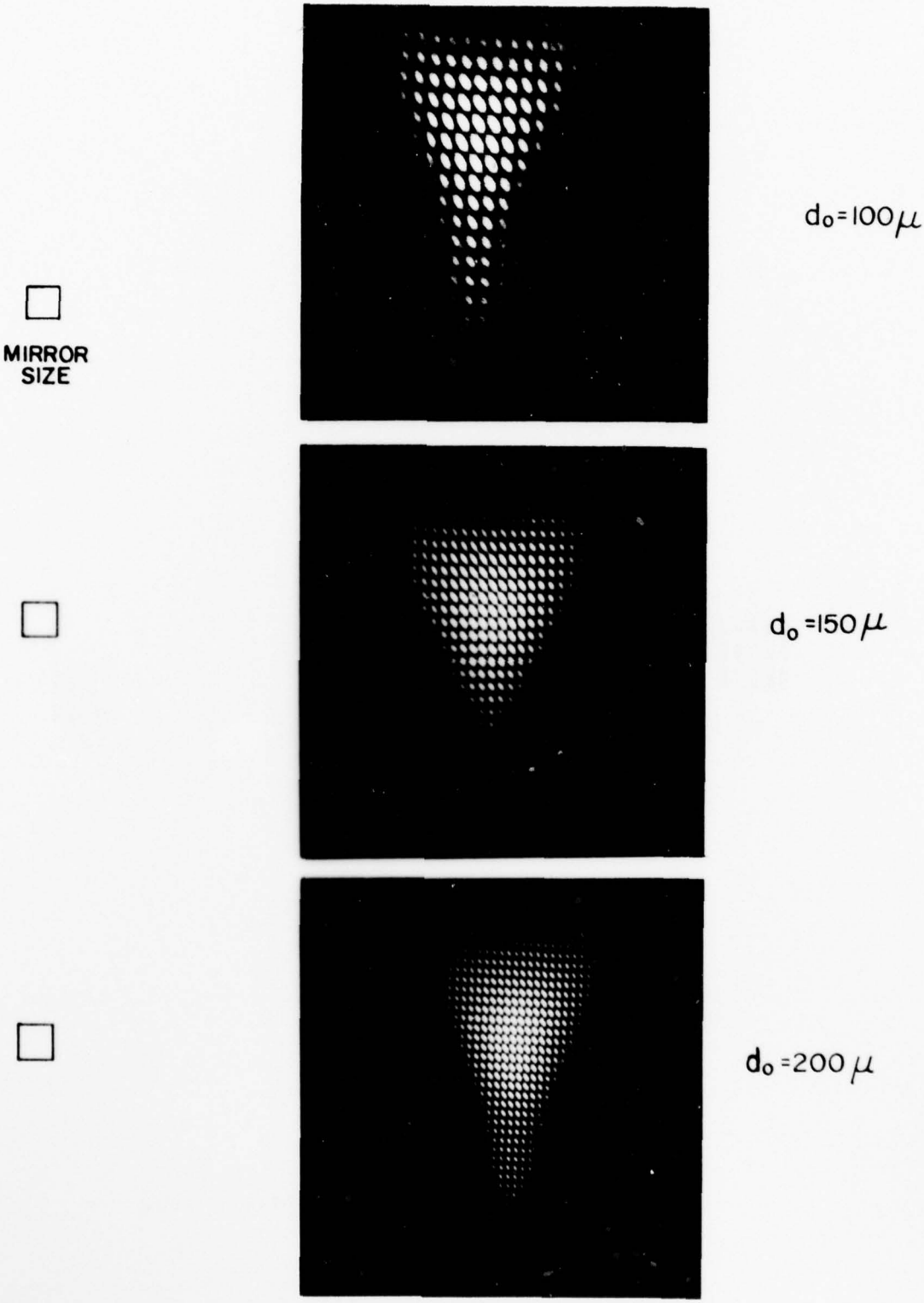

Figure 47 Photographs of fringe patterns for different biaxial spacing. The pictures are full size and were taken 30 cm from the indentations. The size of the 6.4 mm square mirror is also shown.

Fringes from three values of d_o are shown in Figure 47 to show the effect of fringe spacing. If the aperture of the PMT (or mirror reflecting onto the PMT) is small, then not enough spots will shine into it, and the scanned fringe pattern will not have the desired cosine-squared shape. The selection of d_o is determined by the optics of the photodetector system.

The complete 4-channel system as described in Section 2 is required for biaxial measurement.

2. Small Displacement Software

The CTOD system has a resolution of $\sim$ 0.1 micron. Based on a gage-length of 100 microns, this corresponds to a minimum detectable strain of 0.1 percent. More resolution is required, and a completely new approach to measuring and computing fringe movement is necessary. At the completion of the NASA-Langley project [5], a uniaxial program was available that had a resolution of 0.004 micron, but did not have cyclic capability and had only limited range. It was necessary to develop software with cyclic and biaxial capability on this project. The basic approach of the earlier program was followed.

The program is outlined in Figure 48. The mirrors sweep the fringes across the PMT slit in 256 increments--with a voltage recorded for each location. As it scans, the program does a 4-point average, i.e. it adds the three previous values to the value in the current location. This helps to eliminate noise on the voltage signal. Also as it scans, it compares subsequent average values to determine the location of the maxima and minima. The locations of maxima and minima are stored in an array. When the next scan is taken, its max/min locations are compared with the previous one to see whether they are moving to the left or to the right and the amount of their motion. This motion (in the form of number and sign of mirror locations) is fed to a summing counter that does the averaging in Equation 1.

The program sequentially increments and processes each channel. It can print the max/min locations and spacings between them if desired. A typical printout is shown below:

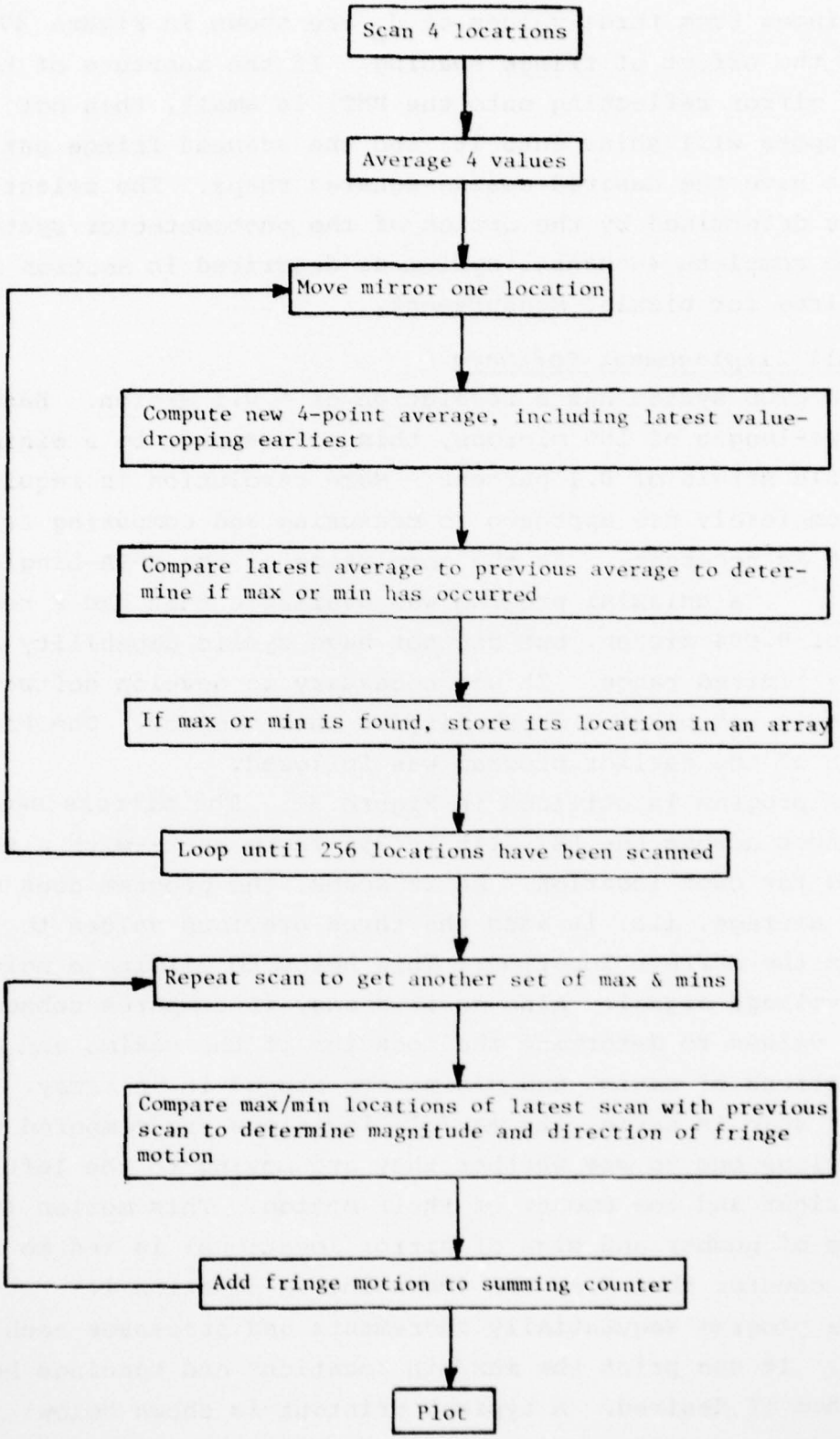

Figure 48 Flowchart of the small displacement program.

```
CH.1
MAX LOC AT: 000A 004D 008F 00D6 00FF
MIN LOC AT: 0026 006D 00B3 00F9
MAX SEP: 0043 0042 0047 0029
MIN SEP: 0047 0046 0046

CH.2
MAX LOC AT: 003C 007C 00C3 00FB
MIN LOC AT: 0010 005A 009F 00E1
MAX SEP: 0040 0047 0038
MIN SEP: 004A 0045 0042

CH.3
MAX LOC AT: 0030 0079 00B8 00F4
MIN LOC AT: 0010 004F 0098 00D6
MAX SEP: 0049 003F 003C
MIN SEP: 003F 0049 003E

CH.4
MAX LOC AT: 0038 0080 00C9
MIN LOC AT: 005C 00A5
MAX SEP: 0048 0049
MIN SEP: 0049

(D,P,R)?R
```

The locations are given in hexadecimal code.

Some other features of the program are:

a) It picks up new max/min as the fringes move by looking for corresponding max or min in positions within 16 locations of the previous one. If none is found (which means the fringe has moved more than 16/256), it selects a new max or min to follow.

b) The program follows the first two maxima in the pattern, ignoring the later ones. This tends to smooth out the motion (as opposed to following only one max).

c) The first 30 locations of the scan are not used because there is a little oscillation as the mirror drops back from its maximum rotation and starts the scan over.

Each scan takes 200 milliseconds; therefore approximately 0.8 ms is required for each increment-to move the mirror, sample the voltage, and perform the calculations.

The ISDG is calibrated using the following equation:

$$\varepsilon = \frac{\text{Number of bits out}}{2 \times 2 \times \text{Fringe Spacing}} \qquad \frac{\lambda}{d_o \sin \alpha_o} \tag{3}$$

One bit is output for each shift of one memory location, so one bit corresponds to a relative fringe shift of 1/fringe-spacing. Note that the fringe spacing must be initially set equal on both channels.

The first "2" in the denominator of Equation (3) comes from Equation (1) because there are two channels for each strain measurement, and the second "2" occurs because the program follows two maxima.

A calibration plot of the small displacement program is shown in Figure 49. The measurand was a flat tensile specimen with two indentations located 200 microns apart. The "true" strain was recorded with a foil resistance strain gage. The calibration plot was taken for several cycles of loading.

In practice, one calibrates the displacement output by increasing the gain on the plotter until individual bits are observed. One bit corresponds to $\sim$ 3 mv.

This program works fine as long as the fringe pattern signals are clean. But as soon as extra peaks or valleys appear from electrical or optical noise, it sees the wrong max/min and puts out useless values. As will be shown in the next section, the operation of the program is critically dependent on the quality of the fringe pattern; electrical or mechanical noise offers no difficulty.

3. Biaxial Strain Results

Seven tests were run in which biaxial measurements were made. The capabilities and limitations of the system are best described by looking at the individual experiments.

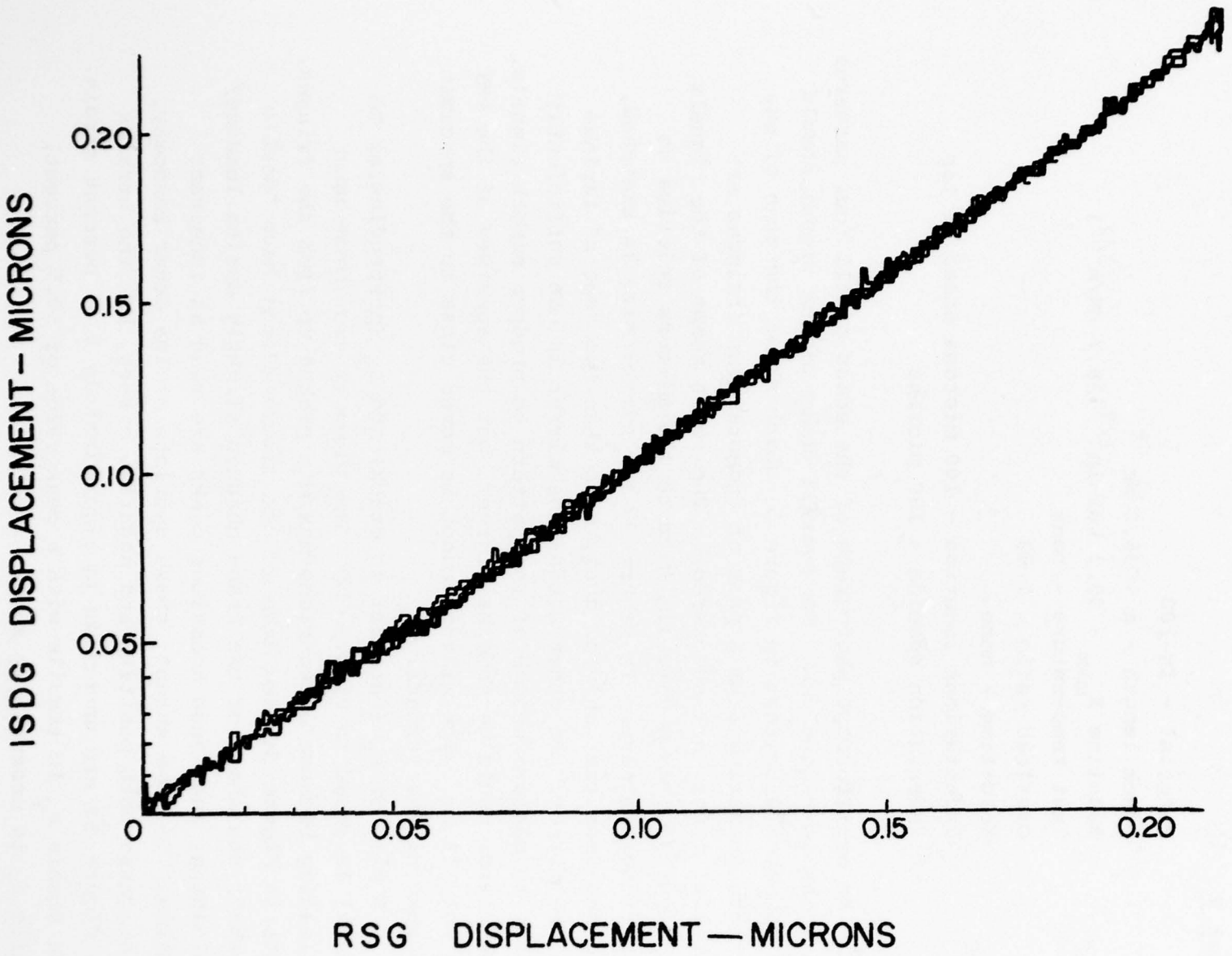

Figure 49 Calibration plot for the small displacement program

Test 9

Material - IN-100
Crack length - a = 36.2 mm
Baseline K_{max} - 35.2 ksi-$in^{1/2}$ (38.7 $MN/m^{3/2}$)
Test temperature - room
Overload ratio - 1.73
Hold-time - none
Indentations location - 100 microns ahead of tip
Indentation spacing - 100 microns

An oscilloscope photograph of the scans of all four patterns is shown in Figure 50. The overall shape of the signal should be compared with that in Figure 51 which shows the scan of one pattern emanating from a pair of indentations (fringes are parallel lines; not checkered). The rough shape of the signals in Figure 50 stems from the size of the mirrors relative to the fringe pattern. In Figure 47 the mirror size is sketched, and one sees that only slightly more than two "spots" impinge on the mirror. In other words, the mirror is not sufficiently large to capture enough of the pattern to produce smooth signals. The mirror could be somewhat larger, but the aperture of the PMT is only 16 mm. The mirror cannot be moved close to the specimen because of the furnace.

A plot of ε_x (parallel to crack) and ε_y (perpendicular to crack) is shown in Figure 52. The plots do not close upon unloading because of spurious max/min picked up from the fringes. Note in Figure 50 that some of the traces almost have "double peaks"; the shape of the trace changes slightly during loading/unloading, and these anomalous peaks are read as incorrect maxima. To some extent, these spurious maxima occur randomly, i.e. cause both positive and negative errors, but the strains in Figure 52 are uncertain by approximately 0.05 percent strain. The strain ε_y is tensile with a peak value of $\sim$0.5 percent, while ε_x is essentially zero.

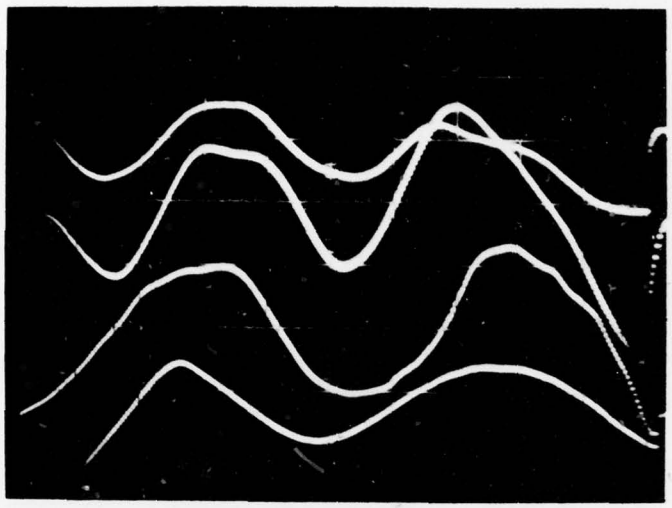

Figure 50 Fringe pattern signals from three indentations spaced 100 microns apart.

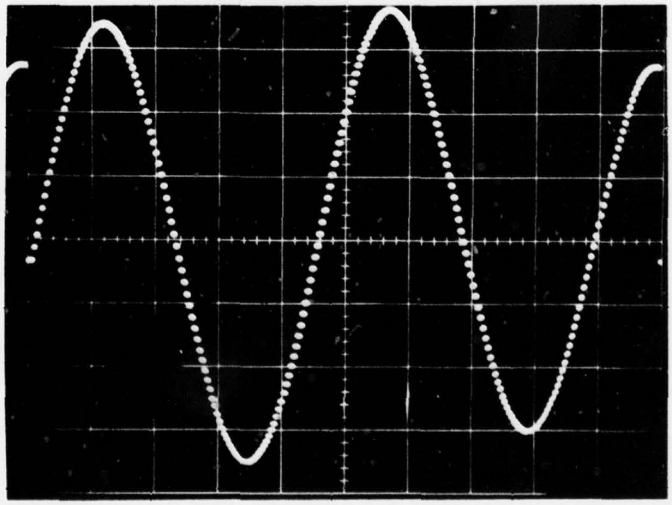

Figure 51 Fringe pattern signal from two indentations.

AD-A057 664 MICHIGAN STATE UNIV EAST LANSING DIV OF ENGINEERING --ETC F/G 11/6
AN OPTICAL GAGE FOR STRAIN/DISPLACEMENT MEASUREMENT AT HIGH TEM--ETC(U)
SEP 77 W N SHARPE, D R MARTIN F33615-76-C-5059

UNCLASSIFIED AFML-TR-77-153 NL

2 OF 2
AD
A057 664

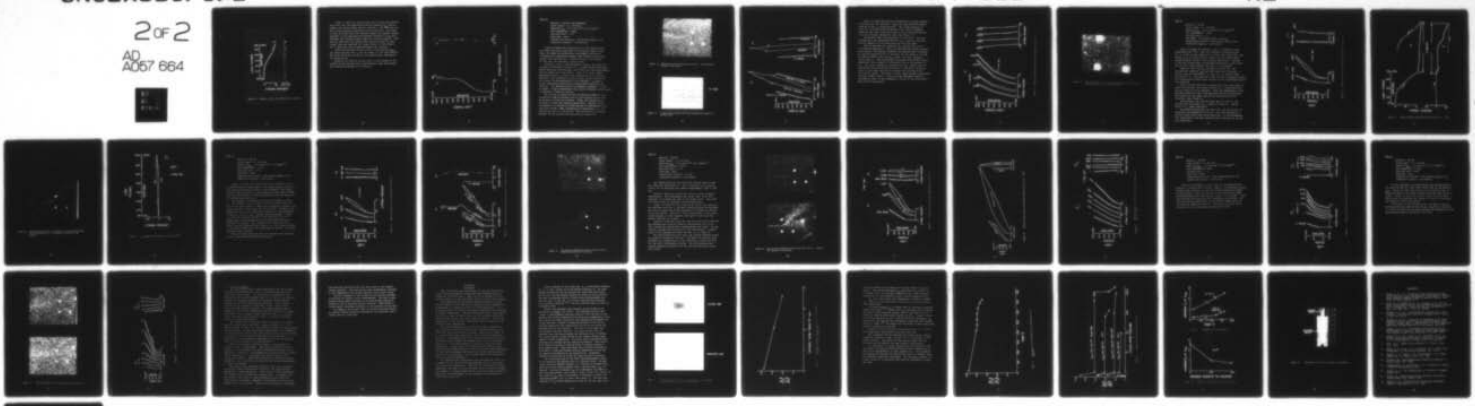

END
DATE
FILMED
9-78
DDC

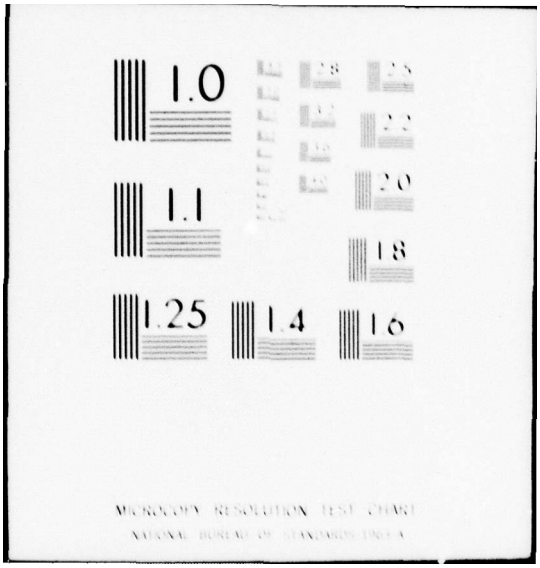
1.0
1.1
1.25
1.4
1.6
2.0
1.8
MICROCOPY RESOLUTION TEST CHART
NATIONAL BUREAU OF STANDARDS-1963-A

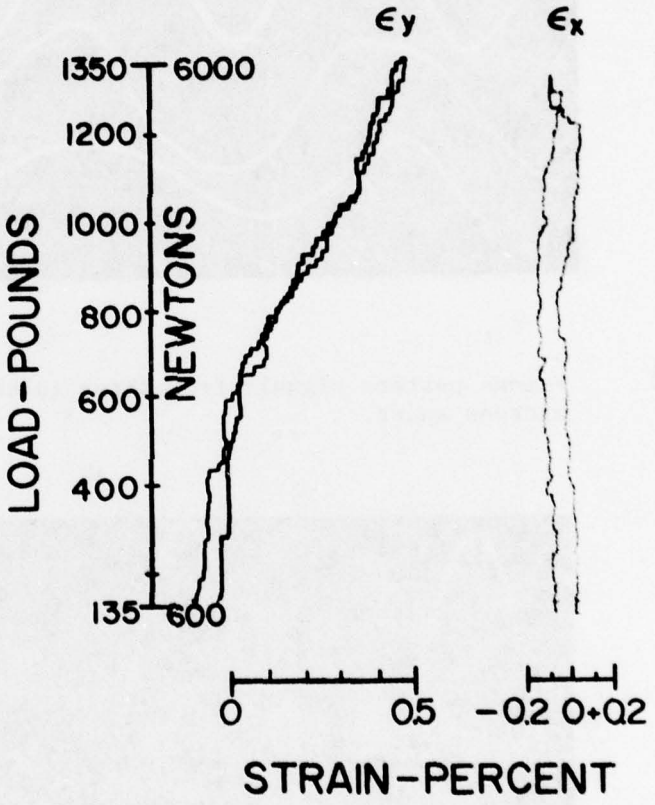

Figure 52 Strains ε_x and ε_y for Test 9 before overload.

Figure 53 shows the strains when the overload was applied. Soon after the load associated with the baseline K_{max} was exceeded, the strain became clearly incorrect. The whole set of four fringe patterns rotated off the four mirrors. The crack at this point was more than halfway through the compact tension specimen, so the specimen was extremely sensitive to any misalignment and rotated slightly when the load was applied. This does not mean that the biaxial ISDG cannot be used for long cracks (data was acquired for longer cracks in later tests), but it does mean that alignment becomes very critical.

After the overload and 100 cycles at the baseline K_{max}, the fringe patterns for ε_y were no longer of very good quality. The crack had grown into one of the indentations, destroying its reflectivity.

Based on the results of this test, it was decided to use another IN-100 specimen with a much shorter crack and enlarge the indentation spacing to 150 microns.

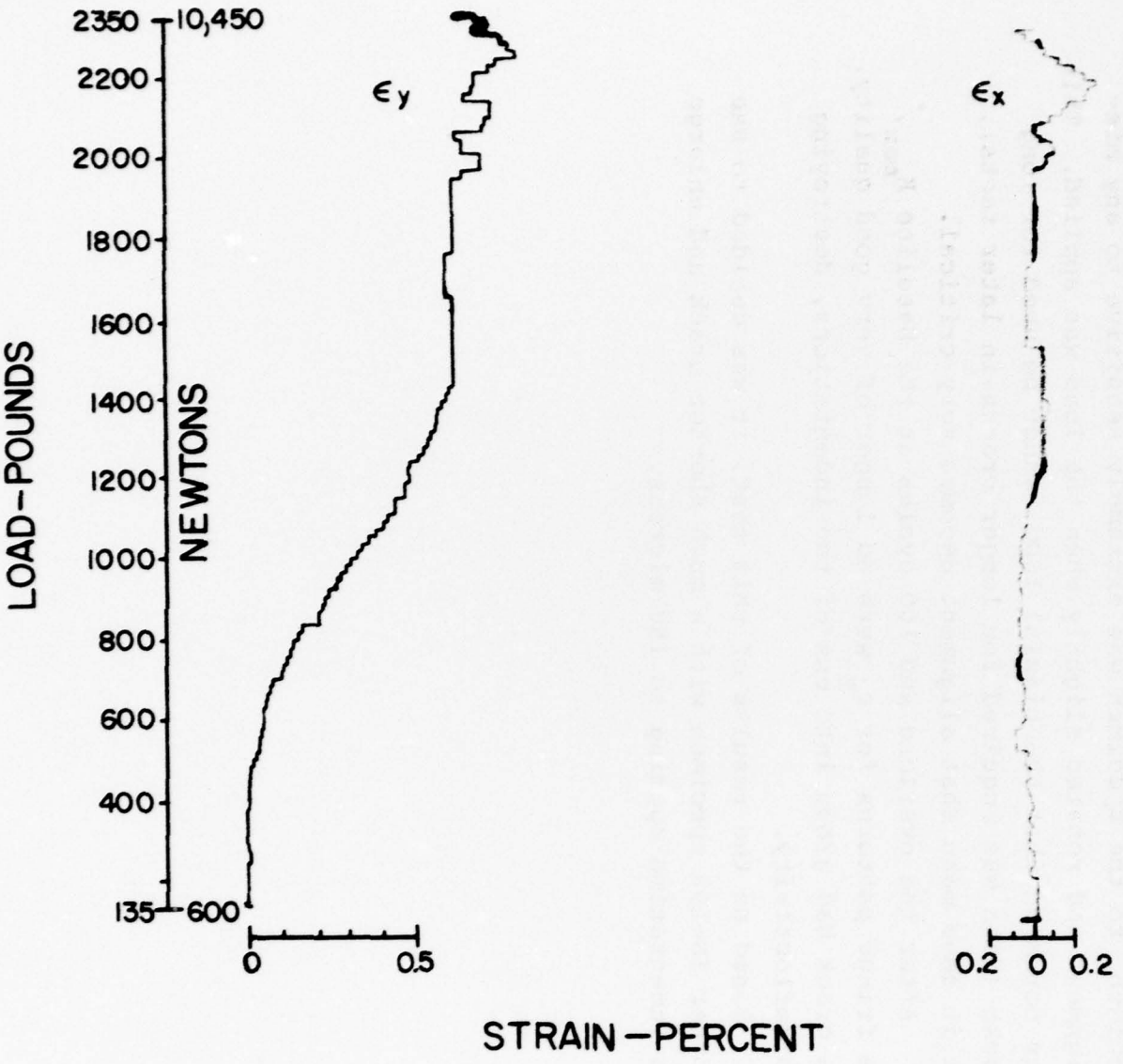

Figure 53 Strains ε_x and ε_y for Test 9 during overload.

Test 10

Material - IN-100 (new specimen)
Crack length - a = 19.54 mm
Baseline K_{max} - 23.2 ksi-$in^{1/2}$ (25.5 $MN/m^{3/2}$)
Test temperature - Room
Overload ratio - 1.73
Hold-time - none
Indentations location - 100 microns ahead of tip
Indentation spacing - 150 microns

Figure 54 shows the configuration of the indentations; this same orientation was used in all biaxial strain tests. Figure 55 shows the considerable improvement attained by increasing the indentation spacing and thereby bringing more "spots" into the PMT slit. Compare Figure 55 with Figure 50, but note the different voltage scales.

Strains ε_x and ε_y recorded before, during, and after the overload are plotted in Figure 56. ε_y shows little difference before and after the overload; recall that the CTOD measurements did not change very much either. There is a large tensile hysteresis loop in ε_y during the overload cycle as could be expected. The increase in tensile strain in the y-direction as a result of the overload is $\sim$ 0.15 percent. ε_x shows a slight compressive strain with loading before and after the overload. The overload strain is somewhat unexpected in that it shows a tensile hysteresis--this requires further investigation to determine if this is correct.

The strains in Figure 56 were recorded by loading with a triangular pulse 40 seconds long for the baseline K data and 80 seconds long for the overload. These long durations are necessary to gain the required sensitivity. One bit output corresponds to a strain of 0.0023 percent (23 microstrain) for this gage length. This translates to a sensitivity of $\sim$ 0.8 percent per volt for the system. The sensitivity is clearly adequate as can be seen from the plots in Figure 56.

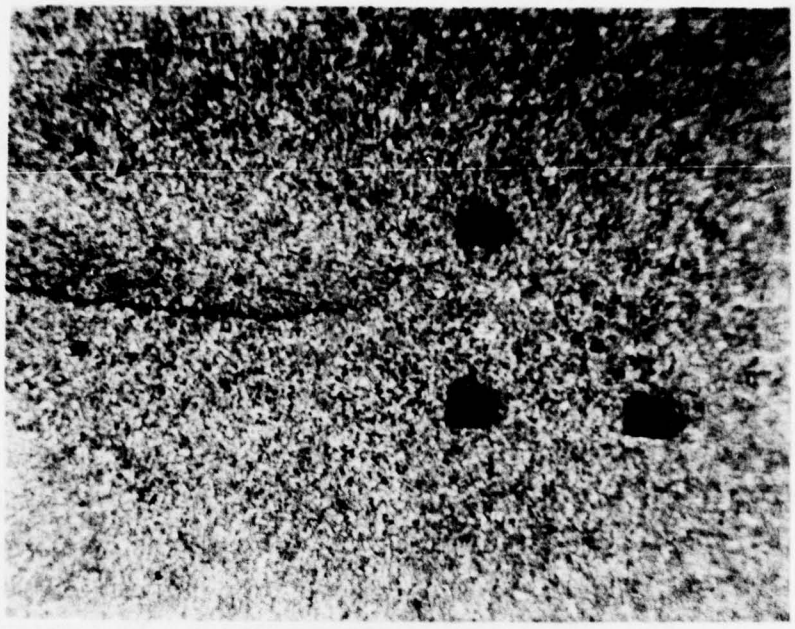

Figure 54 Indentations for Test 10 before overload. The indentation spacing in 150 microns.

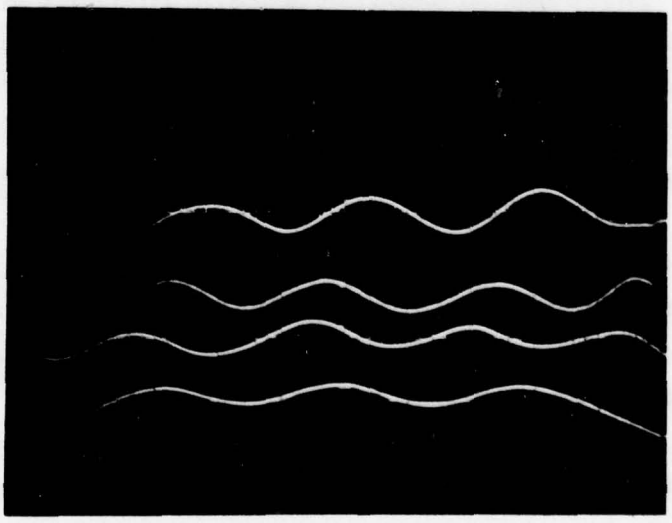

Figure 55 Fringe pattern signals from three indentations spaced 150 microns apart.

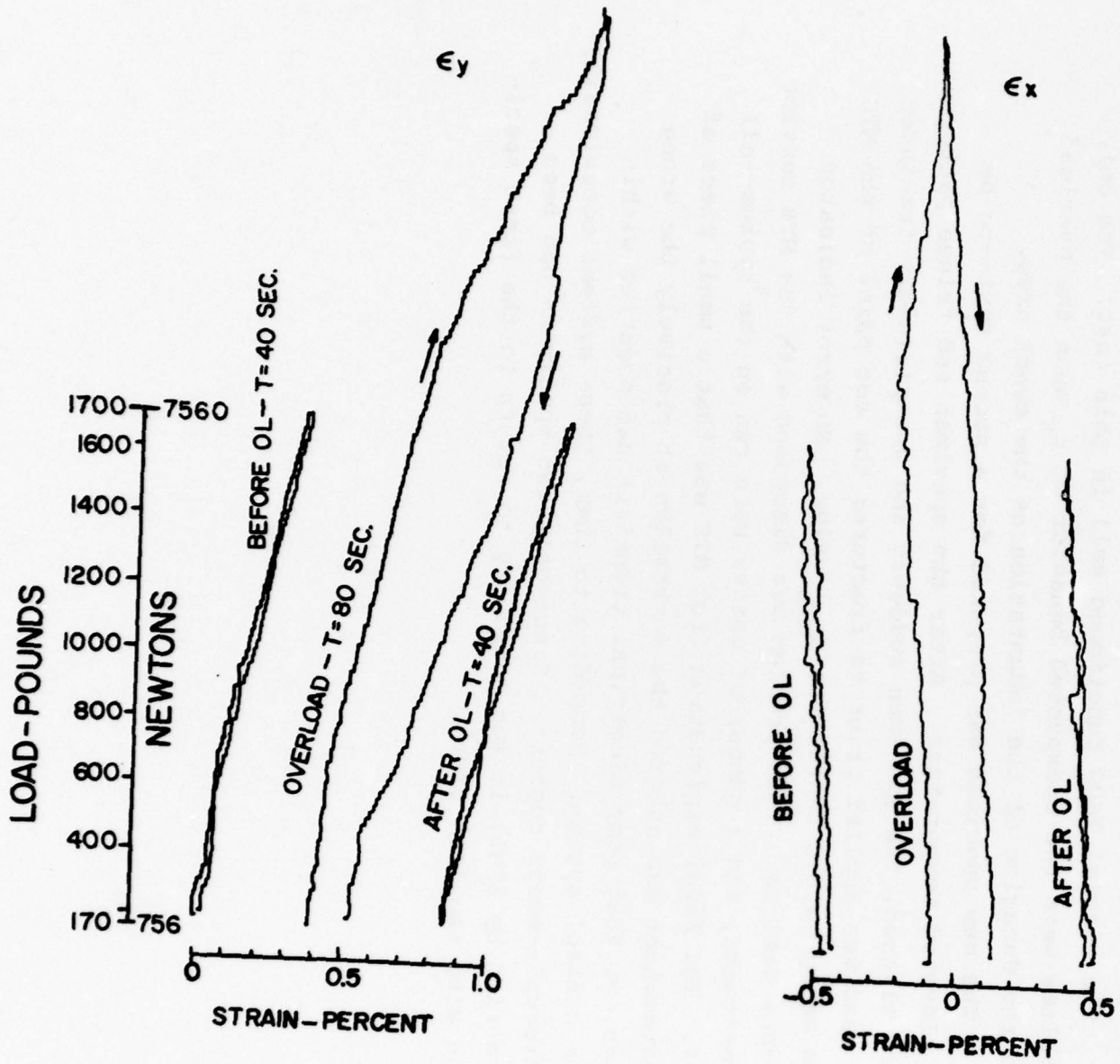

Figure 56 Biaxial strains before, during, and after the overload for Test 10.

Figure 57 shows the strains recorded after various numbers of cycles after the overload. There are some spurious max/min occuring in the ε_y fringe patterns. The fringe patterns on those two channels had deteriorated a bit; this is probably caused by the crack coming so close to one of the indentations as it grew through the plastic zone (see Figure 58).

The biaxial ISDG functioned well in this test. The only problems were the unexpected behavior of ε_x upon the overload and the damaging of the indentation as the crack grew.

The new specimen was prepared for a second test--to be at elevated temperature. After the specimen and fringe patterns were aligned, the specimen suddenly and unexplainedly fractured. No load was applied prior to fracture; the set point of the MTS was being raised to set the K_{min} value. No error indicator lights came on. This problem was discussed with the MTS service department, and a number of checks were run on the system--all O.K. The final explanation from MTS was that a small piece of contaminant had entered the servovalve at precisely the wrong time, or that some electrical transient had occurred within the control system. According to them, these systems occasionally "hiccup"--small comfort. Since only two specimens had been provided by AFML, it was necessary to return to the first specimen with the long crack.

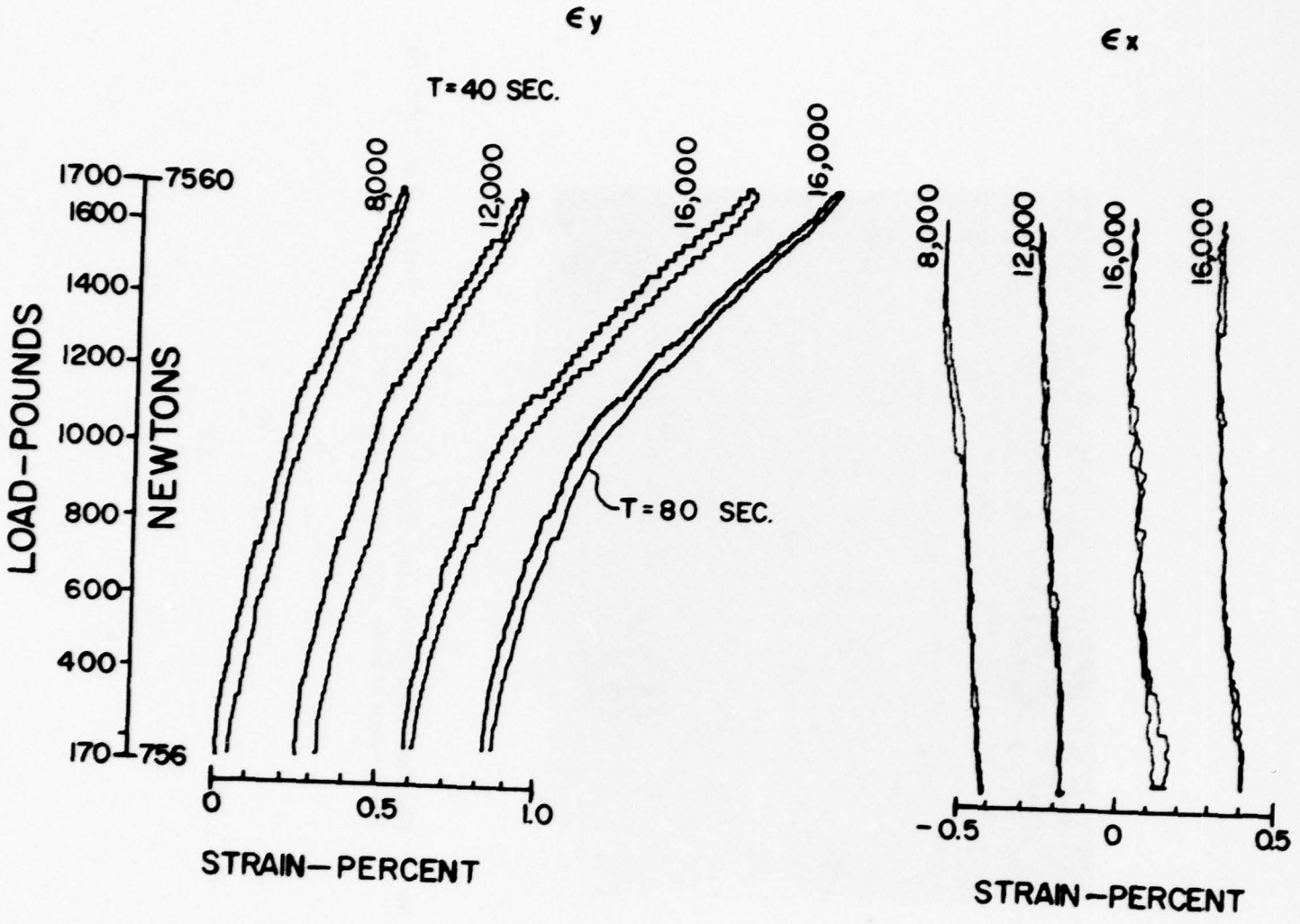

Figure 57. Biaxial strains taken after the overload for Test 10.

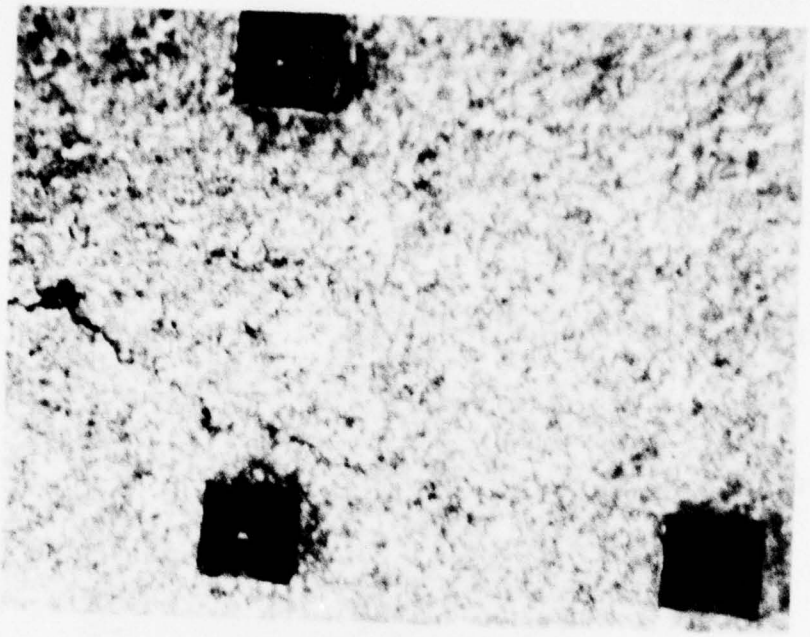

Figure 58 Photomicrograph of the crack and indentations after Test 10. The indentations are 150 microns apart.

Test 11

Material - IN-100
Crack length - a = 39.3 mm
Baseline K_{max} - 23.2 ksi-in$^{1/2}$ (25.5 MN/m$^{3/2}$)
Test temperature - 732°C
Overload ratio - 1.73
Hold-time - 10 minutes before overload
Indentations location - 100 microns ahead of tip
Indentation spacing - 150 microns

Figure 59 shows the strains ε_x and ε_y recorded at room temperature and 732°C. Note the increase in tensile strain for ε_y as well as the addition of a large hysteresis loop. The strain ε_x is not very large in either case, but shifts more towards tensile values at the elevated temperature. Because of the very large strain at elevated temperature, it was necessary to run a slow loading ramp with T = 100 seconds.

Creep at 732°C and K_{max} is shown in Figure 60. The specimen was loaded to K_{max} and held there for 10 minutes. A little creep was observed on ε_y, but a lot of tensile creep was seen for ε_x. The creep of ε_x was not due to spurious max/min; the fringes were actually seen to move on the oscilloscope during the hold-time.

After the hold-time and as preparations were being made to apply the overload, the fringe patterns for ε_y deteriorated to such an extent as to be unusable. Post-test examination of the specimen showed that the crack had grown during the hold-time and curved into the upper indentation--destroying its reflectivity (see Figure 61).

Nevertheless, the overload cycle was run with T = 200 seconds with the result for ε_x shown in Figure 62. The behavior of ε_x seems reasonable.

The program worked well for this test, but one of the indentations was damaged by the crack. The ISDG was shown to function under short-term creep conditions. To avoid damaging the indentations, they were placed further from the tip in the next experiment.

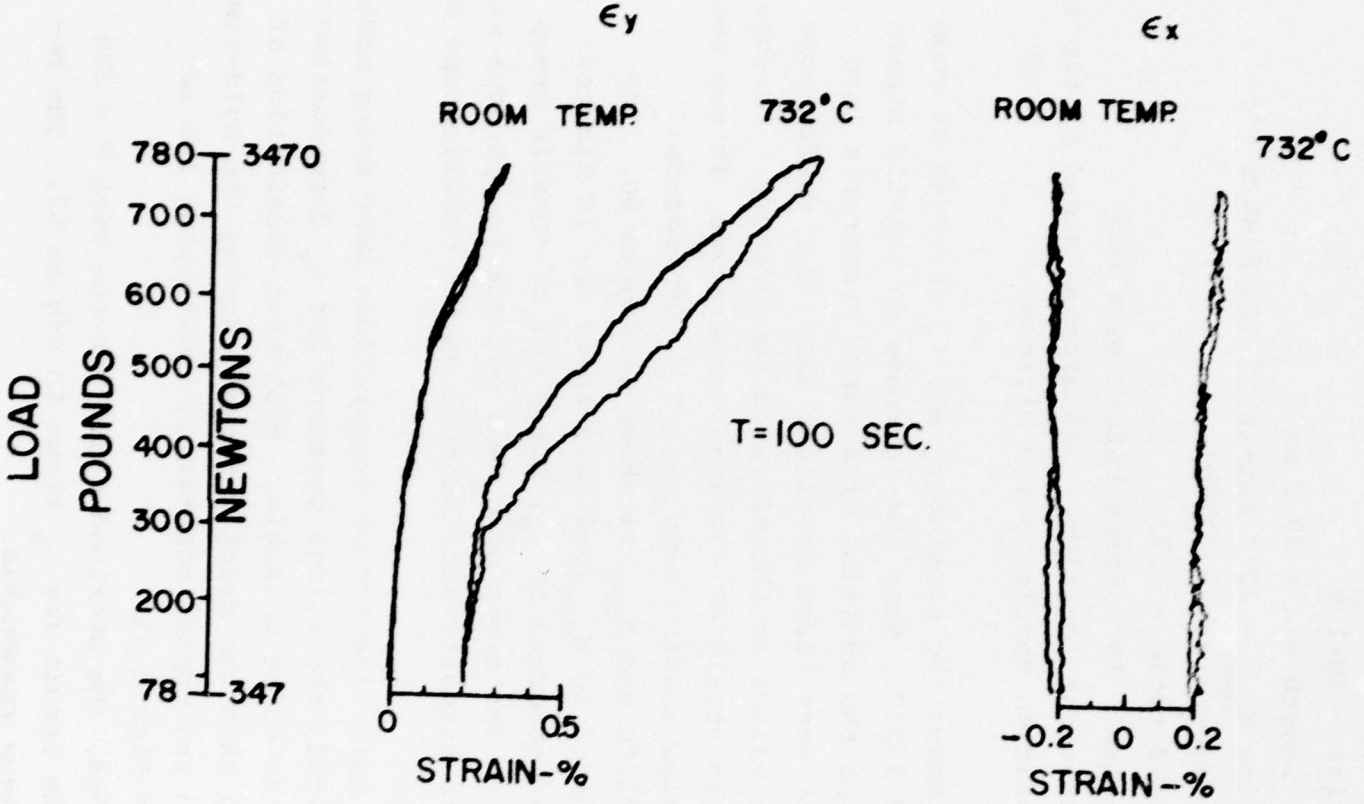

Figure 59 Biaxial strains at room temperature and 732°C for Test 11.

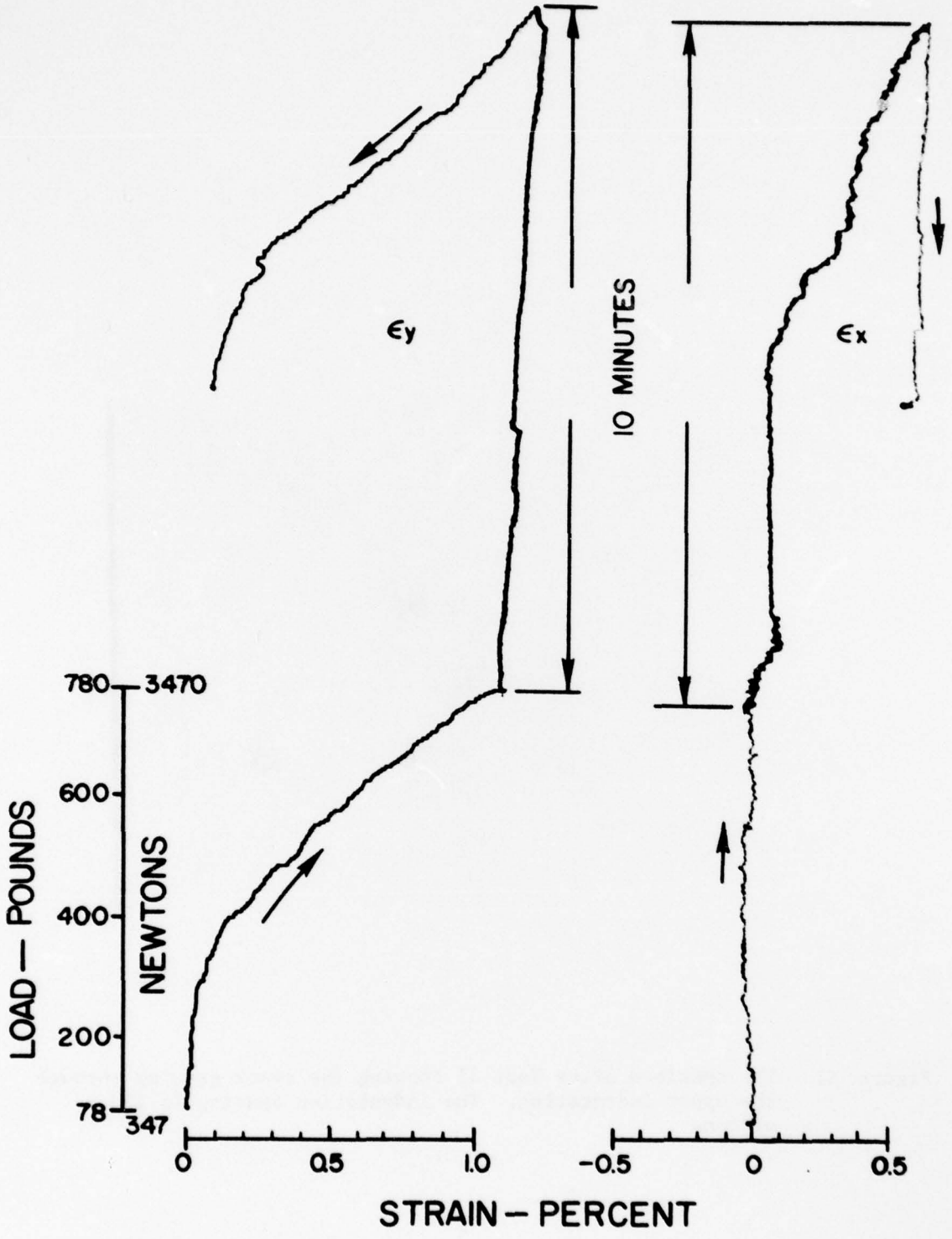

Figure 60 Biaxial strains versus load and time for Test 11. 732°C.

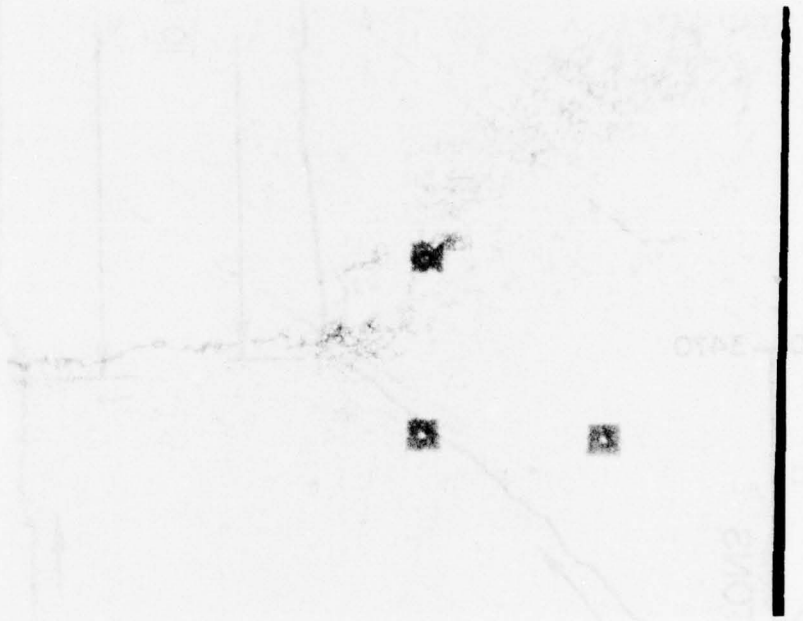

Figure 61 The specimen after Test 11 showing the crack growing through the upper indentation. The indentation spacing is 150 microns

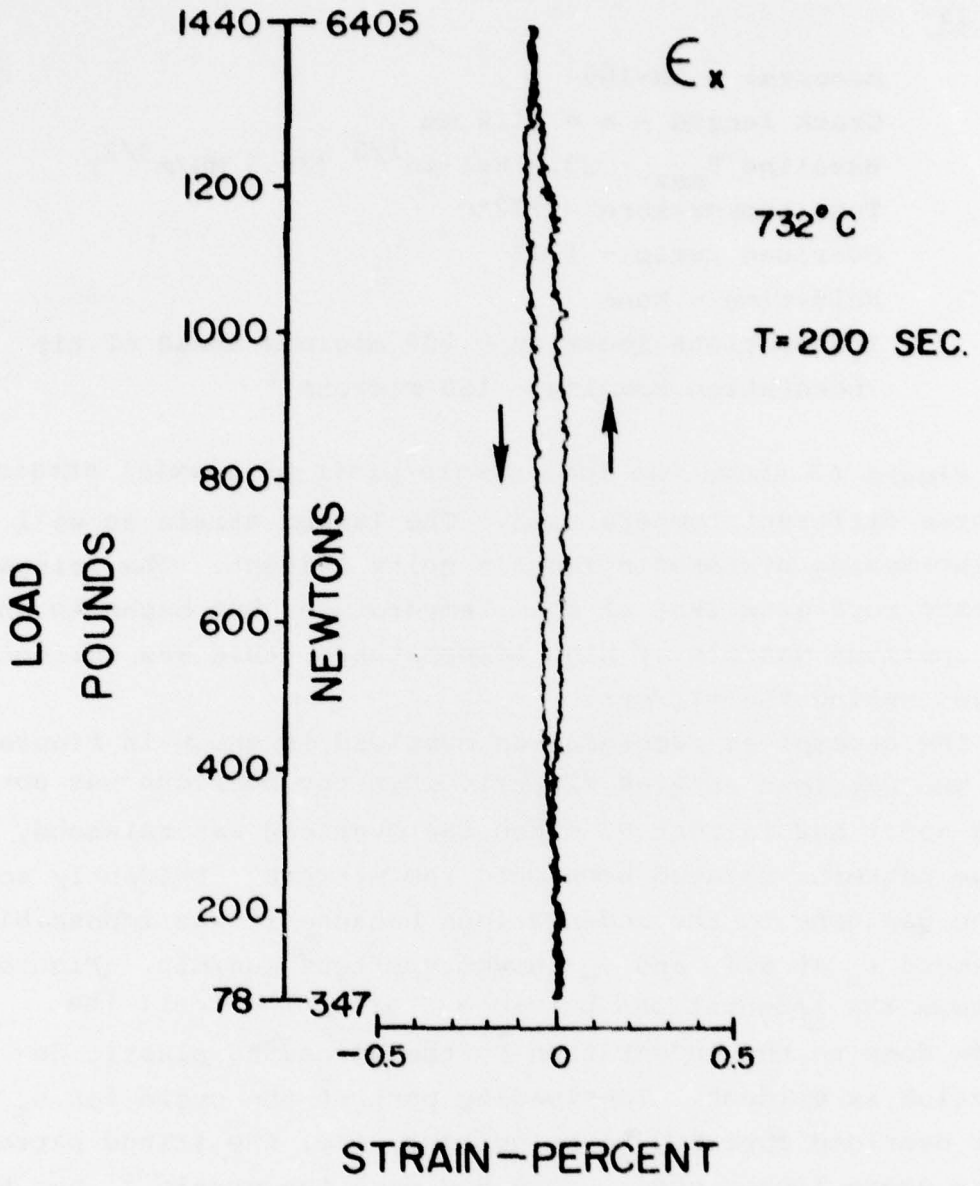

Figure 62 ϵ_x during the overload of Test 11 at 732°C.

Test 12

Material - IN-100
Crack length - a = 41.8 mm
Baseline K_{max} - 23.2 ksi-$in^{1/2}$ (25.5 $MN/m^{3/2}$)
Test temperature - 732°C
Overload ratio - 1.73
Hold-time - None
Indentations location - 200 microns ahead of tip
Indentation spacing - 150 microns

Figure 63 shows the load-strain plots of biaxial strain at three different temperatures. The larger strain as well as the increasing hysteresis loop is quite evident. The fringe patterns were excellent at room temperature, but began to show some spurious max/min at high temperatures; this was corrected by readjusting the mirrors.

The attempt at recording an overload is shown in Figure 64. The specimen rotated slightly when the overload was applied as it had in Test 9. When the overload was released, the fringe patterns rotated back onto the mirrors. Evidently some damage was done to the indentations because it was impossible to record ε_x at all, and ε_y showed spurious max/min. Figure 65 shows the indentations before and after the test; the damage done to the indentation by the spreading plastic deformation is evident. The loading part of the cycle for ε_y after overload appeared to be correct, i.e. the fringe patterns on the scope looked good. Note how much the strain ε_y has been changed by the overload.

The recording difficulty here was caused by the spreading plastic zone associated with the overload.

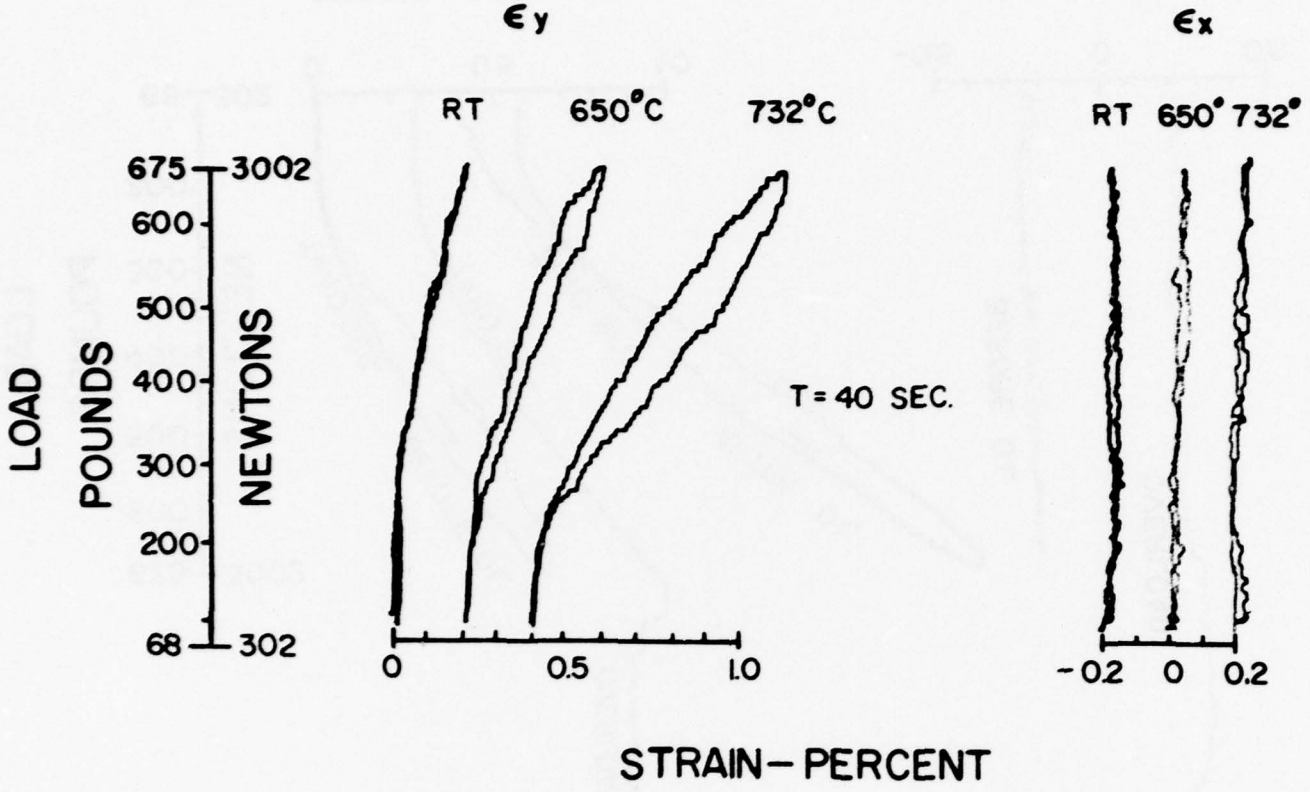

Figure 63 Biaxial strains at three temperatures for Test 12.

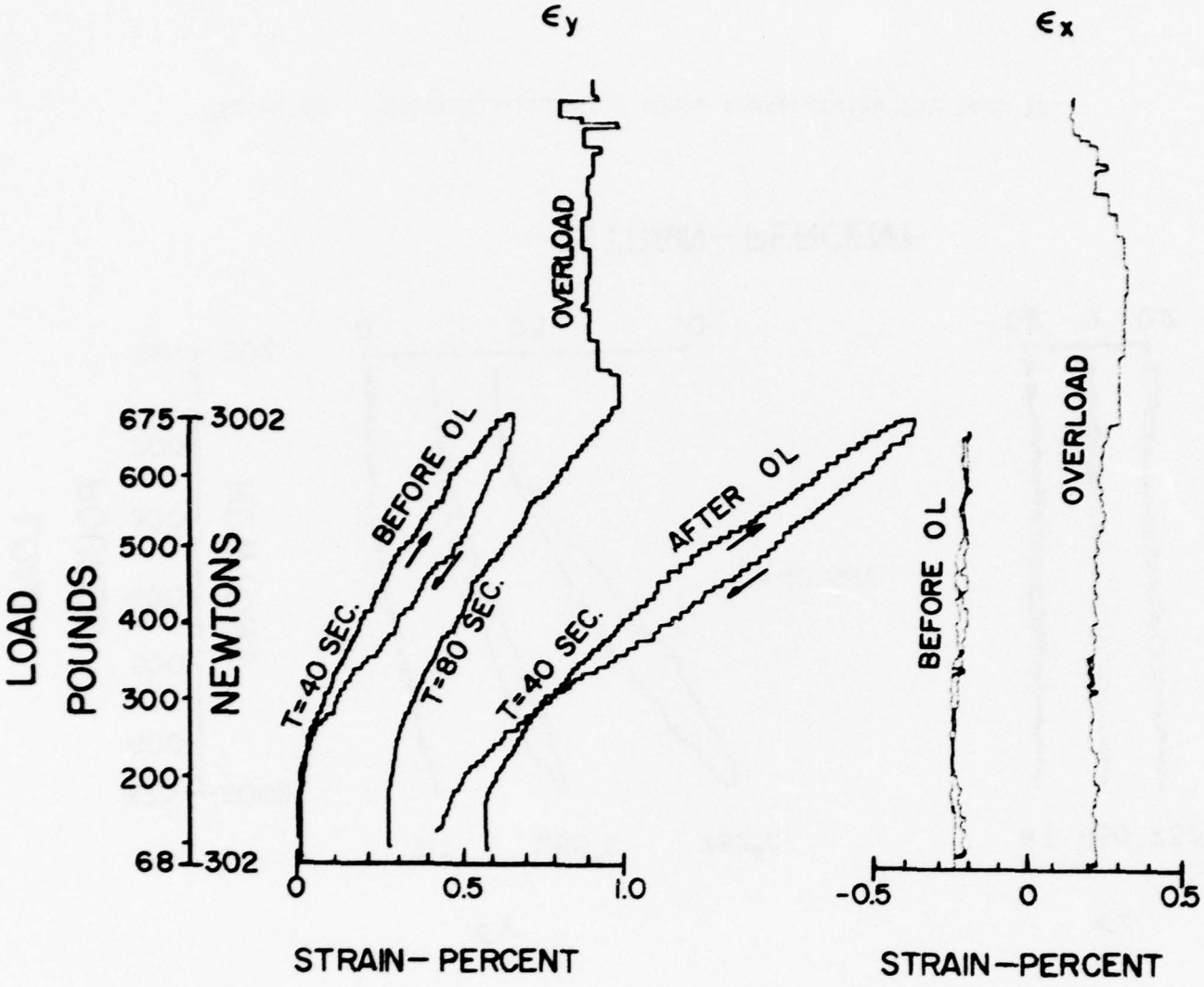

Figure 64 Biaxial strains before, during and after overload for Test 12.

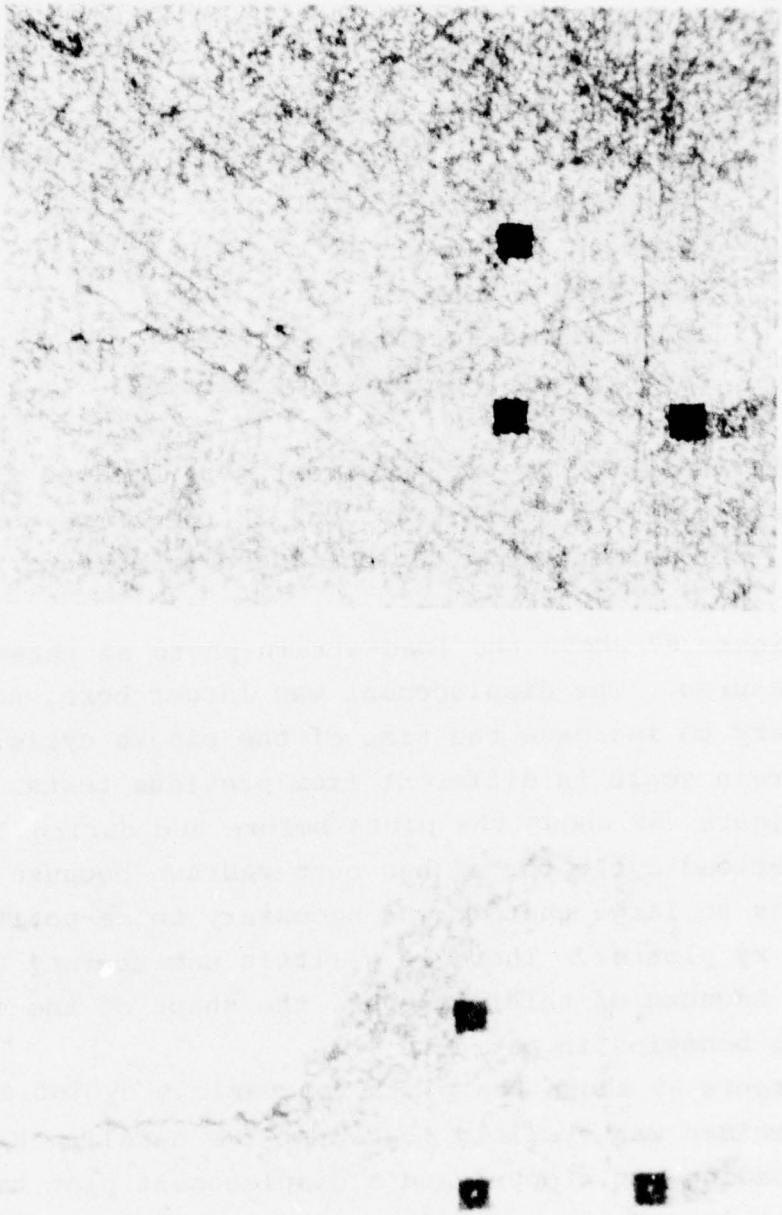

Figure 65 The crack and indentations before and after Test 12. Indentation spacing is 150 microns.

Test 13

Material - IN-100
Crack length - a = 43.0 mm
Baseline K_{max} - 23.2 ksi-$in^{1/2}$ (25.5 $MN/m^{3/2}$)
Test temperature - 732°C
Overload ratio - 1.73
Hold-time - None
Indentations location - at tip
Indentation spacing - 150 microns

The indentations for this test were located right across the crack tip--see Figure 66. One is therefore not measuring strain, but is measuring the opening displacement right at the tip.

Figure 67 shows the load-strain photo at three different temperatures. The displacement was larger here, so it was necessary to increase the time of the single cycle. Note that the strain scale is different from previous tests.

Figure 68 shows the plots before and during the overload. The overload cycle for ε_y has been redrawn because the displacement was so large that it was necessary to re-position the pen on the xy plotter. There is a little uncertainty in the strain values because of this; however, the shape of the curve and general behavior is correct.

Figure 69 shows the plots for various cycles after overload The specimen was cyclicly loaded at the baseline K at 10 Hz; then loading was stopped and a displacement plot taken. No significant changes were noted until after 4000 cycles. A photograph of the indentations after the test is in Figure 66.

The ISDG worked very well here; the fringes remained bright and distinct throughout the test. The amount of relative displacement for indentations at this location is really too much for the small displacement program. The CTOD program would provide adequate resolution for the overload and would record much faster.

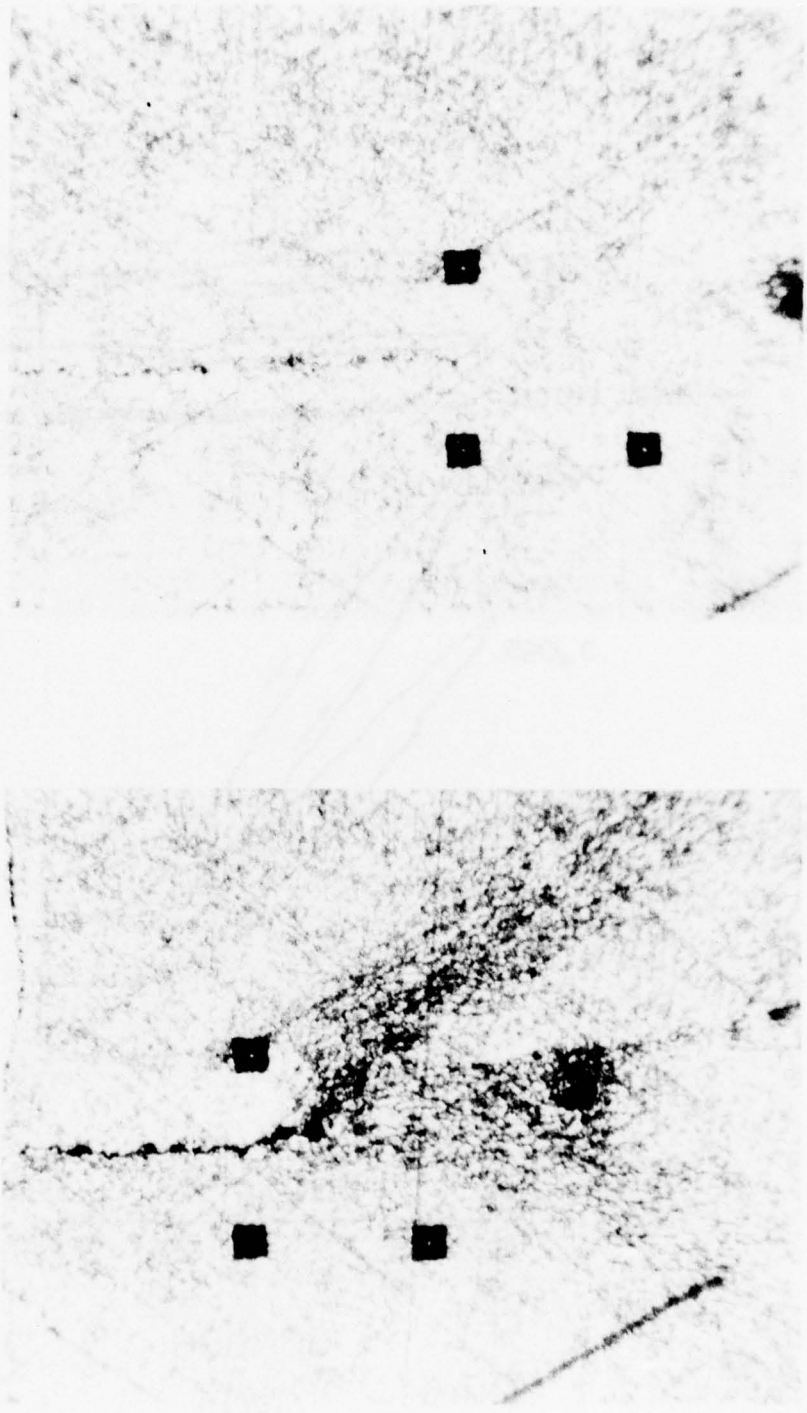

Figure 66 The crack and indentations before and after Test 13. Indentation spacing is 150 microns.

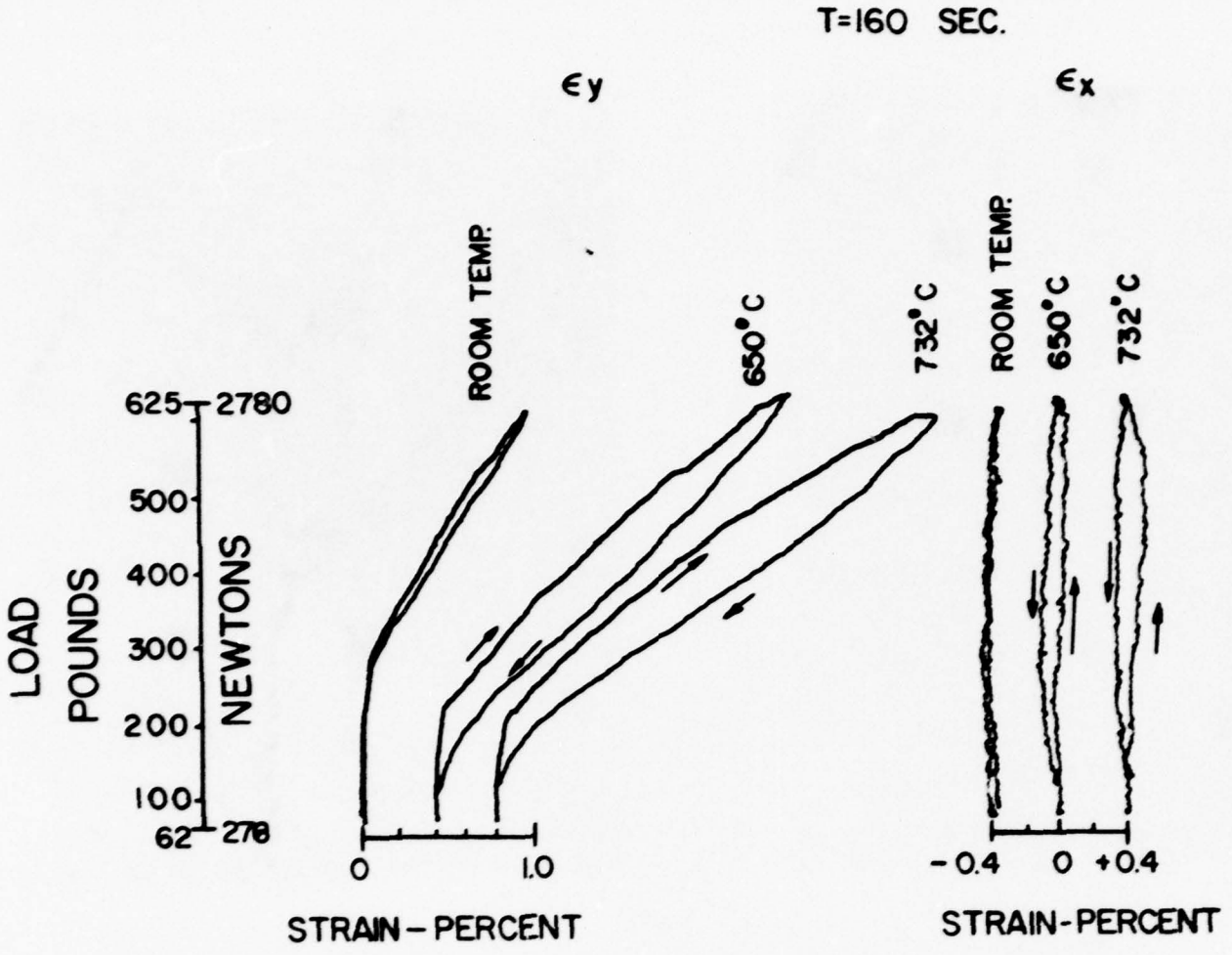

Figure 67 Biaxial strains at three temperatures for Test 13.

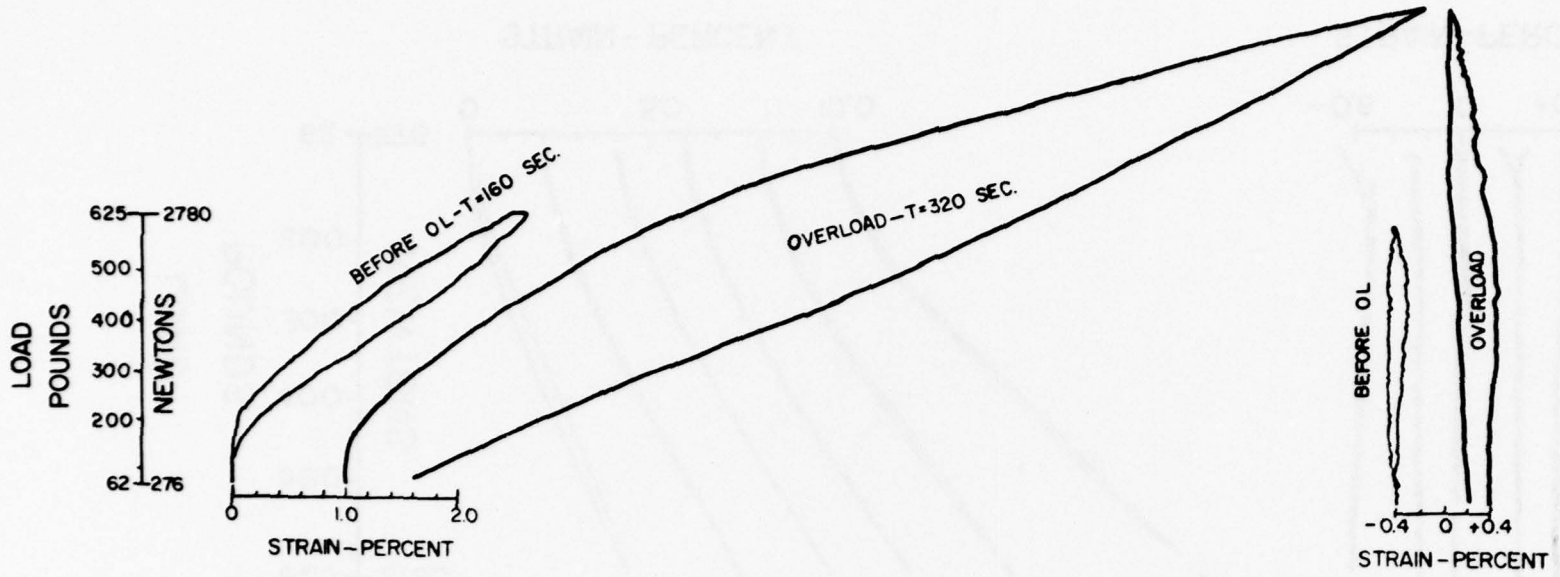

Figure 68 Biaxial Strains before and during overload for Test 13. 732°C.

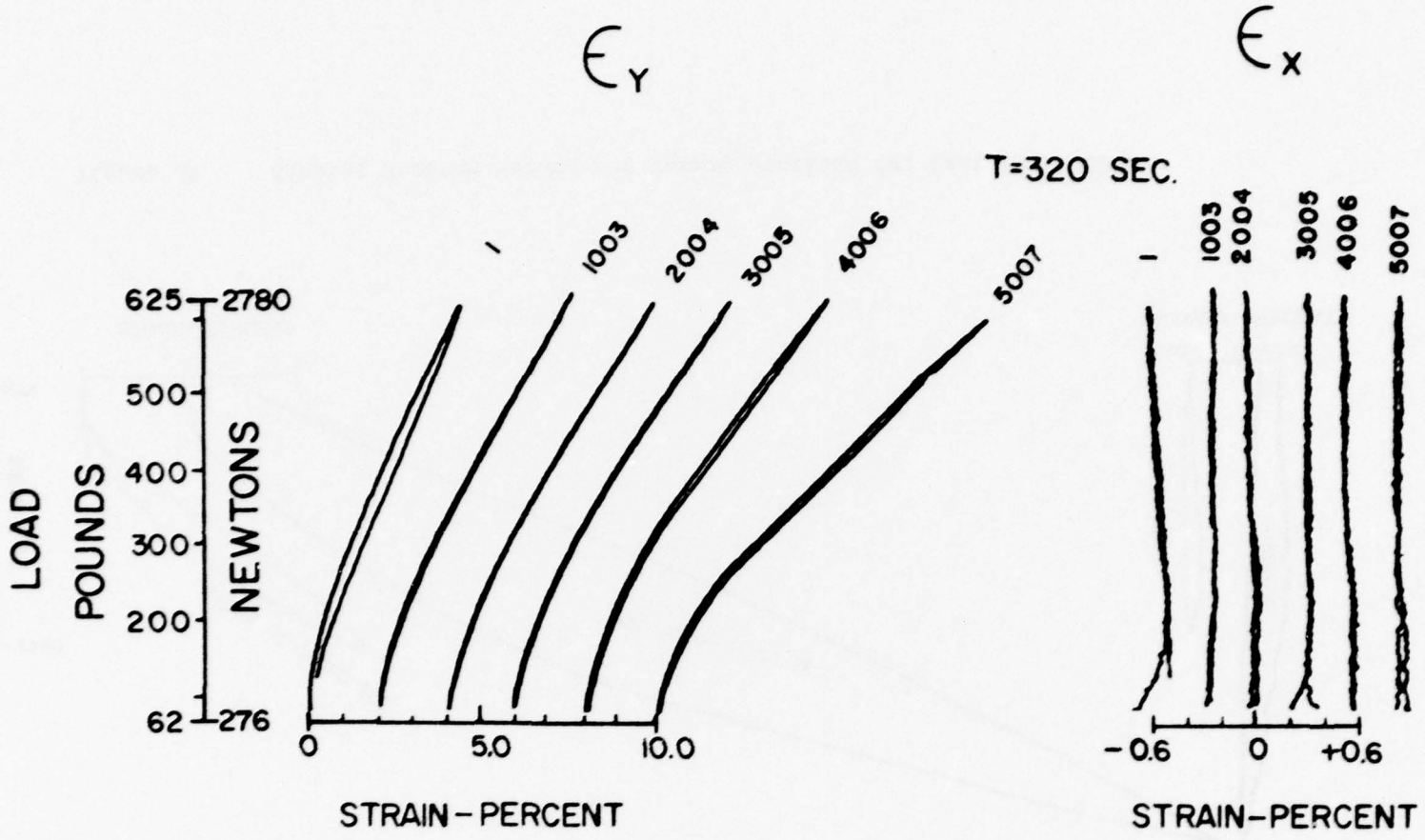

Figure 69 Biaxial strains at various cycles after the overload of Test 13. 732°C.

Test 14

Material - IN-100
Crack Length - a = 44.6 mm
Baseline K_{max} - 23.2 ksi-$in^{1/2}$ (25.5 $MN/m^{3/2}$)
Test temperature - Room
Overload ratio - 1.73
Hold-time - None
Indentations location - 100 microns ahead of tip
Indentation spacing - 150 microns

This was an attempt to repeat Test 10 to examine the behavior of ε_x during the overload. However, the specimen rotated slightly upon overload, so that the fringe patterns no longer hit the mirrors. Bear in mind that Test 10 was on the other IN-100 specimen with a much shorter crack (a = 19.54 mm). After the overload the fringe patterns returned to the mirrors. Biaxial strains recorded before and at various times after the overload are shown in Figure 70. The fringe patterns deteriorated as the crack grew through the plastic zone.

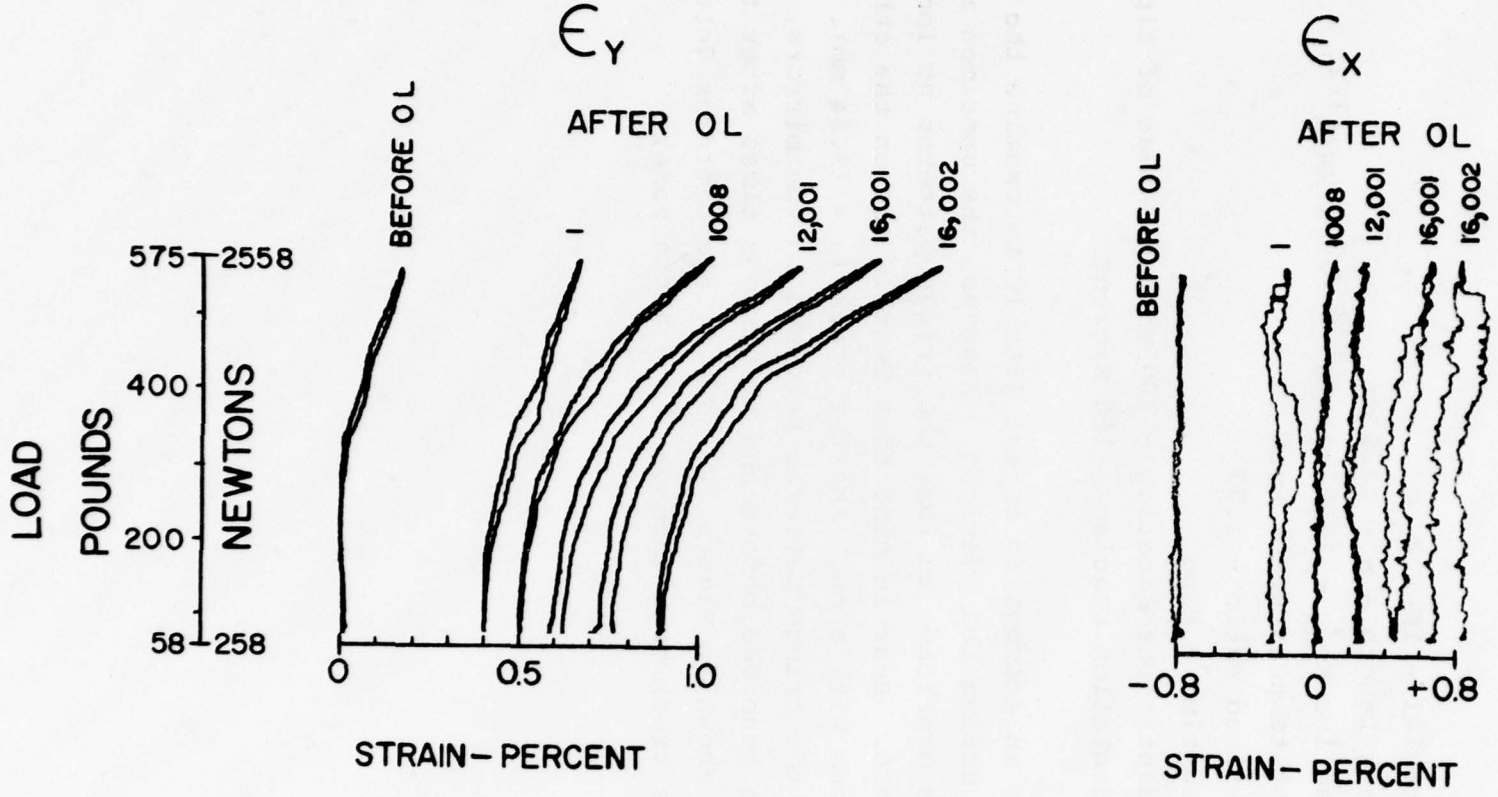

Figure 70 Biaxial strains before and after the overload for Test 14.

Test 15

Material - IN-100
Crack length - a = 45.6 mm
Baseline K_{max} - 23.2 ksi-$in^{1/2}$ (25.5 $MN/m^{3/2}$)
Test temperature - Room
Overload ratio - None
Hold-time - None
Indentations location - 200 microns ahead of tip
Indentation spacing - 150 microns

In this experiment the indentations were placed ahead of the crack tip and the crack grown toward them at the baseline K_{max}. Figure 71 shows the relation of the crack to the indentations before the loading started and after 6000 cycles of growth. Figure 72 plots the biaxial strain recorded every 1000 cycles; the specimen was loaded at a rate of 10 Hz which was slowed to record the strains.

In contrast to the overload tests, the ISDG is able to record the strains ahead of the tip as it grows at a constant K. After the crack tip has grown through the indentations, the CTOD program would be the better one to use.

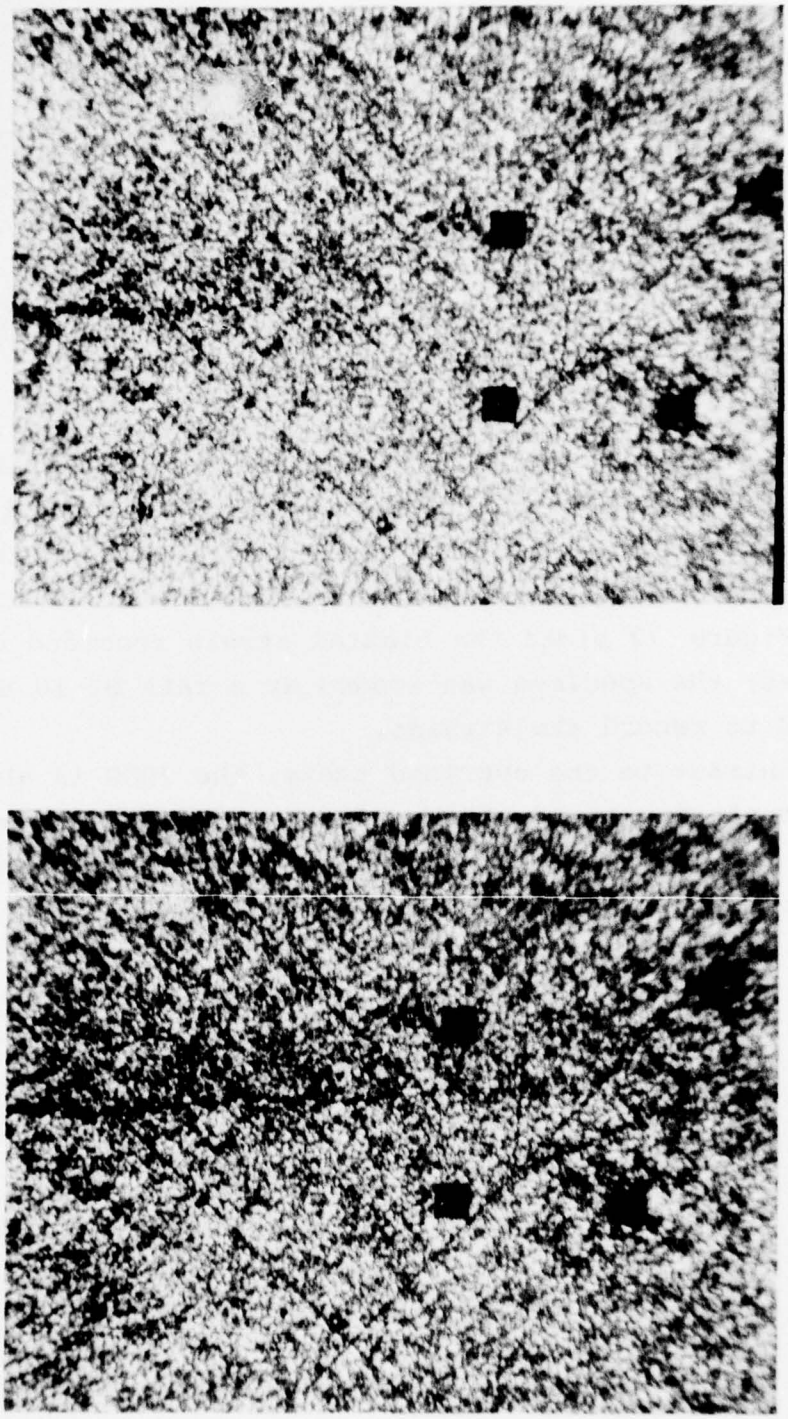

Figure 71 Photomicrographs of the crack before and after Test 15.

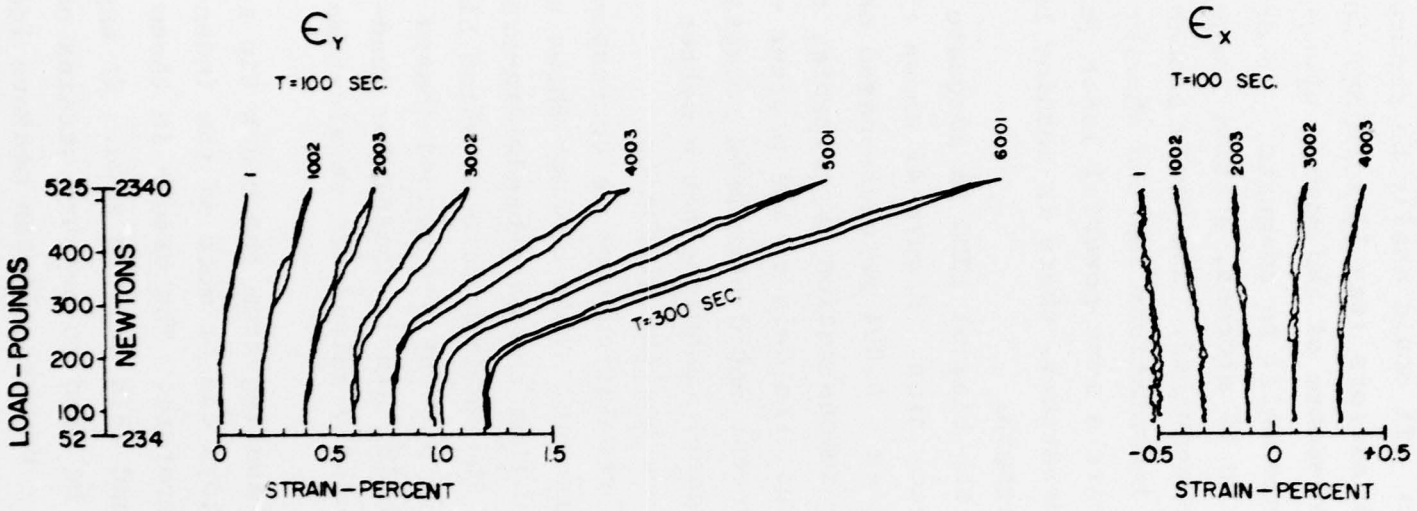

Figure 72 Biaxial strains recorded during Test 15.

4. Concluding Remarks

The gage-length used in these experiments was 150 microns. This was determined by the size of the mirrors and their distance from the specimen. It could easily be reduced to 100 microns by using larger mirrors (say 12 x 12 mm) in the existing system; the frequency response of the mirror system and the aperture of the PMT would still be adequate. If one wished to reduce the gage-length to 50 microns, a still larger mirror and larger PMT would be required. One would probably want to reduce the size of the indentations for the shorter gage-length; this would in turn require a more powerful laser (e.g. 15 mw). Aside from these considerations, there is nothing to prohibit use of a shorter gage-length.

The resolution of the biaxial ISDG is adequate for measurement of strains near crack tips. Figure 49 shows that it can detect strains as small as $\sim$ 0.004 percent--based on a gage-length of 150 microns. In the demonstration experiments, to accommodate the largest strain values, the gain on the plotter was set so that a resolution of 0.05 percent would have been acceptable. In other words, the measurement technique has a better sensitivity than is actually needed--a healthy situation.

With the increased resolution comes a corresponding decrease in rate of measurement. This concept shows up in electronics in the statement that the gain-bandwidth-product of an amplifier is constant. The maximum rate at which biaxial strains can be measured is $\sim$ 0.01 percent per second (based on 150 micron gage-length). While this is useful for load-strain measurements, it is particularly suited for strain-time measurements in creep experiments.

The plastic zone emanating from the crack tip as overload is applied usually destroys one or more of the indentations--especially at high temperature. The cracks in these experiments all tended to curve around this plastic zone. It appears that the biaxial ISDG cannot be used to measure strains near the crack tip for overloads. However, it can measure local strains during cyclic crack growth. Some of the difficulty in recording

overloads was associated with the long crack in the compact-tension specimen. Overload strains were successfully recorded at room temperature for another specimen with a short crack.

Initial alignment of the fringes on the mirrors and PMTs is critical for biaxial strain measurements. The four fringe patterns were always monitored on an oscilloscope during recording to see if spurious max/min occurred. Observation of fringe motion increased confidence in the validity of the data.

In summary, the biaxial ISDG can record real-time strains in regions without excessive deformation with excellent resolution, but at a slow rate.

SECTION VI
DISCUSSION

The capabilities and limitations of both the CTOD and biaxial strain measurement systems have been examined and discussed in Sections 4 and 5. This section is devoted to a few general comments on the techniques and the results they produce.

The demonstration experiments showed that there is very little difference in difficulty in making elevated temperature measurements as compared to those at room temperature. It is no more difficult to align the patterns and operate the programs at higher temperatures. The main difference with a high temperature test is that one has to wait for the specimen to heat up and cool down; hence, they take longer to perform. The greater deformation of the material changes the rates at which one can record at high temperature.

The slow recording rate for strain at high temperatures may seriously restrict the use of the technique because of the creep that may occur during recording. That did not appear to be a problem with this superalloy, but it might be with other materials. Undoubtedly this first version of the biaxial strain program could be speeded up somewhat, but very fast recording rates (e.g. 1 Hz) seem unlikely if one is to retain the high resolution. If one needs to record strain at testing rates, then the only solution appears to be to sacrifice the convenience of real-time measurement and record the fringe pattern signals for post-test processing. On the other hand, both systems are ideal for creep measurements.

The demonstration experiments have provided the first information on the strains and displacements close to the crack tip at elevated temperature. Now that one has an idea of their magnitude, the CTOD or strain program can be selected as needed. For example, it would be much better to use the CTOD program for measuring the displacement at the tip when an overload is applied (see Figure 68).

Strain parallel to the crack tip, ε_x, is very small compared to ε_y; in fact, little is to be gained recording it. At other positions ahead of the tip and off the crack line this would not be true and the biaxial capability would be fully utilized. The most interesting place to record strain/displacement may well be right at the tip. A critical CTOD has been proposed as a fracture criterion [23], but has suffered from an inability to measure CTOD.

Coating the specimen with chromium and platinum is not absolutely necessary for IN-100. The specimen used was subjected to approximately fourteen hours at 732°C as well as the heating and cooling associated with seven high temperature tests. The surface was still reflective and indentations produced good fringe patterns. Figure 73 shows photographs of the fringe patterns emanating from indentations placed on the plated and unplated side of the specimen. The ones on the plated side are brighter and more distinct. One must realize that the unplated side was also polished and oxidized in an rf furnace. One cannot expect to test IN-100 in any furnace without some special surface preparation. The extra effort associated with chromium and platinum plating appears worthwhile. Most metals will require coatings of various kinds to permit testing at high temperatures. This work shows that suitable coatings can be found to raise the maximum working temperature of the IDG for making measurements on two superalloys. Presumably suitable coatings can be found for other metals of interest.

One interesting use of the CTOD load-displacement curves is to establish the opening load of a fatigue crack. Fatigue cracks normally exhibit closure, i.e. they do not become fully open along their entire length until a certain load, P_{op}, is applied. One way to measure P_{op} is to determine the place in the load-displacement curve where a "knee" occurs (see Figure 31). The value of P_{op} that is determined is dependent on where the load-displacement plot is taken--see Figure 74. The best measurement of P_{op} would seemingly be right at the tip, but there

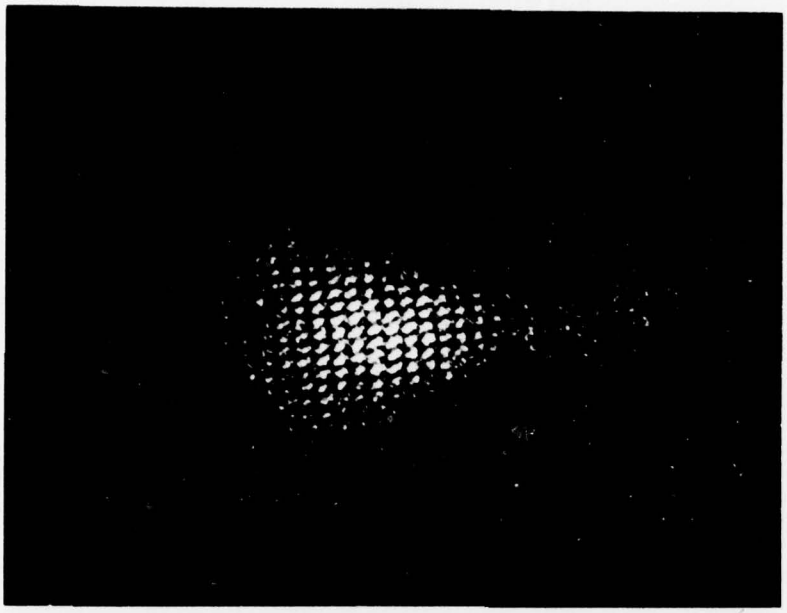

PLATED SIDE

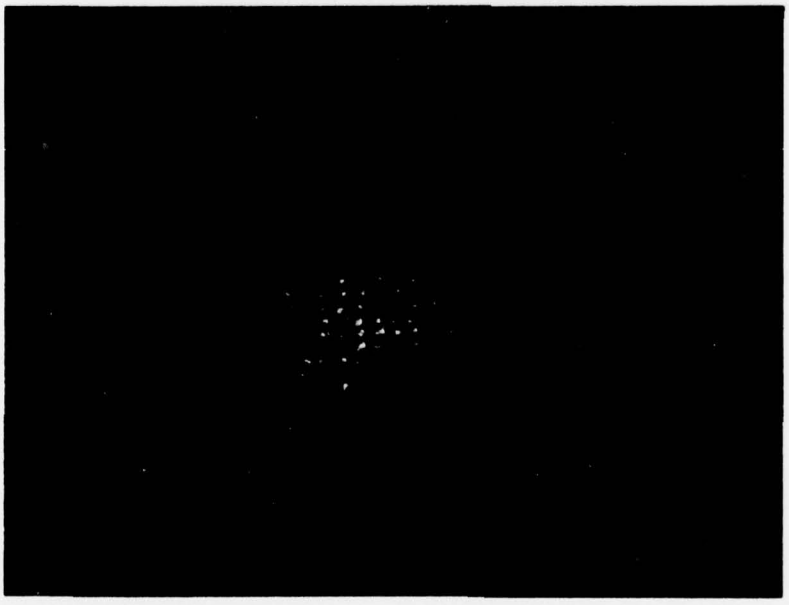

UNPLATED SIDE

Figure 73 Fringe patterns from sets of 3 indentations on the plated and unplated sides of the IN-100 specimen.

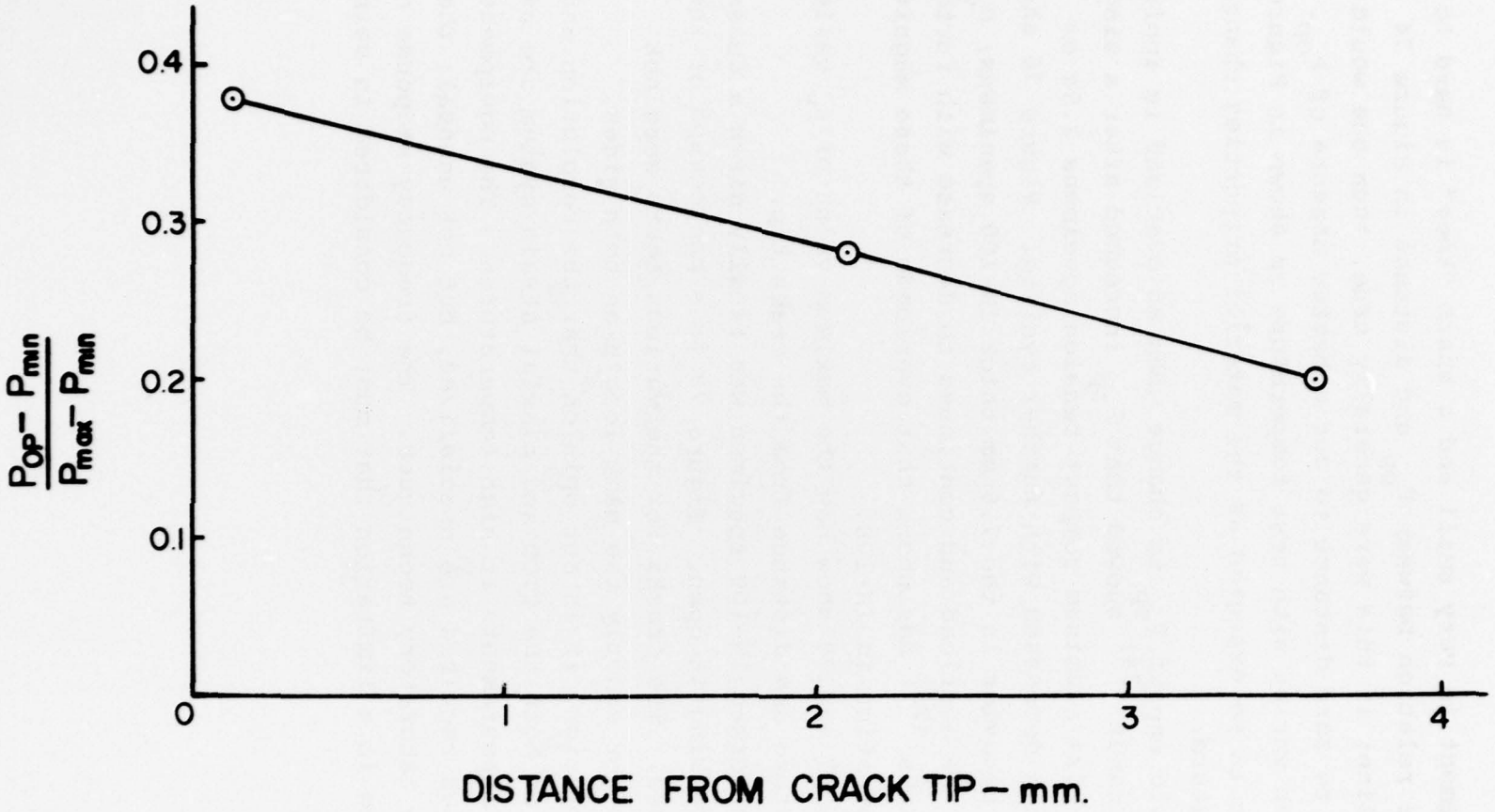

Figure 74 Opening load versus distance from tip for a crack grown at 25.5 $MN/m^{3/2}$ at room temperature.

the displacement is very small and a sharp "knee" is hard to define. The relation between P_{op} and distance in Figure 74 a straight line; if this were generally true, then one would extrapolate to zero distance to get a better measure of P_{op}.

P_{op} also varies with test temperature as shown in Figure 75. This is to be expected as the material properties change with temperature.

One would expect P_{op} to change when an overload is applied. Sharpe and Grandt [24] showed that P_{op} increased after a single overload in 2024 aluminum compact tension specimens 2.54 cm thick and then decreased with further cycling. Figure 76 shows a different behavior in the 7.6 mm thick IN-100 specimens; P_{op} drops after the overload and continues to decrease with further cycling. Macha [25] has shown that overloads of these magnitudes produce retardation in IN-100.

Figures 77 and 78 show how the maximum value of ε_y varies with temperature and distance from the crack tip.

The overworked IN-100 specimen was finally given a decent ending by breaking it open. Figure 79 is a photograph of the crack surfaces. The cracks for the various tests were not straight and not exactly the same length on both sides.

In conclusion, it is our opinion that the resolution and gage-length of both the CTOD and biaxial strain system are excellent for measurements at high temperatures. The equipment and techniques required are specialized, but not unusual; these are workable laboratory techniques. The frequency response of either system is a limitation that must be considered in using the ISDG.

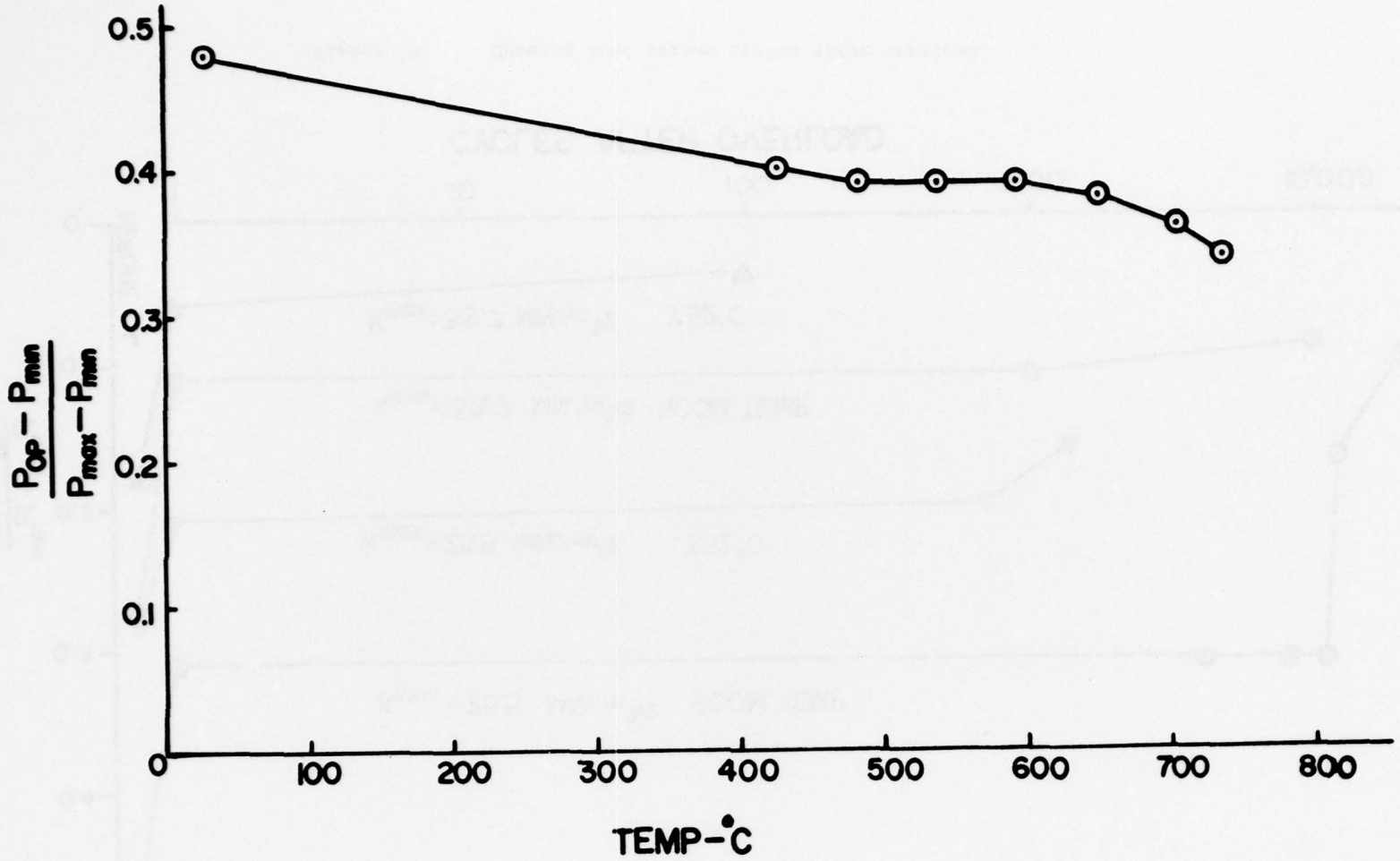

Figure 75 Opening load versus temperature for crack grown at 25.5 $MN/m^{3/2}$.

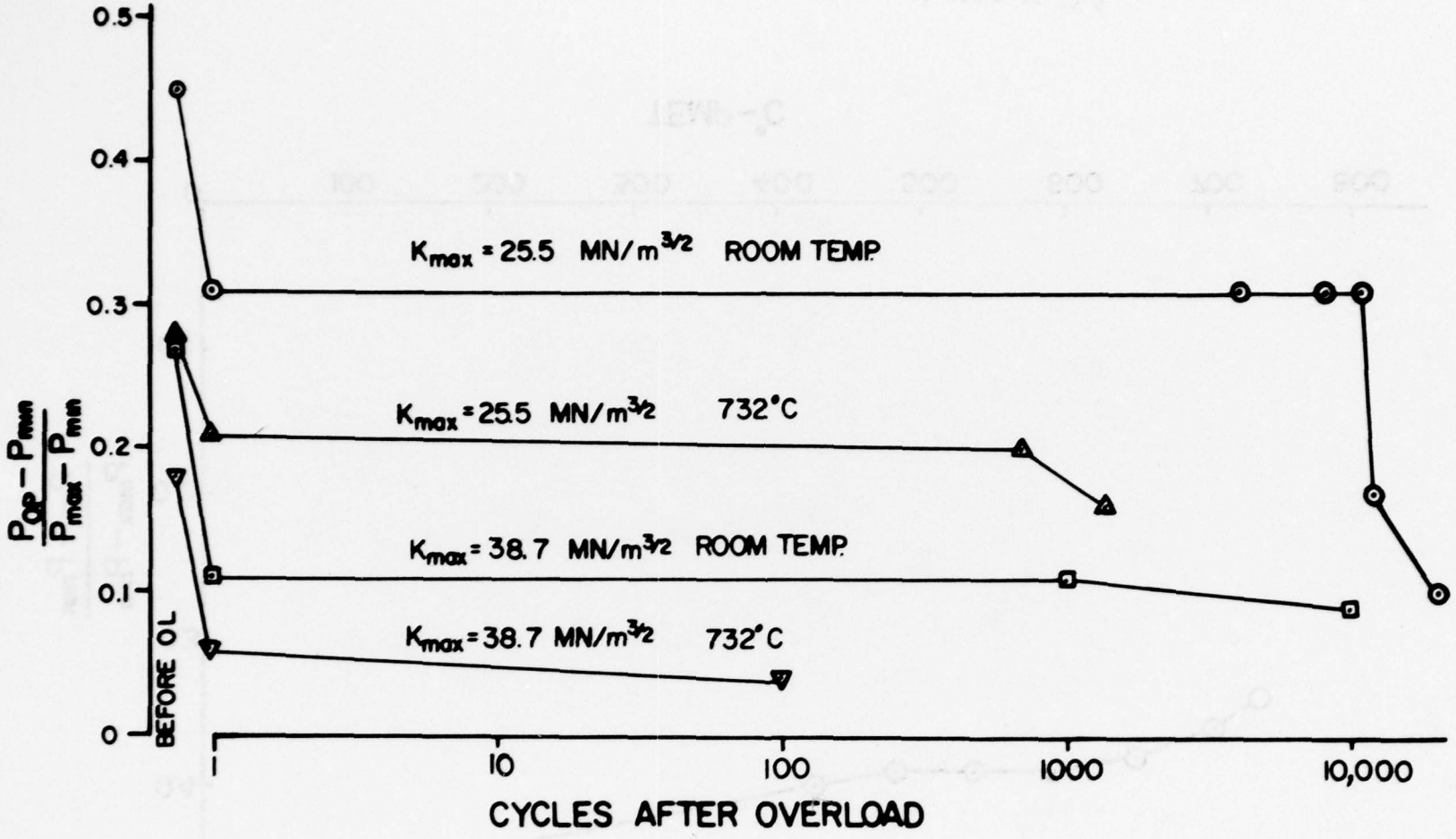

Figure 76 Opening load versus cycles after overload.

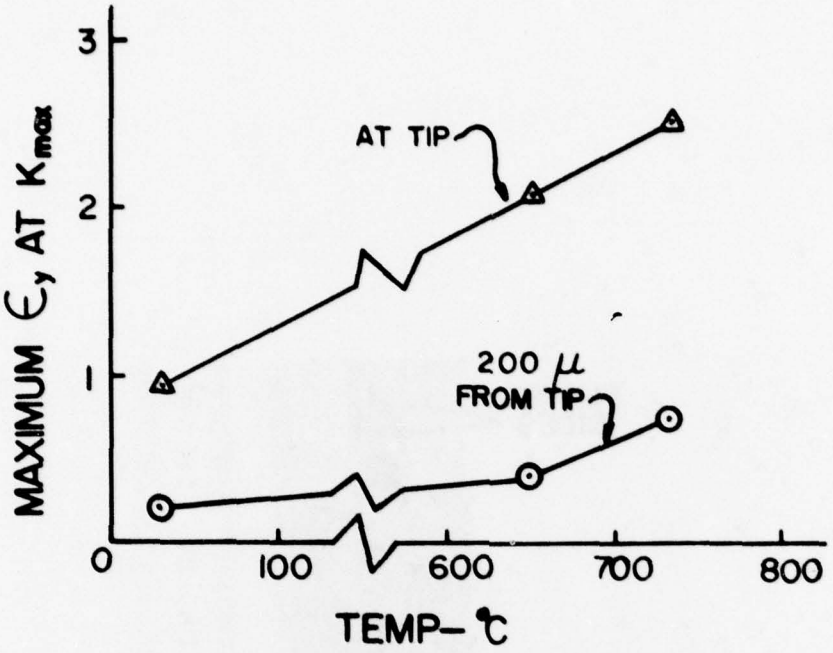

Figure 77 Maximum ϵ_y versus temperature

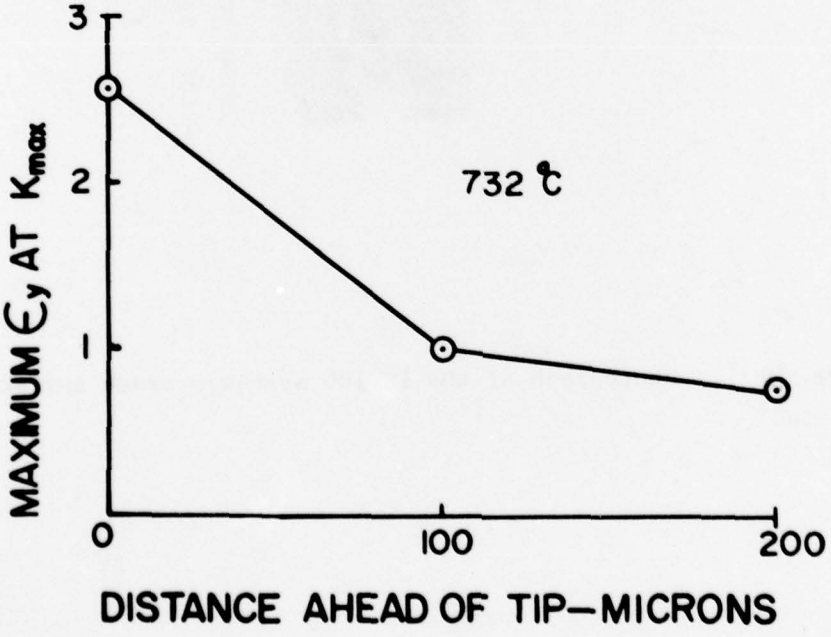

Figure 78 Maximum ϵ_y versus distance from the crack tip.

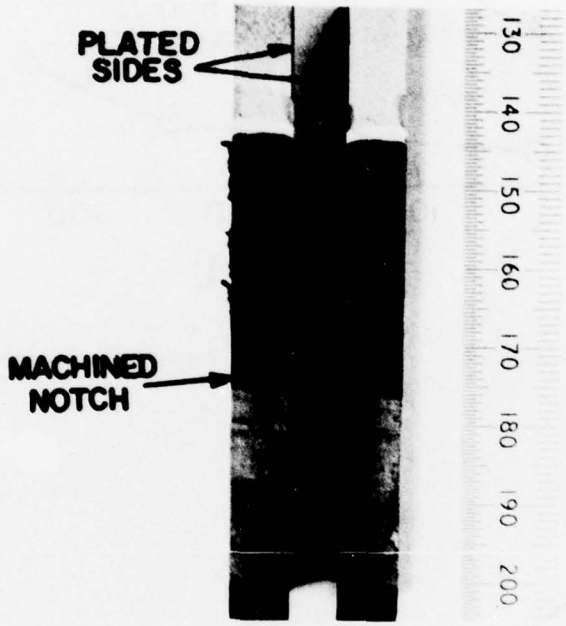

Figure 79 Photograph of the IN-100 specimen crack surfaces.

REFERENCES

1. Sharpe, W. N., Jr., "A Review of the Techniques for Measuring Strains at High Temperatures," Final Report, Pressure Vessel Research Committee, Welding Research Council, New York, New York, December 1973.

2. Macha, D. E., Sharpe, W. N., Jr., Grandt, A. F., Jr., "A Laser Interferometry Method for Experimental Stress Intensity Factor Calibration," Cracks and Fracture, ASTM STP 601, Amer. Soc. Test. Mat., 1976, pp. 490-505.

3. Sharpe, W. N., Jr., "Interferometric surface strain measurement," International Journal of Nondestructive Testing 3, 1971, pp. 56-76.

4. Sharpe, W. N., Jr., "Preliminary development of an interferometric strain gage for use on nosetip materials subjected to thermal shock," AFML-TR-76-63, Air Force Materials Laboratory, Wright-Patterson Air Force Base, June 1976.

5. Sharpe, W. N., Jr., "Development and Application of an Interferometric System for Measuring Crack Displacements," Final Report on NASA grant NSG-1148, N 77-12367, 1977.

6. Sharpe, W. N., Jr., Payne, T. S., and Smith, M. K., "A Biaxial Laser-Based Displacement Transducer," presented at 1977 Spring Meeting of SESA, Dallas, TX, May 1977.

7. Gray, A. G., "Modern Electroplating," J. Wiley & Sons, Inc., 1953.

8. Berry, R. W., Hall, P. M., and Harris, M. T., "Thin Film Technology," D. Van Nostrand Company, Inc., 1968.

9. Powell, C. F., Oxley, J. H., and Blocher, J. M., "Vapor Deposition," J. Wiley & Sons, Inc., 1966.

10. Kofstad, Per, "High-Temperature Oxidation of Metals," J. Wiley & Sons, Inc., 1966.

11. Kubaschewski, O., and Hopkins, B. E., "Oxidation of Metals & Alloys," Butterworths, 1962.

12. Scully, J. C., "The Fundamentals of Corrosion," Pergamon Press, 1975.

13. Molloy, E., "Electro-Plating and Corrosion Prevention," George Newnes Ltd, London, 1954.

14. Mohler, J. B., "Electroplating and Related Processes," Chemical Publishing Co., Inc., 1969.

15. National Research Council, "High-Temperature Oxidation-Resistant Coatings," National Academy of Sciences/National Academy of Engineering, 1970.

16. "New Metallic Diffusion Coatings," Materials in Design Engineering, Vol. 54, No. 6, pg. 133, Nov. 1961.

17. Gedwill, M. A. & Grisaffe, S. J., "Aluminized Alloy Boosts Turbine Blade Life," Metal Progress, Vol. , pp. 66-68, August 1974.

18. Couch, D. E., et al, "Protestion of Molybdenum from Oxidation at Elevated Temperatures," J. Electrochemical Soc., Vol. 105, pp. 450-456, Aug. 1958.

19. Bredzs,, N. T., Miller, F. M., and Peaslee, R. L., "Alloy Coatings for High Temperature Protection," Materials Engineering Quarterly, Vol. 14, pp. 12-18, Feb. 1974.

20. Gedwill, M. A. and Grisaffe, S. J., "Oxidation Resistant Claddings for Superalloys," Metals Engineering Quarterly, Vol. 12, pp. 55-61, May 1972.

21. Wessel, E. T., "State of the Art of the WOL Specimen for KIC Fracture Toughness Testing," Engineering Fracture Mechanics, Vol. 1, 77-103, 1968.

22. Sharpe, W. N., Jr., "A New Biaxial Strain Gauge," Rev. Sci. Instr., Vol. 41, No. 10, pp. 1440-1443, Oct. 1970.

23. Knott, J. F., Fundamentals of Fracture Mechanics, J. Wiley & Sons, New York, N. Y., Ch. 6, 1973.

24. Sharpe, W. N., Jr., and Grandt , A. F., Jr., "A Preliminary Study of Fatigue Crack Retardation Using Laser Interferometry to Measure Crack Surface Displacements," Mechanics of Crack Growth, ASTM STP 590, pp. 302-320, 1976.

25. Macha, D. E., "Fatigue-Crack-Growth Retardation Behavior of IN-100 at Elevated Temperature," presentat at 1977 SESA Spring Meeting, Dallas, TX., May, 1977.

*U.S.Government Printing Office: 1978 — 757-080/634